FEDERAL UNIVERSITY OF ESPÍRITO SANTO

POSTGRADUATE PROGRAM IN MECHANICAL ENGINEERING

MARCIELLYO RIBEIRO DE OLIVEIRA

A MODEL FOR PREDICTING TWO-PHASE FLOW PATTERN TRANSITIONS IN AN ANNULUS: INCLINATIONS FROM HORIZONTAL TO NEAR-VERTICAL

VITÓRIA

2021

MARCIELLYO RIBEIRO DE OLIVEIRA

A MODEL FOR PREDICTING TWO-PHASE FLOW PATTERN TRANSITIONS IN AN ANNULUS: INCLINATIONS FROM HORIZONTAL TO NEAR-VERTICAL

Dissertation submitted to the Postgraduate Program in Mechanical Engineering of the Federal University of Espírito Santo, as a partial requirement for obtaining the title of Master of Science in Mechanical Engineering. Concentration Area: Mechanical Sciences

Advisor: Prof. Dr. Márcio Ferreira Martins

Co-advisor: Prof. Dr. Humberto Belich Junior

VITÓRIA

2021

Ficha catalográfica disponibilizada pelo Sistema Integrado de Bibliotecas - SIBI/UFES e elaborada pelo autor

---

Oliveira, Marciellyo Ribeiro de, 1994-
O48m A model for predicting two-phase flow pattern transitions in an annulus : inclinations from horizontal to near-vertical / Marciellyo Ribeiro de Oliveira. - 2021.
121 f. : il.

Orientador: Marcio Ferreira Martins.
Coorientador: Humberto Belich Junior.
Dissertação (Mestrado em Engenharia Mecânica) - Universidade Federal do Espírito Santo, Centro Tecnológico.

1. Multiphase flows. 2. Flow pattern predictions. 3. Flow pattern maps. 4. Inclined tubes. 5. Annular geometries. I. Martins, Marcio Ferreira. II. Belich Junior, Humberto. III. Universidade Federal do Espírito Santo. Centro Tecnológico. IV. Título.

CDU: 621

PROGRAMA DE PÓS-GRADUAÇÃO EM ENGENHARIA MECÂNICA
CENTRO TECNOLÓGICO
UNIVERSIDADE FEDERAL DO ESPÍRITO SANTO

A MODEL FOR PREDICTING TWO-PHASE FLOW PATTERN TRANSITIONS IN AN ANNULUS: INCLINATIONS FROM HORIZONTAL TO NEAR-VERTICAL

MARCIELLYO RIBEIRO DE OLIVEIRA

COMISSÃO EXAMINADORA

Prof. Dr. Márcio Ferreira Martins
Orientador (PPGEM/UFES)

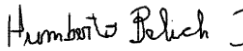

Prof. Dr. Humberto Belich Júnior
Coorientador (PPGEM/UFES)

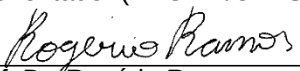

Prof. Dr. Rogério Ramos
Examinador Interno (PPGEM/UFES)

Dr. Leandro Silva Amorim
Examinador Interno (pós-doutorando - PPGEM/UFES)

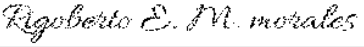

Prof. Dr. Rigoberto Eleazar Melgarejo Morales
Examinador Externo (PPGEM/UTFPR-CT)

Dissertação apresentada ao Programa de Pós-Graduação em Engenharia Mecânica da Universidade Federal do Espírito Santo como parte dos requisitos necessários à obtenção do título de Mestre em Engenharia Mecânica

Vitória (ES), 16 de dezembro de 2021.

Datas e horários baseados em Brasília, Brasil
Sincronizado com o NTP.br e Observatório Nacional (ON)
Certificado de assinaturas gerado em
25/12/2021 às 07:51:18

Docs dissertação Marciellyo

Data e Hora de Criação: 16/12/2021 às 11:54:47

Documentos que originaram esse envelope:

- Questionário CAPES - Marciellyo Ribeiro de Oliveira.pdf (Arquivo PDF) - 1 página(s)
- Aprovação banca Marciellyo Ribeiro de Oliveira.pdf (Arquivo PDF) - 1 página(s)
- Ata 293 - Marciellyo Ribeiro de Oliveira.pdf (Arquivo PDF) - 1 página(s)

Hashs únicas referente à esse envelope de documentos

[SHA256]: 56e57e40a438fcff9ac039114d95e857fa7cfce2fb4cd97f9114fcb09c774aac
[SHA512]: 28b01cdeefea56ce26d50f31434f2b58f37d615c32f9e4e50c58568e5c3a9c241317cd577e2322ae429a8612326c99b40b839c3a3739edb5c40a09fda2ba1f4e

Lista de assinaturas solicitadas e associadas à esse envelope

ASSINADO - Marcio Ferreira Martins (marcio.martins@ufes.br)
Data/Hora: 16/12/2021 - 12:08:31, IP: 200.137.65.107, Geolocalização: [-20.272165, -40.305343]
[SHA256]: 8ea3850f3dd4ba7437cc4e56b1d47ba62fd38fc73025d7b933ad651a0f508823

ASSINADO - Rogério Ramos (rogerio.ramos@ufes.br)
Data/Hora: 17/12/2021 - 09:45:11, IP: 187.36.167.32, Geolocalização: [-20.293222, -40.307916]
[SHA256]: 9a072ecc0f5b0595ad8f7ee0f92542bd7602afbb2841bc3986bf759dfac1a88e

ASSINADO - Humberto Belich Júnior (humberto.belich@ufes.br)
Data/Hora: 18/12/2021 - 16:47:42, IP: 2804:14d:ae84:81f3:1de2:5863:8, Geolocalização: [-20.291750, -40.298641]
[SHA256]: c2f4a2d177033d03a7d05da17441d5d2c859e2a409ece1346f4df4cb179febcf

ASSINADO - Leandro Silva Amorim (lesamorim@gmail.com)
Data/Hora: 24/12/2021 - 00:36:07, IP: 179.180.7.205, Geolocalização: [-20.288725, -40.295421]
[SHA256]: 69a8fe75319d6d5100b9ba5cf689578edadeb3b32e0011eb0a61e8e2097ecdd3

ASSINADO - Rigoberto Eleazar Melgarejo Morales (rmorales@utfpr.edu.br)
Data/Hora: 25/12/2021 - 07:51:18, IP: 191.177.172.67
[SHA256]: 6f89552d80def3710ff7b50c150ffc8478ed8b5fa163a664b142443baf755594

Histórico de eventos registrados neste envelope

25/12/2021 07:51:21 - Envelope finalizado por rmorales@utfpr.edu.br, IP 191.177.172.67
25/12/2021 07:51:18 - Assinatura realizada por rmorales@utfpr.edu.br, IP 191.177.172.67
24/12/2021 16:31:45 - Envelope visualizado por rmorales@utfpr.edu.br
24/12/2021 00:36:07 - Assinatura realizada por lesamorim@gmail.com, IP 179.180.7.205
24/12/2021 00:35:57 - Envelope visualizado por lesamorim@gmail.com, IP 179.180.7.205
18/12/2021 16:47:42 - Assinatura realizada por humberto.belich@ufes.br, IP 2804:14d:ae84:81f3:1de2:5863:8
17/12/2021 16:07:43 - Envelope visualizado por humberto.belich@ufes.br, IP 2804:14d:ae84:81f3:6c77:d071:5
17/12/2021 09:45:11 - Assinatura realizada por rogerio.ramos@ufes.br, IP 187.36.167.32
17/12/2021 09:35:11 - Envelope visualizado por rogerio.ramos@ufes.br, IP 187.36.167.32
16/12/2021 12:08:31 - Assinatura realizada por marcio.martins@ufes.br, IP 200.137.65.107
16/12/2021 12:05:07 - Envelope registrado na Blockchain por marcio.martins@ufes.br, IP 200.137.65.107
16/12/2021 12:05:05 - Envelope encaminhado para assinaturas por marcio.martins@ufes.br, IP 200.137.65.107
16/12/2021 11:54:49 - Envelope criado por marcio.martins@ufes.br, IP 200.137.65.107

ACKNOWLEDGEMENTS

I am deeply indebted and would like to express my appreciation to my advisor and committee chair Professor Márcio Ferreira Martins, whose support, patience and faith in my work were unflinching. His valuable and constructive suggestions during the planning and development of this dissertation were immeasurable.

I would also like to extend my deepest gratitude to my co-advisor, Professor Humberto Belich Junior. His encouragement throughout this dissertation was indispensable. Besides, I am grateful to Dr. Leandro Amorim for his help with the formulation/calculation of equations.

I am specially grateful to my parents Maria da Penha and Marcelo Luiz, for their love, prayers, caring, and sacrifices for educating and preparing me for my future. Also, I express my thanks to my sisters Marielly and Marcelly and brother Marcellyo for their support. My special thanks to Isabela Dalvi and Gabriel Xavier for the many times they listened to me and supported me as well as teaching me to "enjoy the journey."

I would like to acknowledge the technical assistance of the 2Solve, particularly Maurício Calheiros, for his help in setting up the test facility that originated this work. I would also like to extend my gratitude to my working team from LFTC Lab, Flávio Bittencourt, Cleyton Mendonça, and Adriana da Mata for their countless practical suggestions. I would also wish to recognize the assistance of the Nemog Lab team, Tiago Guerzet, for his help and tips on the development of the algorithm, and Ligia Franco for her constructive criticism.

I very much appreciate the Postgraduate Program in Mechanical Engineering (PPGEM) of the Federal University of Espírito Santo for providing space and support to work through this programme.

Finally, my acknowledgment to Petrobras for financing the project that originated this work.

ABSTRACT

The flow of a two-phase mixture is a complex phenomenon. One reason is that interactions between phases depend on variations in operating conditions (velocity of the phases, pressure, tube geometry, etc). These operating conditions impose the formation of different flow patterns that can undergo pattern transition depending on the change in geometric cross-section. This work proposes a mechanistic model for any tube inclination from horizontal to near-vertical and considers the concentric annulus condition as a particular case of a pipe. Mathematical relationships are developed to calculate shear stresses and velocity profiles in an annulus under different inclinations. Based on geometric parameters, a new methodology helps obtain the wetted area and perimeter of the liquid and gas phase. Furthermore, two scenarios are considered to verify the model's reliability: horizontal piping and vertical piping, and good performance was found in both scenarios. Finally, a generalized air-water flow pattern map based on dimensionless groups is obtained. Furthermore, the influence of the inner tube on the stratified liquid level is studied, and it is found that the insertion of the inner tube causes an increase in the liquid level as the superficial gas velocity increases. Also, the influence of the tube inclination in the following transitions between flow patterns is verified: smooth stratified/wavy stratified, wavy stratified/annular dispersed liquid, stratified/intermittent, annular dispersed/intermittent, and intermittent/dispersed bubble. Regardless of the direction, the intermittent flow pattern is the most affected, increasing its area as the inclination increases if the flow is upward and decreasing its area as the inclination increases if the flow is downward.

Keywords: Multiphase flows. Flow pattern predictions. Flow pattern maps. Inclined tube. Annular geometries

LIST OF FIGURES

LIST OF TABLES

LIST OF SYMBOLS

Abbreviations

ESP	Electrical Submersible Pump
FPSO	Floating, Production, Storage and Offloading
MOBO	Pumping Module ("Módulo de Bombeio" in portuguese)
NEMOG	Research Group for Oil and Gas Flow and Measurements ("Núcleo de Estudos em Escoamentos de Óleo e Gás" in portuguese)
NPP	Nuclear Power Plant
NSSS	Nuclear Steam Supply System
PDF	Power Density Function
PSD	Power Spectral Density
RTNR	Real-Time Neutron Radiography

Latin Letters

A	Flow cross-section area
AD	Annular-dispersed flow pattern
c	Wave's velocity
C	Coefficient dependent on the magnitude of disturbance, also constant in the friction factor correlation, Equations 3.28 and 3.29
D	Tube diameter
DB	Dispersed bubble flow pattern
DBC	Distance between tube centers
e	Degree of eccentricity
f	Friction factor
F	Modified Froude number

g	Acceleration of gravity
h	Liquid level or gas gap
I	Intermittent flow pattern
K	Wavy flow pattern dimensionless parameter
L	Tube's length, also triangle basis
m	Exponent, Equation 3.29
n	Exponent, Equation 3.28
N	Integration constant
p	Pressure
P	Pressure
r	Tube radius
R	Outer tube diameter
Re	Reynolds number
s	Jefferey's sheltering coefficient
S	Perimeter over which shear stress acts, also stratified flow pattern
SS	Stratified smooth flow pattern
SW	Stratified wave flow pattern
T	Dispersed bubble flow pattern dimensionless parameter
u	Velocity in x direction
v	Velocity normal to the x direction
W	Specific weight
X	Lockhart-Martinelli parameter
Y	Dimensionless inclination parameter

Greek Symbols

α	Angle between the pipe longitudinal axis and the horizontal, positive for downward flow

β	Angle that measures the height of liquid in the inner tube
Γ	Auxiliary variable
Δ	Differential
θ	Angle that measures the height of liquid in the outer tube
κ	Diameter ratio
λ	Unknown distance from the pipe center
μ	Dynamic viscosity
ν	Kinematic viscosity
ξ	Modified pressure
ρ	Density
τ	Shear stress
ϕ	Function
φ	Momentum transport by all possible mechanisms, convective and molecular
Ω	Auxiliary variable

Subscript

ABC	Vertices of the triangle
abc	Vertices of the triangle
B	Buoyancy
f	Final
G	Gas
h	Hydraulic
i	Inner tube, also gas-liquid interface
int	Interest
L	Liquid, also length of the infinitesimal element
m	Mean
o	Outer tube

r	Radial direction
rz	rz direction
S	Superficial
T	Turbulence, also triangle
zz	zz direction
$\sim$	Dimensionless variable
$'$	Disturbed variable
0	Initial
1	Relating to the outer tube
2	Relating to the inner tube

CONTENTS

1 INTRODUCTION

Multiphase flow is defined as the simultaneous flow of a mixture containing two or more phases or components. It is a complex phenomenon that is difficult to understand, predict, and model (ANUMBE, 2018). The aforementioned flow generates different topologies, known as flow regimes or flow patterns, whose existence depends on the relative magnitudes of the forces acting on the fluid, such as buoyancy, inertia, viscosity, and surface tension. The acting forces are altered substantially according to the phase's properties, turbulence intensity, relative phase flow velocities, flow direction (co-current or counter-current), and geometric parameters such as channel diameter, inclination, entrance length, and cross-sectional geometry (circular, annular, etc.) (OSAMUSALI, 1988; BRILL; MUKHERJEE, 1999; FIROUZI *et al.*, 2015; WU *et al.*, 2017; OLIVEIRA *et al.*, 2019; WU *et al.*, 2019). Specifically about flows in an annulus, some examples are double pipe heat exchangers for evaporation and condensation, pumping modules (MOBO), food-processing plants, and centrifugal pumps in the petroleum industry (ROMERO; HUPP, 2014; WU *et al.*, 2017; EYO; LAO, 2019).

The pumping module has great importance on offshore oil extraction in Brazilian oil basins (RIBEIRO *et al.*, 2005). It consists of a series of equipment, one of which is the electric submersible pump (ESP), which produces heat during its operation due to high electromagnetic dissipation losses, that must be removed by the passage of oil through the annulus between the motor wall and the shroud.

Given the complexity of multiphase flows in an annulus, most previous works focused on determining the flow pattern transition (OSAMUSALI, 1988; CHEN *et al.*, 1997; LAGE; TIME, 2000; IBARRA *et al.*, 2019) or flow pressure drop (SALCUDEAN *et al.*, 1983b; WONGWISES; PIPATHATTAKUL, 2006; OSGOUEI *et al.*, 2015), void distribution (SALCUDEAN *et al.*, 1983a) through experimental techniques or (a few) on developing mathematical/empirical relations for predicting flow pattern transition (KELESSIDIS; DUKLER, 1989; HASAN; KABIR, 1992; FILHO *et al.*, 1992a; FILHO *et al.*, 1992b; DAS *et al.*, 1999b; LAGE; TIME, 2000; OZBAYOGLU; OMURLU, 2007; YU *et al.*, 2010). The reason is that there is a slight nuance in defining a methodology to describe the so-called 'wet perimeter' and then modeling the wall shear stress, see Bird *et al.* (2002).

Ekberg *et al.* (1999) measured the following two-phase flow patterns parameters: void fraction and pressure drop, associated with air-water flow in concentric annular test sections. Bubbly,

slug/plug, churn, stratified, and annular were the flow patterns observed. The flow pattern maps made a distinction between small and large horizontal channels with regular cross-sections (circular, rectangular, triangular) and typical maps. The correlations by Taitel and Dukler (1976) and Mandhane *et al.* (1974) were used; nevertheless, those correlations were made for pipes. Inclination effects were not studied either.

With respect to the need to promote the experimental and theory interplay, models have been developed but they were strongly dependent on statistical analyses of the measurements (KELESSIDIS; DUKLER, 1989), or the practical cross-section geometry (FILHO *et al.*, 1992a; FILHO *et al.*, 1992b). The models developed for regular or annular cross-section flows were restricted to a given inclination (horizontal, vertical, or inclined) and a flow direction (upward or downward). For instance, the works by Kelessidis and Dukler (1989) and Filho *et al.* (1992a) were verified against experimental data for air-water flow in an upward vertical annulus, similarly to the work of Hasan and Kabir (1992). In the case of the practical models, Ozbayoglu and Omurlu (2007) introduced a new equivalent diameter concept (hydraulic diameter), to represent the flow through an annulus, and Gschnaidtner (2014) adapted the Taitel and Dukler (1976) model to predict intermittent and bubbly flows in a horizontal annulus. Between horizontal and vertical inclinations, Hasan and Kabir (1992) presented an approach to predict the transition in an upward inclined annulus.

Since the efforts to have a general model are still incipient, running experiments for inclined tubes is still necessary. Recently, Bolarinwa (2016) tested both single-phase and two-phase flows in an annulus. His experiments were conducted to observe flow patterns in several inclinations, from horizontal to 15, 30, 45 and, 60 degrees. The flow pattern maps were generated from experimental data. The angle of inclination, size of the duct, and the working fluids' viscosity all played a considerable role in the flow pattern observed on their transitions points and the size of flow pattern maps. However, no correlation was developed, leaving the flow maps without a transition boundary between the flow patterns.

It is noteworthy that, among the works summarized in Table 1, a research gap is identified, where, at present, a model for predicting flow patterns in an annular channel in a horizontal position is still missing in the literature (except for Ozbayoglu and Omurlu (2007), who developed a specific model for flow in a horizontal annulus). That may have been because multiphase flow occurs, usually in pipes and channels, predominantly in the vertical position.

However, specific sub-sea solutions using the pumping module mentioned before, exist in the horizontal (RODRIGUES *et al.*, 2005b; COLODETTE *et al.*, 2007).

1.1 MOTIVATION AND RESEARCH BACKGROUND

The world's daily oil consumption is estimated to be around 88.5 million barrels and the demand for oil and gas increases as populations grow and the economy of developing countries expands (BP, 2021). According to Barcellar (2016), during the 20th century, the consumption of oil in the world grew significantly and it is estimated that its demand will continue to grow over the next 25 years, increasing around 60% from current levels and remaining the main source of the world's energy matrix .

Figure 1 shows the worldwide oil production and consumption over the last 55 years, with a slight gap between consumption and production between the years 1965 and 2020, where from then on, the roles are reversed (mainly due to use from other energy sources - solar, wind, etc.). However, oil consumption is still high and should remain so for the next few years.

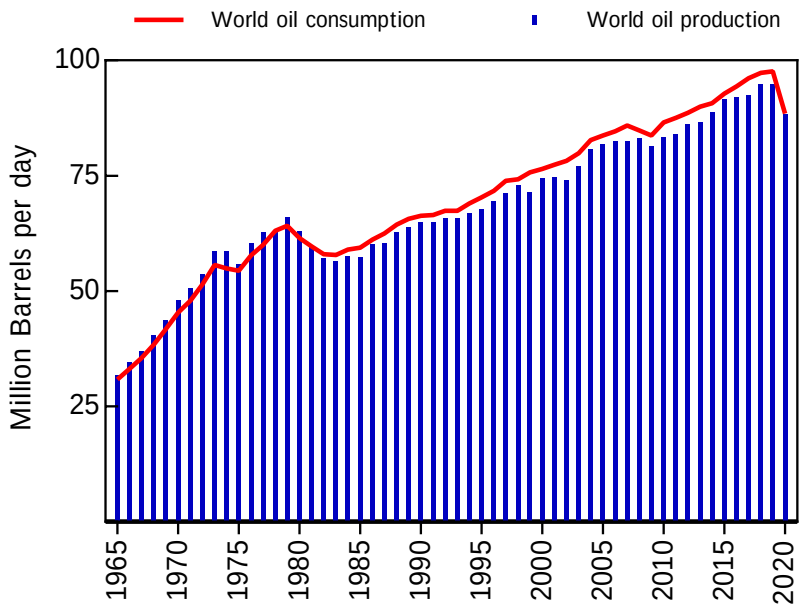

Figure 1 – Production vs. Oil Consumption in the world (1965 - 2020)
Source: Made by the author using BP (2021) data

In this context, it is not surprising that several research centers appear around the world. Among these research centers, the Research Group for Oil and Gas Flow and Measurement (NEMOG, in Portuguese) stands out, addressing many issues found in the industry, with a

focus on the petrochemical industry. The lab's facilities, which according to Franco and Ramos (2021) are all fully instrumented and automated (due to academic and safety reasons), carry out research on flare gas flow measurements (Martins *et al.* (2019), Franco (2020)), water-in-oil emulsions, three-phase flow in pipes (oil, air, and water), and two-phase (air and water) flow.

Concerning this last facility, it meets the need to understand the hydrodynamic behavior of electrical submersible pump (ESP) - which according to Ribeiro *et al.* (2005) is a pioneering technique developed by Petrobras[1] - which together with other components are part of the so-called MOBO piece of equipment - see Rodrigues *et al.* (2005a). This set has an annular cross-sectional and it is illustrated by Figure 2.

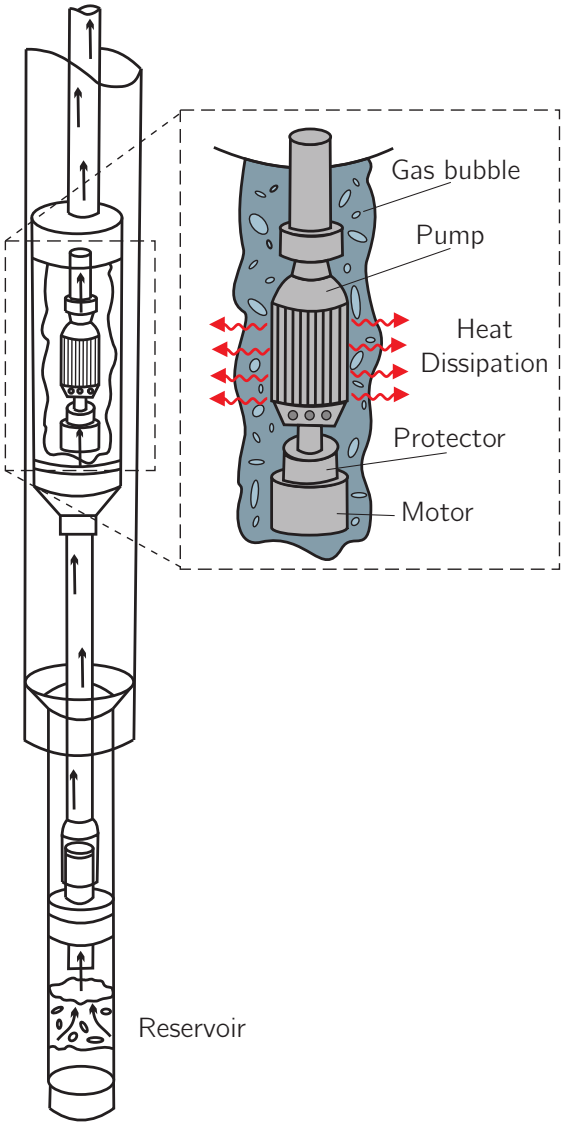

Figure 2 – Conventional ESP installation
Source: Author

[1] Brazilian state-owned oil company

In light of this, an experimental test facility was built consisting of two concentric borosilicate glass tubes which enable the visualization of the flow (air-water) inside. Figures 3 and 4 show the facility at horizontal and inclined positions respectively.

Figure 3 – ESP test facility - horizontal position
Source: Author

Figure 4 – ESP test facility - inclined position
Source: Author

However, after a set of experiments (on horizontal, inclined, and vertical inclinations), an issue arose: "how are flow patterns affected by the tube inclination?" Thus, a literature survey (see Table 1) was carried out and a research gap was identified: at present, a prediction flow pattern

modeling for the annular channel is restricted to a specific position (either horizontal or vertical) with the majority of the developed models addressed for the vertical position (that might be because multiphase flow occurs, usually in pipes and channels predominantly in the vertical). On the other hand, for horizontal position, models are still missing in the literature, except for Ozbayoglu and Omurlu (2007) that developed a specific model for flow in a horizontal annulus.

It should be noted that although the work originates from a laboratory experiment, no experimental data from this test facility had been used, and therefore the work proposed herein is purely analytical.

1.2 OBJECTIVES

To the author's knowledge, a general model independent of the tube inclination is presented for the first time. The proposal considers the unique characteristics of flow in an annulus: the asymmetry in shear stress and velocity profiles. Therefore, the dissertation aims to generalize the Taitel and Dukler (1976) model for any tube inclination, ranging from horizontal to near-vertical and considering a concentric annulus as a particular case of a circular cross-section tube. The outcomes are two-phase flow pattern maps, identifying the transitions from: stratified smooth to stratified wavy, stratified wavy to annular dispersed liquid, stratified to intermittent, annular dispersed liquid to intermittent, and intermittent to dispersed bubble. The dissertation's objectives are:

- To propose a new approach for calculating the shear stress and velocity profile in an inclined annulus.
- To develop a new methodology based on geometric parameters to obtain the area and wetted perimeters;
- To present the influence of inclination on the flow pattern transitions.

1.3 DISSERTATION OUTLINE

Chapter 1 - Introduction: this chapter provides a brief introduction to multiphase flow and delineates the motivation and research background also the objectives of this dissertation.

Chapter 2 - Theoretical Review: this chapter presents the main issues about multiphase flows that are pertinent to the understanding of this dissertation, focusing firstly in presenting

the multiphase flow in pipes. Moreover, it shows the procedures to identification of flow patterns focusing mainly on the mechanistic models (which is the scope of this work), and last but not least, it is discussed about the multiphase flow through an annulus.

Chapter 3 - Formulating the mechanistic model: this chapter presents the basic premise of the dissertation, which is the idea of equilibrium stratified flow, in addition to a new approach to calculating shear stress that considers two parameters: the tube's inclination and its annular cross section. The concept of equilibrium stratified flow together with shear stress are used for the development of transitions between flow patterns. A version of this chapter has been published: Marciellyo Ribeiro de Olivera, Marcio Ferreira Martins, Humberto Belich and Leandro Amorim, "A model for predicting two-phase flow patterns transitions in an annulus: inclinations from horizontal to near-vertical", Chemical Engineering Science Journal. https://doi.org/10.1016/j.ces.2021.117379

Chapter 4 - Adapting the transition criteria for annuli: this chapter provides the development of transitions between the various flow patterns using the ideas developed in chapter 3. The resulting equations are presented in two ways: dimensional and dimensionless. A version of this chapter has been published: Marciellyo Ribeiro de Olivera, Marcio Ferreira Martins, Humberto Belich and Leandro Amorim, "A model for predicting two-phase flow patterns transitions in an annulus: inclinations from horizontal to near-vertical", Chemical Engineering Science Journal. https://doi.org/10.1016/j.ces.2021.117379

Chapter 5 - Results and Discursion: this chapter presents the results obtained from the equations developed in the chapter 4, in addition to discussing the possible causes that led to such results.

Chapter 6 - Conclusions: this chapter summarizes the principal conclusions of the dissertation. Besides, it is given a series of recommendations for future research.

Appendix A: presents a supplementary material to adapting the equations developed by Taitel and Dukler (1976) from the condition of pipe to annulus. Such equations are part of the development proposed in chapter 4. A version of this chapter has been published: Marciellyo Ribeiro de Olivera, Marcio Ferreira Martins, Humberto Belich and Leandro Amorim, "A model for predicting two-phase flow patterns transitions in an annulus: inclinations from horizontal to near-vertical", Chemical Engineering Science Journal. https://doi.org/10.1016/j.ces.2021.117379

Appendix B: presents a supplementary material describing the procedure to convert the

equations developed in appendix A for a dimensionless form. A version of this chapter has been published: Marciellyo Ribeiro de Olivera, Marcio Ferreira Martins, Humberto Belich and Leandro Amorim, "A model for predicting two-phase flow patterns transitions in an annulus: inclinations from horizontal to near-vertical", Chemical Engineering Science Journal. https://doi.org/10.1016/j.ces.2021.117379

Appendix C: presents a supplementary material to generalize the proposal developed in appendix A using two angles (referenced in the center of the tube) that rotate from 0 to π, thus the previous method that divides the cross section into four sections now needs only three sections, making the analysis simpler. A version of this chapter has been published: Marciellyo Ribeiro de Olivera, Marcio Ferreira Martins, Humberto Belich and Leandro Amorim, "A model for predicting two-phase flow patterns transitions in an annulus: inclinations from horizontal to near-vertical", Chemical Engineering Science Journal. https://doi.org/10.1016/j.ces.2021.117379

Appendix D: presents a supplementary material with the code routines written in Matlab^{TM} used to solve the iterative problem that equation 3.33 requires. Furthermore, the codes generate the flow pattern maps.

2 THEORETICAL REVIEW

2.1 MULTIPHASE FLOW

Present as one of the many topics of research in the field of fluid mechanics, many authors have defined the multiphase flow in distinct ways (LIMA, 2016): Soo (1990) defined the flow as constituted of a liquid (fluid medium) and a dispersed phase (particulate) regardless of the numbers of chemical components. Furthermore, either the liquid or the gaseous medium is taken as the continuous phase whereas either the solid particles, gas bubbles, or liquid drops are taken as the dispersed phase. While Paladino (2005) defined the multiphase flow as a region in the space where two or more immiscible fluids are separated by an interface. Finally, Brennen (2005) and Yadigaroglu and Hetsroni (2018) defined multiphase flow in a slightly different manner that could be summarized as the flow of a mixture containing two or more phases or components.

Multiphase flow presents a wide variety of phenomena associated with it, and the occurrence of two or more phases makes the analysis much more difficult (ANUMBE, 2018). Therefore, ways must be found so as to show how such flow behaves.

2.1.1 Important Multiphase Flow System

Multiphase flow is a complex phenomenon which is difficult to understand, predict, model and objectively interpret. Such a phenomenon is present in everyday life, in nature, in industrial processes, in power plants, in the oil and gas industry, etc. The following large engineering systems are examples among many others in which multiphase flow plays a dominant effect in the design and operation (ANUMBE, 2018; YADIGAROGLU; HETSRONI, 2018).

- **Electric power production from oil, coal or gas**

A bulk of power plants use the water as the working fluid in a steam cycle. Figure 5 illustrates the steam cycle of a modern plant. Water is vaporized in the high-pressure steam generator section and the low-pressure steam exiting from the turbine condensers in the condenser; the two-phase flow takes place throughout the steam plant, specially in the condenser. (YADIGAROGLU; HETSRONI, 2018).

Further informations can be found in the work of Wu *et al.* (2015).

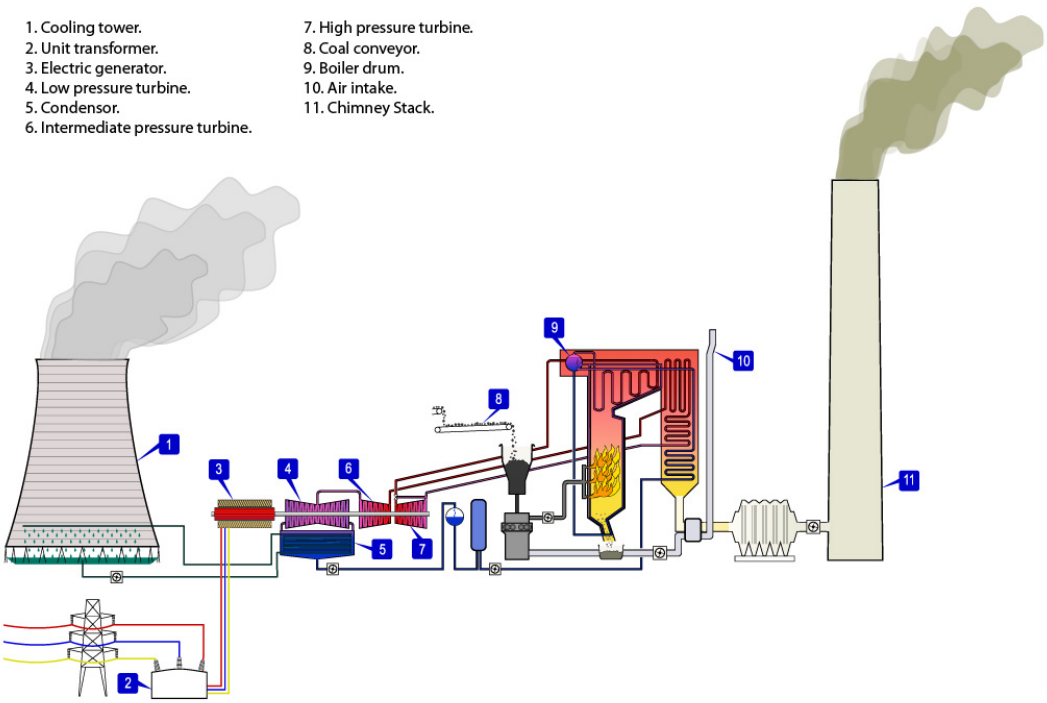

Figure 5 – Modern Steam Power System
Source: ZeroCO2 (2017?)

- **Nuclear Power Plant (NPP)**

According to Yadigaroglu and Hetsroni (2018), in a nuclear power plant (NPP), the Nuclear Steam Supply System (NSSS) is the part of the plant where water at high pressure is heated in the reactor vessel by the nuclear chain reaction taking place in the fuel rods. Steam is then produced (either in a steam generator, as in a pressurized water reactor, figure 6, or in the reactor vessel, as in a boiling water reactor, figure 7) and used in the turbine-generator to produce electric power.

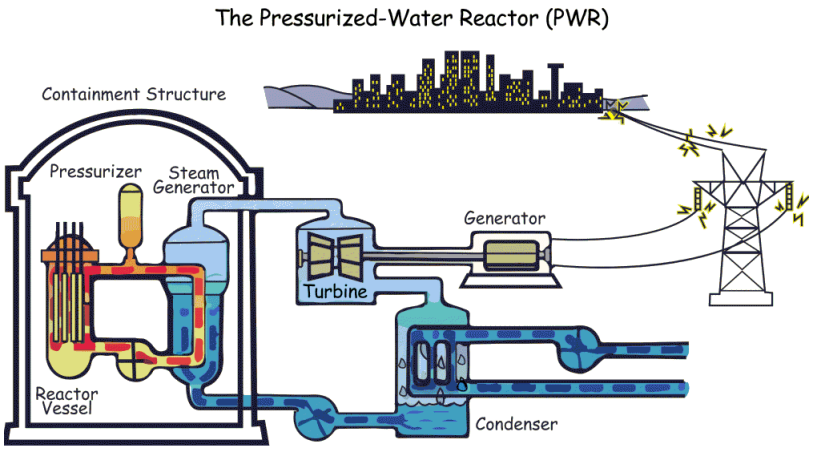

Figure 6 – Pressure Water Reactor (PWR)
Source: NRSC (201?)

Both plants are very onerous; therefore, a safe and efficient operation during the lifetime of the equipment depends on detailed knowledge of the multiphase flow inherent to the process.

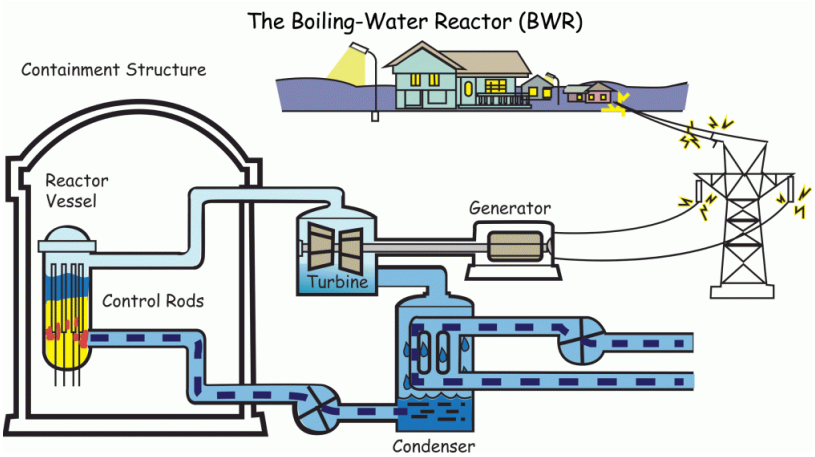

Figure 7 – Boling Water Reactor (BWR)
Source: NRSC (201?)

- **Offshore production**

The offshore production usually involves a drilling platform which operates a number of wells to produce crude oil. The oil comes out of the ground usually as a mixture of crude oil, sea water, sand and gas (YADIGAROGLU; HETSRONI, 2018). Figure 8 illustrates the production wells, drilling platforms, and a floating production, storage and offloading (FPSO) vessel.

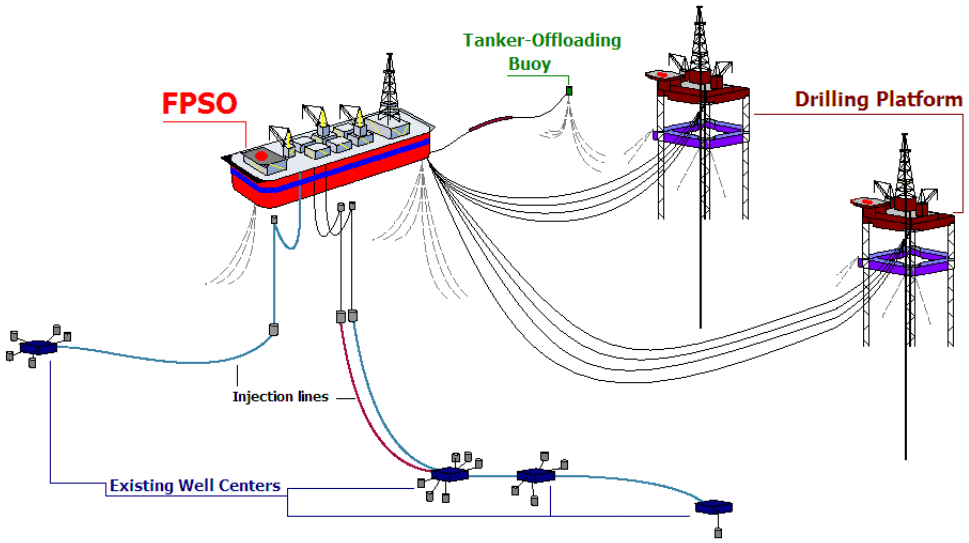

Figure 8 – FPSO diagram
Source: Yadigaroglu and Hetsroni (2018)

Furthermore, according to Lima (2016), as oil flows from the reservoir to the surface, lighter hydrocarbons tend to undergo phase change due to pressure drop; such a phase change can be

both ways; that is, from liquid to gas, the most common, and from gas to liquid (retrograde condensation). Therefore, the multiphase phenomenon inherent to the oil lifting process needs attention during the operation as it leads to problems such as severe head losses and gas lock, which in turn affects submersible centrifugal pumps under high gas fractions in the oil flow.

2.2 FLOW PATTERN

In single-phase flow, assuming that the channel's geometry is known, one can straightforwardly determine, either experimentally or theoretically, the system's velocity distribution or pressure drop. However, if two or more different fluids are flowing simultaneously, one cannot tell a priori how the phases are distributed. Therefore, the determination of the velocity distribution or pressure drop gains further complexity. In addition, as a consequence, the mass, momentum, and energy transfer rates become pretty sensitive to this geometric/topological phase distribution (BRENNEN, 2005; YADIGAROGLU; HETSRONI, 2018).

As discussed before, the interfaces' geometric/topological configuration is known as flow regime or flow pattern, whose existence depends on the relative magnitudes of the forces acting on the fluid, such as buoyancy, inertia, viscosity, and surface tension. The acting forces are altered noticeably according to to the properties of the phases, turbulence intensity, the relative velocity between the phases, flow direction, and geometric parameters such as the channel diameter, inclination, entrance length, and cross-section geometry [2] (circle, annulus, etc.) (OSAMUSALI, 1988; BRILL; MUKHERJEE, 1999; CHENG *et al.*, 2008; OLIVEIRA *et al.*, 2019; WU *et al.*, 2019).

Other parameters such as the heat transfer and the pressure drop are also affected by this topological distribution, and thereby without knowing such distribution, these parameters cannot be calculated (YADIGAROGLU; HETSRONI, 2018). Furthermore, the two phases are not expected to flow at the same average speed; actually, the gas is most likely to flow at a higher average axial velocity than the liquid, thus inducing a change in the void fraction. Consequently, until the flow patterns are determined, there is no way to precisely model and calculate other parameters of engineering significance. Therefore, one of the first problems that must be addressed when dealing with the multiphase flow is determining the flow patterns.

[2] The geometry may strongly affect the interfacial area available for mass, momentum or energy exchange between the phases.

2.3 FLOW PATTERN IDENTIFICATION PROCEDURE

Many flow pattern identification procedures are found in the literature, and these procedures are divided into two main methods: the Flow Pattern Prediction Method and the Flow Pattern Determination Method. Figure 9 presents a flowchart with both methods.

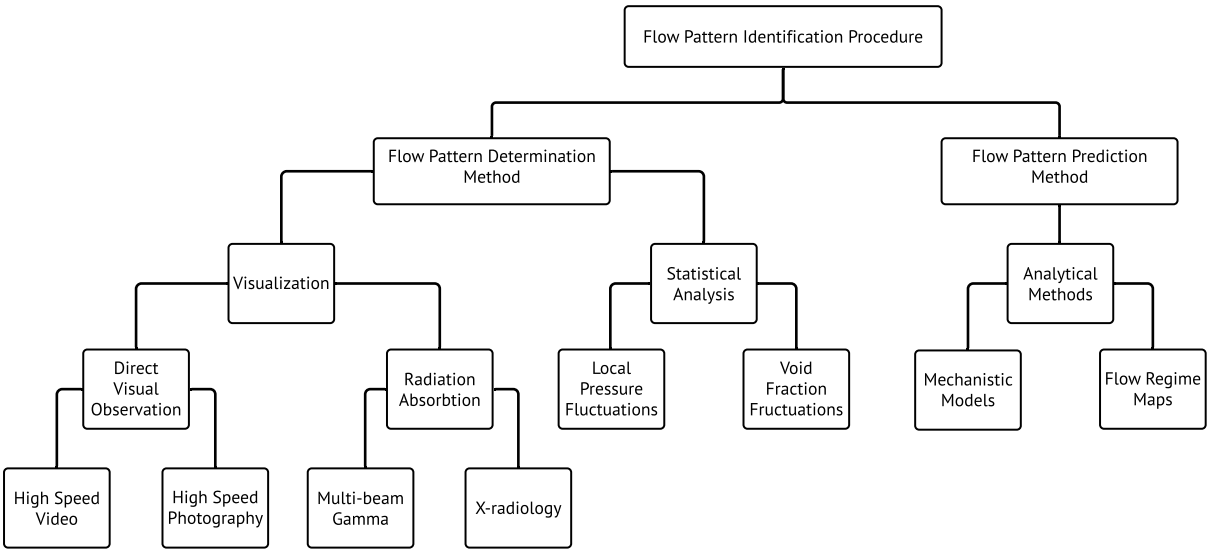

Figure 9 – Flow identification procedure
Source: Adapted from Anumbe (2018)

2.3.1 Flow Pattern Determination Method

There are various flow pattern determination methods and several ways to group the available procedures. Whereas no single technique has delivered excellent results, to improve the confidence in the results, one technique can be used to validate the another (ANUMBE, 2018). Within the branch of flow pattern determination, these methods can be classified into the Visualization Method and the Statistical Analysis Method categories.

The visualization method uses techniques to reconstruct the flow topology visually. This reconstruction is done through:

- **Direct visual observation:** high speed cameras capture the flow pattern through a transparent section (usually glass) in the tube.
- **Radiation absorption:** radiation attenuation measurements with gamma densitometer, Real-Time Neutron Radiography (RTNR) or High speed X-ray Computed Tomography (High Speed X-CT) use ionizing or non-ionizing radiation to determine the flow behavior

(CHAN; BANERJEE, 1981; CHAN; BZOVEY, 1990; HARVEL *et al.*, 1996; ANUMBE, 2018).

Differently from the visualization (visual inspection) method, the statistical analysis for determining flow pattern is objective; this method is based on measuring and quantifying the fluctuations of natural flow parameters such as the differential pressure (Tutu (1982) and Matsui (1986)) or the void fraction (Jones and Zuber (1975), Barnea *et al.* (1980), Vince and Lahey (1982), Tsoukalas *et al.* (1997), and Costigan and Whalley (1997)), which can reflect the prevailing flow patterns in pipes under different conditions (ANUMBE, 2018).

During the experiments, the time-series signals of both quantities (differential pressure and void pressure) are collected by using a variety of instruments (Electrical Impedance flowmeter is an example) and then analyzed with the aid of statistical measures such as Power Density Function (PDF) and Power Spectral Density (PSD) functions.

2.3.2 Flow Pattern Prediction Method

There are at least two main methods within the branch of flow pattern prediction: flow pattern maps and mechanistic models; both methods are presented as follows.

2.3.2.1 Flow Pattern Maps

When certain flow conditions are achieved, the flow topology changes from one pattern to another, and the flow pattern transitions take place (YADIGAROGLU; HETSRONI, 2018). The usual way of presenting these changes in the flow patterns is to plot them on a graph whose axes represent the flow rates of the two phases; an alternative is to plot total mass flux (total mass flow rate divided by total flow area) on one axis, and the mass fraction of the vapor or gas on the other axis (HEWITT; HALL-TAYLOR, 1970).

This graph is a two-dimensional map known as *flow pattern map*, which according to Anumbe (2018), once the abscissa and ordinate coordinates of the map are known, it can help a project engineer, for example, to immediately predict the flow pattern of a system, given its specific conditions.

These maps are generally plotted using data extracted from experimental investigations and can be characterized into two groups: maps based on physical coordinates or maps based on dimensionless groups (TAITEL *et al.*, 1978; HAND; SPEDDING, 1993). Physical coordinates

include quantities such as the superficial and the mixture velocities, mass flow rates, etc. On the other hand, dimensionless coordinates include the Reynolds number, or the Lockhart-Martinelli parameter for example. Several researchers have studied multiphase flow over the years and proposed different sets of parameters or coordinate types. At least three types of coordinates have stood out (ANUMBE, 2018):

- Dimensional Coordinates containing only dimensional parameters such as mass-flow rates or superficial velocities.
- Dimensionless coordinates such as multiphase Reynolds and Weber numbers.
- Mixed coordinates, which are a combination of dimensional and non-dimensional parameters.

Baker (1953) was pioneered in his field and proposed one of the best-known flow pattern maps for horizontal flow, which is widely used in the petroleum industry (MANDHANE *et al.*, 1974; GSCHNAIDTNER, 2014). Figure 10 shows the Baker's map modified by Scott (1964) to broaden the map's boundaries so as to reflect the inherent uncertainty.

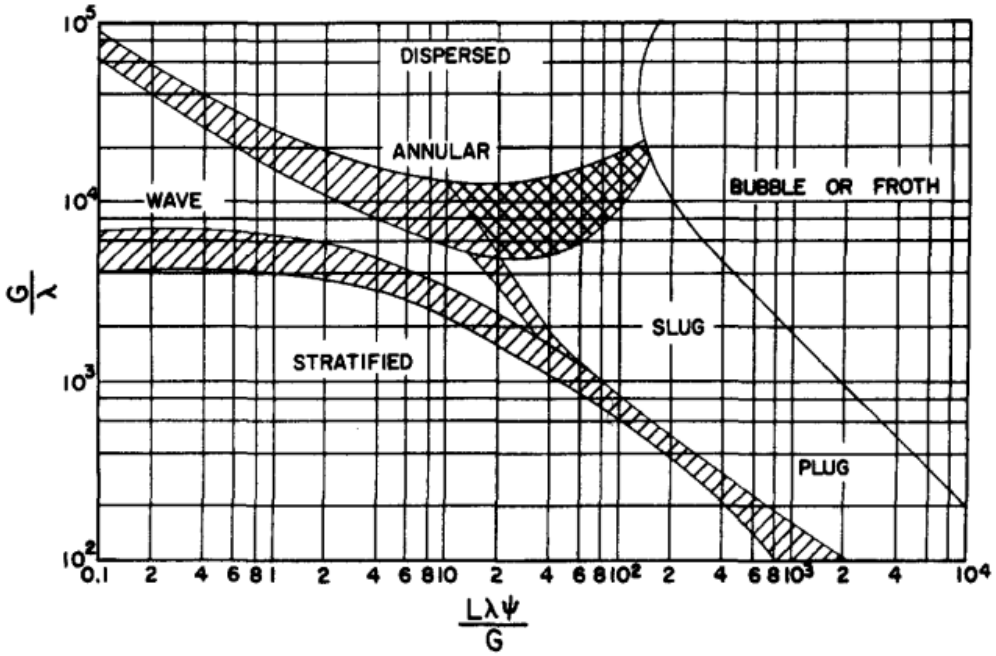

Figure 10 – Modified Baker's map for horizontal flow
Source: Scott (1964)

As an attempt to produce a generic map, Baker (1953) used $\frac{G}{\lambda} \quad vs \quad \frac{L}{G}\lambda\psi$ as coordinates, where L and G are the mass fluxes of the liquid and the gas phases respectively and the parameters λ (Eq. 2.1) and ψ (Eq. 2.2) represent allowances for the fluid physical properties in the given system.

$$\lambda \equiv \left[\frac{\rho_G}{\rho_{air}} . \frac{\rho_L}{\rho_{water}} \right]^{0.5} \tag{2.1}$$

and

$$\psi \equiv \frac{\sigma_{water}}{\sigma} \left[\frac{\mu_L}{\mu_{water}} . \left(\frac{\rho_{water}}{\rho_L} \right)^2 \right]^{2/3} \tag{2.2}$$

Both equations are in the form of ratios of physical properties of the fluids to those of air and water at atmospheric temperature and pressure (HEWITT; HALL-TAYLOR, 1970).

In Baker's map, the horizontal coordinate is dimensionless, whereas the vertical coordinate has dimension of mass flux. This suggests that this map cannot be very general (YADIGAROGLU; HETSRONI, 2018). Indeed, some authors such as Mandhane *et al.* (1974), Spedding and Nguyen (1980), Rouhani and Sohal (1983), and Spedding and Spence (1993) have shown that Baker's map does not correctly predict horizontal flow regime in many situations.

For vertical tubes, Hewitt and Roberts (1969) presented a more generalized map in terms of the momentum fluxes of the phases ($\rho_k U_{sk}^2$). Figure 11 shows the flow pattern map they obtained.

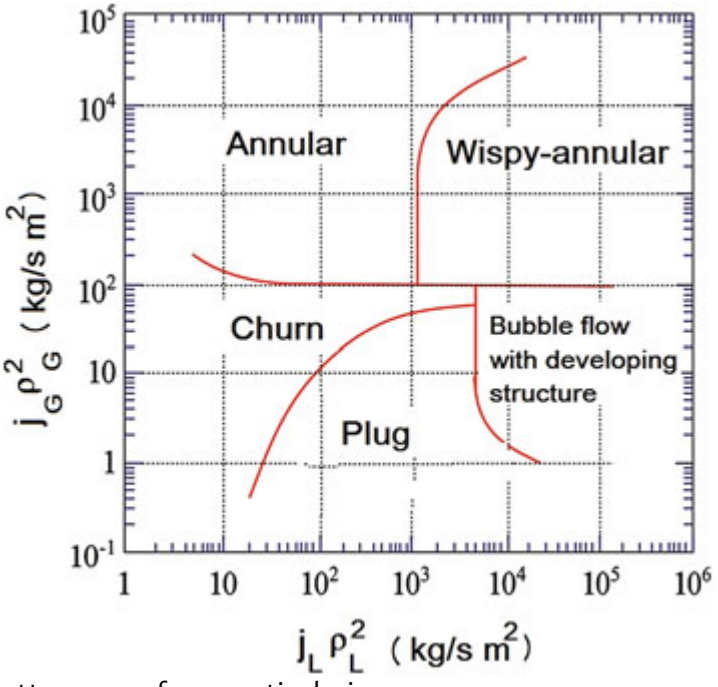

Figure 11 – Flow pattern map for a vertical pipe
Source: Hewitt and Roberts (1969)

According to Yadigaroglu and Hetsroni (2018), this map is still recommended as it fits a reasonably wide range of data for both low and high pressures and with several fluid pairs.

2.3.2.2 Mechanistic Models

For predicting flow pattern transitions, the application of mechanistic models is a very resourceful approach. The mechanistic model involves understanding the behavior of the flow around the boundary region and the identification of the transition mechanism for each pair of flow patterns (TAITEL, 1990).

Unlike the empirical models which often prove inadequate in that they are limited by the range of data on which they were based and, usually, cannot be used with confidence for all kinds of fluids and conditions found in multiphase problems, the mechanistic models produce accurate results for conditions beyond those based on which the model was developed since they are based on the fundamental physics laws (BRILL; ARIRACHAKARAN, 1992; PETALAS; AZIZ, 2000; ANUMBE, 2018).

The earliest realistic mechanistic model for predicting two-phase flow pattern transitions was developed by Taitel and Dukler (1976). Since then, many efforts have been made by several researchers in order to develop physical models that allow the analytical prediction of flow patterns and transition boundaries (ZHAO, 2005). Besides, due to its pioneering and importance, the model proposed by Taitel and Dukler (1976) has been the benchmark for the comparison of all following models (ANUMBE, 2018).

As aforementioned, the analytical[3] methods have been an essential tool in the prediction of flow patterns. However, they have some inherent issues that must be addressed, since the model according to Anumbe (2018):

- **Involves modeling of the transition boundaries:** The model involves the modeling of transition boundaries where transition mechanisms, such as flow velocity, pipe orientation, and shape, etc., are identified for each pair of flow patterns.
- **Has reliability issues:** Results are generally unreliable when the flow conditions are close to the transition boundaries, owing to the fact that the flow structure generally becomes very unstable on the verge of transition from one pattern to another. In addition, the models are based on the assumption that the flow is steady-steady and developed, which

[3] Flow maps and Mechanistic models

is rarely the case in practice (especially) around the boundaries, therefore, experienced designers are usually wary of the reliability of model results near the transition boundaries

- **Requires stability on the flow:** Although rarely achievable in practice, as noted above, there is a requirement that the flow is steady and fully developed for the models to be applied.
- **Requires prior knowledge of flow parameters:** The model can only be used if the flow parameters are previously known. Furthermore, there are also reliability issues for the flow around the transition boundaries between the flow patterns.

2.4 MULTIPHASE FLOW THROUGH AN ANNULUS

In the literature, many studies on two-phase flow in circular cross-sections are available, see sections 2.2 and 2.3. On the other hand, a scarce number of theoretical and/or experimental investigations discussing the two-phase flow through an annulus have been found. Table 1 summarizes the main works for air-water flow in a concentric annulus.

As there are no guarantees that the mathematical correlations developed for pipes still apply to annulus, efforts have been made in recent decades to develop theories concerning this issue; however, most of the works were concerned with determining parameters such as the phase distribution (Furukawa and Sekoguchi (1986), Das *et al.* (2000), and Ozar *et al.* (2008)), the flow pattern transition (Osamusali (1988), Ekberg *et al.* (1999), Sun *et al.* (2004), and Ibarra *et al.* (2019)) , flow pressure drop (Sadatomi *et al.* (1982), Salcudean *et al.* (1983b), Osamusali (1988), Ekberg *et al.* (1999), Wongwises and Pipathattakul (2006), Osgouei *et al.* (2015), and Gschnaidtner (2014)), or void fraction (Salcudean *et al.* (1983a), Ekberg *et al.* (1999), Hibiki *et al.* (2003), Ozar *et al.* (2008), Julia *et al.* (2009), and Gschnaidtner (2014)) through experimental facilities. On the other hand, a few works focus on developing mathematical/empirical relations for predicting flow patterns transitions. The reason is that there is a slight nuance in defining a methodology to describe the so-called wetted perimeter and then modeling the wall shear stress, see Bird *et al.* (2002).

Among the few mechanistic models that predict the transition between flow patterns in a concentric annulus, the works developed by Kelessidis and Dukler (1989), Hasan and Kabir (1992), Filho *et al.* (1992a), Filho *et al.* (1992b), Das *et al.* (1999b), Lage and Time (2000), Ozbayoglu and Omurlu (2007), and Yu *et al.* (2010) consider a unique tube's inclination

Work	Diameter [mm] ID	OD	Orientation	Flow Pattern[a]	Type
Sadatomi *et al.* (1982)	15.0	30.0	Vertical	B/S/A	Experimental
Furukawa and Sekoguchi (1986)	13.0	10.0	Vertical	B/S/C/A	Experimental
Kelessidis and Dukler (1989)	50.8	76.2	Vertical	B/S/C/A	Experimental/ Theoretical
Hasan and Kabir (1992)	48	127	Vertical	B/S/C/A	Experimental/ Theoretical
Filho *et al.* (1992a)	42.2	76.2	Vertical	B/S/C/A	Experimental/ Theoretical
Ekberg *et al.* (1999)	33.2	35.2	Horizontal	B/S/P/C/S/A	Experimental
Das *et al.* (1999a)	12.7	38.1	Vertical	B/S/C	Experimental
Das *et al.* (1999b)	12.7	38.1	Vertical	B/S/C	Theoretical
Lage and Time (2000)	88.9	159.4	Vertical	B/DB/S/C/A	Experimental/ Theoretical
Das *et al.* (2000)	12.7	38.1	Vertical	B/DB/S/C	Experimental
Sun *et al.* (2004)	19.1	38.1	Vertical	B/C	Experimental
Wongwises and Pipathattakul (2006)	8.0	12.5	Inclined	B/DB/C/I/A	Experimental
Ozbayoglu and Omurlu (2007)	88.9	127.0	Horizontal	S/DB/I/A	Theoretical
Ozar *et al.* (2008)	19.1	38.1	Vertical	B/S/C	Experimental
Julia *et al.* (2009)	19.1	38.1	Vertical	B/S/C/A	Experimental
Yu *et al.* (2010)	-	-	Vertical	B/S/C/A	Theoretical
Julia *et al.* (2011)	19.1	38.1	Vertical	S/C/A	Experimental
Mendes *et al.* (2013)	75.0	111.0	Horizontal Inclined Vertical	B/DB/C/A	Experimental
Gschnaidtner (2014)	33.3	51.5	Horizontal	B/I	Experimental
Firouzi *et al.* (2015)	-	-	Vertical	S	Theoretical
Wu *et al.* (2019)	70.0	170.0	Vertical	S/C/A	Experimental

[a] B: Bubble; S: Slug; C: Churn; A: Annular; P: Plug; S: Stratified; DB: Dispersed Bubble; I: Intermittent

Table 1 – Summary of experimental/theoretical works for air-water flow in concentric annulus
Source: Author

(vertical or horizontal), so its use is conditioned to such operational condition.

2.4.1 Flow patterns in an annulus

Since there are several flow pattern definitions available in the literature (ROUHANI; SOHAL, 1983), the definitions presented in this section are exclusively qualitative, although we are aware that investigators usually do not agree about such definitions. Some consensus regarding specific nomenclature for some fundamental flow patterns in pipes might converge but the flow characteristics are substantially different from those flowing through an annulus (ANUMBE, 2018; FILHO *et al.*, 1992a). Figure 12 shows a sketch of the main flow patterns in the concentric annulus analyzed in this work.

For the sake of simplicity, a general definition is given as follows; for further details please refer to the references given below together with the respective flow pattern definition:

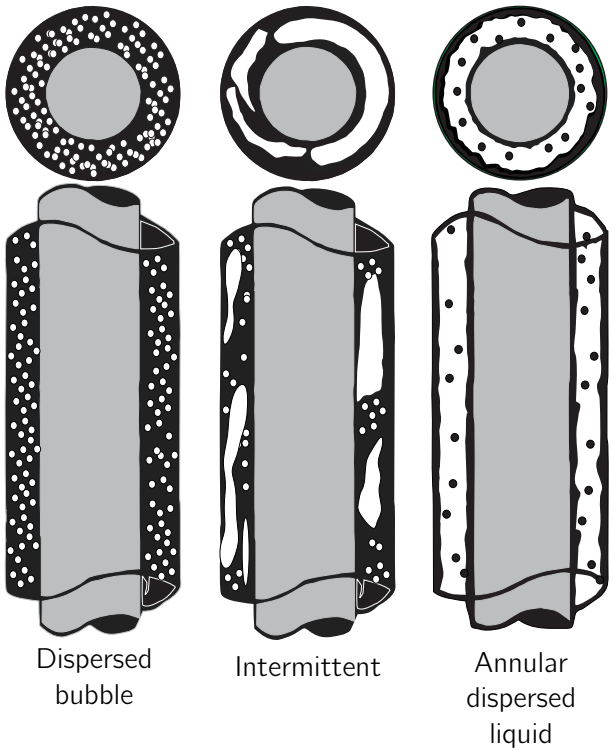

Figure 12 – Sketch of main flow pattern found in annulus. Liquid phase is represented by black color, while gas phase is in white

Source: Author

Stratified Smooth: This flow pattern occurs at low liquid and gas velocities in which the gas plugs coalesce to produce a continuous gas phase. In this pattern, liquid and gas phases flow fully separated by an undisturbed interface, with the liquid at the bottom and the gas at the top of the tube (AL-LABABIDI *et al.*, 2012; YADIGAROGLU; HETSRONI, 2018; HEWITT; HALL-TAYLOR, 1970; De Schepper *et al.*, 2008).

Stratified Wavy: As the gas velocity increases in stratified flow, large surface waves begin to build upon the liquid layer; such waves travel in the flow direction. The amplitude of the waves depends on the relative velocity between the phases and the properties of the fluids (YADIGAROGLU; HETSRONI, 2018; HEWITT; HALL-TAYLOR, 1970; De Schepper *et al.*, 2008).

Intermittent: As the gas velocity increases in the wavy flow pattern, the waves eventually become large. As a consequence, they reach the top of the channel. These waves propagate at high speed and wet the entire surface of the channel, leaving a liquid film covering the surface between successive binding waves (HEWITT; HALL-TAYLOR, 1970).

Annular Dispersed Liquid: As the gas velocity increases still further, the slugs (found in the intermittent flow pattern) become fragmented with a gas core, and the flow becomes

essentially annular with droplets usually dispersed on it. Furthermore, the film formed at the bottom of the channel is thicker than at the top. The liquid film that forms may or may not be continuous around the periphery of the channel (HEWITT; HALL-TAYLOR, 1970; YADIGAROGLU; HETSRONI, 2018).

Dispersed Bubble: Bubbles with a considerably smaller diameter are dispersed in the continuous liquid, even though their concentrations tend to be higher in the upper part of the tube. At a higher velocity, the relative importance of gravity is minor, and the bubbles tend to be more dispersed in the channel, i.e. their concentration is more uniform (YADIGAROGLU; HETSRONI, 2018).

3 FORMULATING THE MECHANISTIC MODEL

3.1 SHEAR STRESS EVALUATION

According to Filho *et al.* (1992b), two major geometrical parameters identify an annulus: the diameter ratio and the degree of eccentricity. The annulus diameter ratio takes into account, to some extent, the flow area and is expressed by Eq.3.1.

$$\kappa = \frac{D_i}{D_o} \tag{3.1}$$

where D_o is the inner diameter of the outer tube (casing), and D_i is the outer diameter of the inner tube (tubing). Similarly, the degree of eccentricity, which takes the displacement between the centers of the inner and outer tubes into account, is given by Eq.3.2.

$$e = \frac{2DBC}{(D_o - D_i)} \tag{3.2}$$

where DBC is the distance between the tube center, and the eccentricity is considered to be equal to zero in this work, if $DBC = 0$.

Bird *et al.* (2002) presented a theory for shear stress in an annulus. This theory is modified herein to take the tube inclination into account (Figure 13). Note that the momentum-flux distribution changes sign at the same value of r for which the velocity profile has a maximum.

By making a momentum balance over a thin cylindrical shell of liquid, Eq.3.3 yields.

$$(2\pi rL\varphi_{rz})\Big|_r - (2\pi rL\varphi_{rz})\Big|_{r+dr} + (2\pi r\Delta r)(\varphi_{zz})\Big|_{z=0} - (2\pi r\Delta r)(\varphi_{zz})\Big|_{z=L} + (2\pi r\Delta rL)W\sin\alpha = 0 \tag{3.3}$$

where $(2\pi rL\varphi_{rz})\Big|_r$ is the rate of z-momentum in, across cylindrical surface r; $(2\pi rL\varphi_{rz})\Big|_{r+dr}$ is the rate of z-momentum out, across cylindrical surface $r + dr$; $(2\pi r\Delta r)(\varphi_{zz})\Big|_{z=0}$ is the rate of z-momentum in, across the annulus surface at $z = 0$; $(2\pi r\Delta r)(\varphi_{zz})\Big|_{z=L}$ is rate the z-momentum out, across the annulus surface at $z = L$; and $(2\pi r\Delta rL)W\sin\alpha$ is the gravity force acting along the z direction in the cylindrical shell.

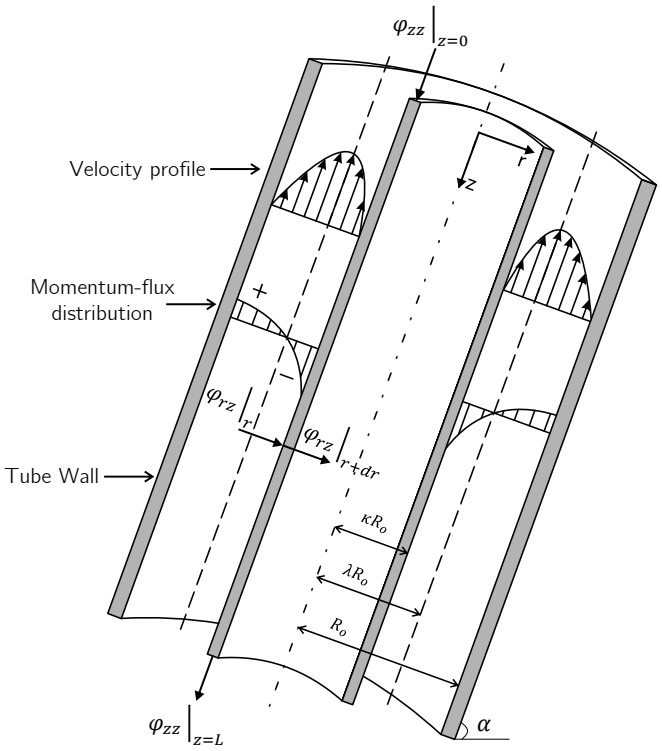

Figure 13 – Momentum-flux distribution and velocity profile in inclined concentric annulus.
Source: Adapted from Bird *et al.* (2002)

By dividing Eq.3.3 by $2\pi L\Delta r$ and taking the $\lim_{\Delta r\to 0}$; Eq.3.3 simplifies to,

$$\lim_{\Delta r\to 0}\left(\frac{(r\varphi_{rz})\Big|_{r+dr}-(r\varphi_{rz})\Big|_{r}}{\Delta r}\right)=r\left(\frac{\varphi_{zz}\Big|_{z=0}-\varphi_{zz}\Big|_{z=L}}{L}+\rho g\sin\alpha\right) \tag{3.4}$$

The expression on the left hand side of Eq.3.4 is the definition of the first derivative of $r\tau_{rz}$ with respect to r. Therefore, Eq.3.4 is rewritten as,

$$\frac{\partial}{\partial r}(r\varphi_{rz})=r\left(\frac{\varphi_{zz}\Big|_{z=0}-\varphi_{zz}\Big|_{z=L}}{L}+\rho g\sin\alpha\right) \tag{3.5}$$

where

$$\varphi_{rz}=\tau_{rz}+\rho v_r v_z=-\mu\frac{\partial v_z}{\partial r}+\rho v_r v_z \tag{3.6}$$

and

$$\varphi_{zz} = p + \tau_{zz} + \rho v_z v_z = p - 2\mu \frac{\partial v_z}{\partial z} + \rho v_z v_z \tag{3.7}$$

The radial velocity $v_r = 0$, so the terms $\rho v_r v_z$ in Eq.3.6 can be neglected. Besides, the longitudinal velocity $v_z = v_z(r)$, hence at both tube edges the terms $\rho v_z v_z$ and $-2\mu \frac{\partial v_z}{\partial z}$, in Eq.3.7 are equal and therefore both terms cancel themselves out. By coupling the, now modified, Eqs.3.6 and 3.7 into Eq.3.5, Eq.3.8 arises.

$$\frac{d}{dr}(r\tau_{rz}) = r\left(\frac{p_0 - p_L}{L} + \rho g \sin\alpha\right) \tag{3.8}$$

By integrating Eq.3.8 twice,

$$\tau_{rz} = \left(\frac{p_0 - p_L}{L} + \rho g \sin\alpha\right)\frac{r}{2} + \frac{N}{r} \tag{3.9}$$

A problem now arises because no information about the momentum flux (τ_{rz}) at the boundary surface ($r = \kappa R$ and $r = R$) is known, hence the constant N in Eq.3.9 cannot be directly determined. However, it is known that the velocity profile has a maximum value at a distance (yet unknown) $r = \lambda r$ from the tube's center and, at this distance, the momentum flux is zero, thus the constant N can now be determined and Eq.3.9 becomes:

$$\tau_{rz} = \frac{\xi R}{2}\left[\left(\frac{r}{R}\right) - \lambda^2\left(\frac{R}{r}\right)\right] \tag{3.10}$$

where $\xi = \left(\frac{p_0 - p_L}{L} + \rho g \sin\alpha\right)$. The constant N is eliminated and another constant (λ) appeared. The advantage of this change is that the geometrical meaning of λ is known (BIRD *et al.*, 2002). Substituting Newton's law of viscosity into Eq.3.10, a differential equation for v_z arises.

$$\frac{dv_z}{dr} = \frac{\xi R}{2\mu}\left[\left(\frac{r}{R}\right) - \lambda^2\left(\frac{R}{r}\right)\right] \tag{3.11}$$

Integrating Eq.3.11:

$$v_z = \frac{-\xi R^2}{4\mu}\left[\left(\frac{r}{R}\right)^2 - 2\lambda^2 \ln\left(\frac{R}{r}\right) + C_2\right] \tag{3.12}$$

Applying the no-slip condition on each surface boundary, i.e. at $r = \kappa R$,$v_z = 0$ and at $r = R$, $v_z = 0$, both constants of integration are found, so Eqs.3.10 and 3.12 become Eqs.3.13 and 3.14, respectively.

$$v_z = \frac{\xi R^2}{4\mu}\left[1 + \frac{(1-\kappa^2)}{\ln(1/\kappa)} \ln\left(\frac{R}{r}\right) - \left(\frac{r}{R}\right)^2\right] \tag{3.13}$$

$$\tau_{rz} = \frac{\xi R}{2}\left[\left(\frac{r}{R}\right) - \frac{(1-\kappa^2)}{2\ln(1/\kappa)}\left(\frac{R}{r}\right)\right] \tag{3.14}$$

Equations 3.13 and 3.14 describe the velocity profile and the momentum flux on an inclined annulus, respectively. Equation 3.14 can be rewritten as.

$$\tau_{rz} = \left(\frac{p_0 - p_L}{L} + \rho g \sin\alpha\right)\frac{R}{2}\left[\left(\frac{r}{R}\right) - \frac{(1-\kappa^2)}{2\ln(1/\kappa)}\left(\frac{R}{r}\right)\right] \tag{3.15}$$

To estimate the pressure drop, it is usual to handle the Moody friction factor, which is defined as (INCROPERA; DEWITT, 2006):

$$f \equiv \frac{-(dP/dx)D}{\rho u_m^2/2} \tag{3.16}$$

where dP/dx is the pressure drop, and u is the phase's mean velocity, Eq.3.16 can be rewritten as:

$$\frac{dP}{dx} \approx \left(\frac{p_0 - p_L}{L} + \rho g \sin\alpha\right) = \frac{-f\rho u_m^2}{2D_h} \tag{3.17}$$

where D_h is the hydraulic diameter defined by Eq.3.18.

$$D_h = D_o - D_i \tag{3.18}$$

The modified gas and liquid shear stresses can be obtained by coupling Eq.3.17 into Eq.3.15.

$$\tau_{WG} = \left(f_G \frac{\rho_G u_G^2}{2} \right) \phi(r) \tag{3.19}$$

$$\tau_{WL} = \left(f_L \frac{\rho_L u_L^2}{2} \right) \phi(r) \tag{3.20}$$

where

$$\phi(r) = \left[\left(\frac{r}{R} \right) - \frac{(1-\kappa^2)}{2\ln(1/\kappa)} \left(\frac{R}{r} \right) \right]$$

3.2 EQUILIBRIUM STRATIFIED FLOW

The analysis is based on the stratified flow pattern condition, i.e. from a condition of stratified liquid, the mechanism that triggers the transition from one flow pattern to another is sought. Considering a smooth, equilibrium stratified flow pattern, Fig.14 schematizes this equilibrium.

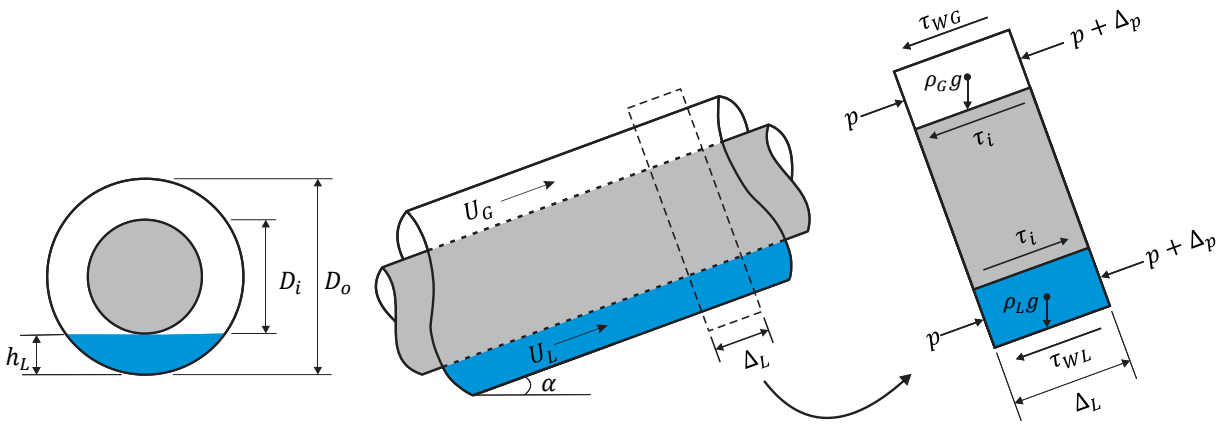

Figure 14 – Stratified liquid level at equilibrium in an annulus; blue represents the liquid phase and white represents the gas phase.

Source: Author

By making a momentum balance for the liquid phase and gas phase, Eqs. 3.21 and 3.22 arrise.

$$-A_L \left(\frac{dP}{dx} \right) - \tau_{WL} S_L + \tau_i S_i + \rho_L A_L g \sin\alpha = 0 \tag{3.21}$$

where A_L is the liquid flow cross-sectional area, dP/dx is the pressure drop, τ_{WL} is the shear stress acting on a tube surface wetted by the liquid, S_L is the perimeter over which the liquid shear stress acts, τ_i is the shear stress at the gas-liquid interface, S_i is the perimeter over which the gas-liquid interface shear stress acts, ρ_L is the density of the liquid, g is the acceleration due to gravity, and α is the inclination between the longitudinal axis and the horizontal plane.

$$-A_G\left(\frac{dP}{dx}\right) - \tau_{WG}S_G - \tau_i S_i + \rho_G A_G g \sin\alpha = 0 \tag{3.22}$$

where A_G is the gas flow cross-sectional area, τ_{WG} is the shear stress acting on a tube surface wetted by the gas, S_G is the perimeter over which the gas shear stress acts, and ρ_G is the gas density. By equating the pressure drop on Eq.3.21 and Eq.3.22, yields:

$$-\tau_{WG}\frac{S_G}{A_G} - \tau_i\frac{S_i}{A_G} + \rho_G g\sin\alpha = -\tau_{WL}\frac{S_L}{A_L} + \tau_i\frac{S_i}{A_L} + \rho_L g\sin\alpha \tag{3.23}$$

Rearranging Eq.3.23:

$$\tau_{WG}\frac{S_G}{A_G} - \tau_{WL}\frac{S_L}{A_L} + \tau_i S_i\left(\frac{1}{A_L} + \frac{1}{A_G}\right) + (\rho_L - \rho_G)g\sin\alpha = 0 \tag{3.24}$$

The gas-liquid interface shear stress is defined by Eq.3.25.

$$\tau_i = f_i\frac{\rho_G(u_G - u_i)^2}{2} \tag{3.25}$$

where f_i is the gas-liquid interface friction factor, u_G and u_i are the gas velocity and the gas-liquid interface velocity, respectively.

Gazley (1948) demonstrated that the gas-liquid friction factor at the interface is approximately equal to the gas-phase friction factor for the stratified smooth flow pattern, that is, $f_i \simeq f_G$. Although the flow patterns considered in this work occur as stratified flow with a wavy interface, the error arising from such an assumption is small (TAITEL; DUKLER, 1976). Therefore, at flow rate conditions required to trigger the flow pattern transition, the gas superficial velocity is greater than the gas-liquid interface one, i.e. $u_G \gg u_i$. As a result, the gas-liquid interface's

shear stress (Eq.3.25) is estimated in the same way as the gas phase shear stress (Eq.3.19). After some simplifications, Eq.3.24 becomes:

$$\tau_{WG}\left(\frac{S_G}{A_G}+\frac{S_i}{A_L}+\frac{S_i}{A_G}\right)-\tau_{WL}\frac{S_L}{A_L}+(\rho_L-\rho_G)g\sin\alpha=0 \tag{3.26}$$

Substituting Eq.3.19 and Eq.3.20 into Eq.3.26.

$$\phi(r)\left(f_G\frac{\rho_G u_G^2}{2}\right)\left(\frac{S_G}{A_G}+\frac{S_i}{A_L}+\frac{S_i}{A_G}\right)-\phi(r)\left(f_L\frac{\rho_L u_L^2}{2}\right)\left(\frac{S_L}{A_L}\right)+(\rho_L-\rho_G)g\sin\alpha=0 \tag{3.27}$$

The liquid and gas friction factor are evaluated from Eqs.3.28 and 3.29, respectively (TAITEL; DUKLER, 1976).

$$f_L=C_L\left(\frac{D_L u_L}{\nu_L}\right)^{-n} \tag{3.28}$$

$$f_G=C_G\left(\frac{D_G u_G}{\nu_G}\right)^{-m} \tag{3.29}$$

where D_L and D_G are the hydraulic diameters of the liquid and gas phase, respectively. Agrawal *et al.* (1973) presented two correlations for the hydraulic diameter of both phases:

$$D_L=\frac{4A_L}{S_L} \tag{3.30}$$

$$D_G=\frac{4A_G}{S_G+S_i} \tag{3.31}$$

Substituting Eqs.3.30 and 3.31 into Eqs.3.28 and 3.29, respectively, and coupling Eqs.3.28 and 3.29 to Eq.3.27, yields:

$$\phi(r)\left[C_L\left(D_L\frac{u_L}{\nu_L}\right)^{-n}\frac{\rho_L u_L^2}{2}\right]\left(\frac{S_L}{A_L}\right)-\phi(r)\left[C_G\left(D_G\frac{u_G}{\nu_G}\right)^{-m}\frac{\rho_G u_G^2}{2}\right]\left(\frac{S_G}{A_G}+\frac{S_i}{A_L}+\frac{S_i}{A_G}\right)-(\rho_L-\rho_G)g\sin\alpha=0 \tag{3.32}$$

It is convenient to change the Eq.3.32 to a dimensionless form; hence the following characteristics scales are used: D_o for length, ${D_o}^2$ for area, u_L^S for the superficial liquid velocity, and u_G^S for the superficial gas velocity. The dimensionless quantities are identified by a tilde ($\sim$), so Eq.3.32 takes the form:

$$X^2\left[(\tilde{u}_L\tilde{D}_L)^{-n}\tilde{u}_L^2\frac{\tilde{S}_L}{\tilde{A}_L}\right]-\left[(\tilde{u}_G\tilde{D}_G)^{-m}\tilde{u}_G^2\left(\frac{\tilde{S}_G}{\tilde{A}_G}+\frac{\tilde{S}_i}{\tilde{A}_L}+\frac{\tilde{S}_i}{\tilde{A}_G}\right)\right]-4Y \tag{3.33}$$

where

$$X^2=\frac{\frac{4C_L}{D_o}\left(\frac{{u_L}^S D_o}{\nu_L}\right)^{-n}\frac{\rho_L({u_L}^S)^2}{2}\phi(r)}{\frac{4C_G}{D_o}\left(\frac{{u_G}^S D_o}{\nu_G}\right)^{-m}\frac{\rho_G({u_G}^S)^2}{2}\phi(r)}=\frac{|(dP/dx)_{L^S}|}{|(dP/dx)_{G^S}|} \tag{3.34}$$

$$Y=\frac{(\rho_L-\rho_G)g\sin\alpha}{\frac{4C_G}{D_o}\left(\frac{{u_G}^S D_o}{\nu_G}\right)^{-m}\frac{\rho_G({u_G}^S)^2}{2}\phi(r)}=\frac{(\rho_L-\rho_G)g\sin\alpha}{\phi(r)|(dP/dx)_{G^S}|} \tag{3.35}$$

In Eqs.3.34 and 3.35, the term $|(dP/dx)^S|$ concerns to the pressure drop of a single-phase, flowing alone along the channel. The parameter X is known as the parameter introduced by Lockhart and Martinelli (1949). Similarly, the parameter Y, equal to zero for a horizontal annulus, refers to the relative forces acting on the liquid in the flow direction due to gravity and pressure drop. This parameter differs from Taitel and Dukler (1976) model by a factor $\phi(r)$; and so this geometrical factor weighs the model.

All dimensionless variables in Eq.3.33 are dependent only on the dimensionless height of the liquid ($\tilde{h}_L$). Appendix A presents all the development of the necessary formulae, and Appendix B presents the results in dimensionless forms. Following Taitel and Dukler (1976), this work adopted the values for the coefficients as follows: $C_G = C_L = 16$, $m = n = 1.0$ for the laminar flow and $C_G = C_L = 0.046$, $m = n = 0.2$ for the turbulent flow.

4 ADAPTING THE TRANSITION CRITERIA FOR AN ANNULUS

4.1 TRANSITION BETWEEN STRATIFIED AND INTERMITTENT OR ANNULAR DISPERSED LIQUID FLOW PATTERNS

The following analysis is made with no distinction between the slug, plug, or elongated bubble flow. Such flow patterns are considered to be different conditions of the intermittent flow pattern.

At flow rate conditions over which intermittent flow occurs, the flow at the tube's inlet is primarily stratified. Hence, as the liquid rate increases, the liquid height rises, forming a wave that grows quickly, blocking the flow of the gas phase (TAITEL; DUKLER, 1976). The blockage forms a competent bridge at a lower gas rate; either slug or plug flow patterns occur in such a condition. As the gas flow rate increases, there is little liquid flowing to keep or, in some cases, even create the liquid bridge; hence, if the gas rate is high enough, the gas flows in the tube center, forming an annular liquid film carrying some liquid droplets. According to Milne-Thomson (1960), the Kelvin-Helmholtz theory establishes the criterion for the formation of infinitesimal amplitude waves generated on a flat sheet between horizontal plates. Such a wave grows if

$$u_G > \left[\frac{g(\rho_L - \rho_G)h_G}{\rho_G}\right]^{1/2} \tag{4.1}$$

where h_G is the distance between the plates. Equation 4.1 can be extend to inclined tubes to give (TAITEL; DUKLER, 1976).

$$u_G > \left[\frac{2(\rho_L - \rho_G)g\cos\alpha(h'_L - h_L)}{\rho_G}\frac{{A'_G}^2}{A_G^2 - {A'_G}^2}\right]^{1/2} \tag{4.2}$$

where h'_L is the liquid height underneath the wave crest, h_L is the liquid height at rest, and A'_G is the gas flow cross-section area over the wave crest. For a small, finite disturbance, ${A_G}'$ may be expanded in terms of A_G as a Taylor series:

$${A_G}' = A_G - \frac{dA_G}{dh_L}(h_L - {h_L}') + O(h_L - {h_L}')^2 \tag{4.3}$$

Ignoring terms of order $(\Delta h_L)^2$ and higher, the criterion for the wave growth becomes

$$u_G > C\left[\frac{(\rho_L - \rho_G) g \cos\alpha}{\rho_G} \frac{A_G}{dA_L/dh_L}\right]^{1/2} \tag{4.4}$$

where A_G is found in Appendix A. According to Taitel and Dukler (1976), the constant C is estimated as,

$$C = 1 - \frac{h_L}{D_o} \tag{4.5}$$

Equations 4.4 and 4.5 describe the criterion for the transition in an annulus from a stratified to intermittent or from stratified to annular dispersed liquid flow pattern. In dimensionless form, the criterion becomes

$$F^2\left[\frac{1}{C^2}\frac{\tilde{u}_G d\tilde{A}_L/d\tilde{h}_L}{\tilde{A}_G}\right] \geq 1 \tag{4.6}$$

where F is the Froude number, modified by the density ratio and is given by Eq.4.7.

$$F = \sqrt{\frac{\rho_G}{(\rho_L - \rho_G)}} \frac{{u_G}^S}{\sqrt{D_o g \cos\alpha}} \tag{4.7}$$

The term $\frac{d\tilde{A}_L}{d\tilde{h}_L}$ is found in Appendix B.

4.2 TRANSITION BETWEEN INTERMITTENT AND ANNULAR DISPERSED LIQUID FLOW PATTERNS

The criterion for finite wave formation/growing in the stratified liquid is presented in Eq.4.6. Two events may occur while the wave grows: if the liquid in the film is large enough to supply the liquid required to establish a stable slug, the slug flow pattern occurs. Otherwise, if the liquid height is insufficient, the wave is swept around the wall, forming either annular or annular mist flow patterns. Consequently, intermittent or annular flow patterns are developed exclusively by the liquid height present in the equilibrium stratified flow. In other words, if the liquid height is above the center-line of the annulus (i.e. for $\frac{h_L}{D_o} > 0.5$), intermittent flow

occurs. On the other hand, if $\frac{h_L}{D_o} < 0.5$, annular dispersed liquid results (TAITEL; DUKLER, 1976). Other authors have reported small values for $\frac{h_L}{D_o}$ (BARNEA *et al.*, 1982; OZBAYOGLU; OMURLU, 2007). However, in this work we used a value of 0.5 to mark the transition.

In light of the fact that the transition occurs at a constant value of $\frac{h_L}{D_o} = 0.5$, a unique value of X defines the change in the flow pattern for any value of Y, as demonstrated in Fig.15. For horizontal tubes ($Y = 0$), the value of $X = 1.15$ is found and it is plotted as a solid line in Fig.22, as boundary B, while for $Y = 100$ and $Y = 1000$, a value of $X = 49.84$ and $X = 498.40$ are found, respectively.

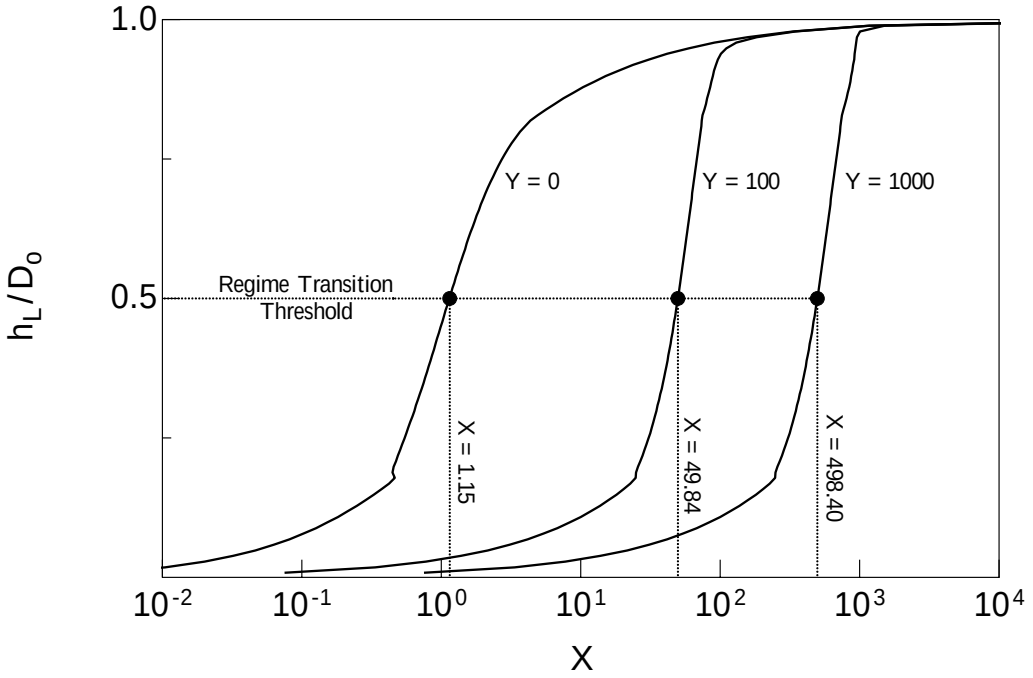

Figure 15 – The procedure for obtaining the Lockhart-Martinelli parameter, X (Eq. 3.34), from the flow pattern transition threshold, $h_L/D_o = 0.5$, for several inclinations parameters, Y (Eq. 3.35).

Source: Author

4.3 TRANSITION BETWEEN STRATIFIED SMOOTH AND STRATIFIED WAVY FLOW PATTERNS

At this flow pattern transition, the gas flow causes waves under a condition at which the velocity of the gas is just enough to produce waves but slower than that needed for the rapid wave growth required to either intermittent or annular flow patterns to occur. Hence, the transition mechanism is associated with the minimum velocity of the gas required to trigger and maintain

the wave. Jeffreys (JEFFREYS; TAYLOR, 1925; JEFFREYS, 1926) postulated such a criterion for wave generation, considering a non-accelerating flow; he derived the following equation:

$$(u_G - c)^2 c > \frac{4\nu_L g(\rho_L - \rho_G)}{s\rho_G} \tag{4.8}$$

where c is the velocity of the wave, ν_L is the kinetic viscosity of the liquid phase, and s is the sheltering coefficient. Jeffreys (JEFFREYS; TAYLOR, 1925; JEFFREYS, 1926) suggested a value for the sheltering coefficient of about 0.3; however, other authors suggested much smaller values of around 0.01 to 0.03 (OSAMUSALI, 1988; TAITEL; DUKLER, 1976; BENJAMIN, 1959). In this work, a value of 0.01 was considered to be appropriate. At the flow conditions in which the transition takes place, $u_G \gg c$, therefore the term in the parentheses on the left hand side of Eq.4.8 is approximately u_G. Hence, Eq.4.8 becomes

$$u_G \geq \left[\frac{4\nu_L(\rho_L - \rho_G)g\cos\alpha}{s\rho_G u_L}\right]^{1/2} \tag{4.9}$$

Equation 4.9 describes the criterion for the transition in the annulus from stratified smooth to stratified wavy flow pattern. In dimensionless form, the criterion becomes

$$K \geq \frac{2}{\sqrt{\tilde{u}_L \tilde{u}_G \sqrt{s}}} \tag{4.10}$$

where K is equal to the product of the square root of the superficial Reynolds number of the liquid to the modified Froude number (Eq.4.7),

$$K^2 = {Re_L}^s F^2 = \left[\frac{D{u_L}^s}{\nu_L}\right]\left[\frac{\rho_G({u_G}^s)^2}{(\rho_L - \rho_G)D_o g\cos\alpha}\right] \tag{4.11}$$

4.4 TRANSITION BETWEEN INTERMITTENT AND DISPERSED BUBBLE FLOW PATTERNS

At the flow conditions in which intermittent (slug or plug) flow patterns occur, the elongated bubble is formed and flows over the liquid surface due to the buoyancy effects. By increasing the liquid flow rate to levels higher than those found in the intermittent flow pattern, the gas

phase tends to mix with the fast-flowing liquid phase, forming dispersed gas bubbles in the liquid phase. According to Levic *et al.* (1962), the force due to the turbulence is estimated as:

$$F_T = \frac{1}{2}\rho_L u_L \left(\frac{f_L}{2}\right)^{1/2} \tag{4.12}$$

where f_L is given by Eq.3.28. According to Taitel and Dukler (1976), the buoyancy force per unit length of the gas region is estimated as:

$$F_B = g\cos\alpha(\rho_L - \rho_G)A_G \tag{4.13}$$

The transition occurs when the turbulent fluctuations in the liquid phase are strong enough to overcome the buoyancy force[4], i.e. $F_T \geq F_B$.

$$\frac{1}{2}\rho_L u_L \left(\frac{f_L}{2}\right)^{1/2} \geq g\cos\alpha(\rho_L - \rho_G)A_G \tag{4.14}$$

Equation 4.14 may be rearranged, thus the criterion to transition in the annulus from intermittent to dispersed bubble flow pattern yields:

$$u_L \geq \left[\frac{4A_G}{S_i}\frac{g\cos\alpha}{C_L\left(\frac{4A_L}{S_L}\frac{u_L}{\nu_L}\right)^{-n}}\left(1 - \frac{\rho_G}{\rho_L}\right)\right]^{1/2} \tag{4.15}$$

In dimensionless form, Eq.4.15 becomes

$$T^2 \geq \frac{8\tilde{A}_G}{\tilde{S}_i\tilde{u}_L^2(\tilde{u}_L\tilde{D}_L)^{-n}} \tag{4.16}$$

where

$$T = \left[\frac{\frac{4C_L}{D_o}\left(\frac{{u_L}^S D_o}{\nu_L}\right)^{-n}\frac{\rho_L {u_L}^{S2}}{2}}{(\rho_L - \rho_G)g\cos\alpha}\right]^{1/2} = \left[\frac{|(dP/dx)_{L^S}|}{(\rho_L - \rho_G)g\cos\alpha}\right]^{1/2} \tag{4.17}$$

[4] The buoyancy force tends to maintain the bubbles over the liquid surface

Table 2 shows the all developed equations for transition between one flow pattern to another.

Table 2 – Sumarry of the flow pattern transition equations

Transition	Dimensional Equation	Dimensionless Equation
Equilibrium Stratified Flow	$\phi(r)\left(f_G\frac{\rho_G u_G^2}{2}\right)\left(\frac{S_G}{A_G}+\frac{S_i}{A_L}+\frac{S_i}{A_G}\right)$ $-\phi(r)\left(f_L\frac{\rho_L u_L^2}{2}\right)\left(\frac{S_L}{A_L}\right)$ $+(\rho_L-\rho_G)g\sin\alpha=0$	$X^2\left[(\tilde{u}_L\tilde{D}_L)^{-n}\tilde{u}_L^2\frac{\tilde{S}_L}{\tilde{A}_L}\right]-\left[(\tilde{u}_G\tilde{D}_G)^{-m}\tilde{u}_G^2\left(\frac{\tilde{S}_G}{\tilde{A}_G}+\frac{\tilde{S}_i}{\tilde{A}_L}+\frac{\tilde{S}_i}{\tilde{A}_G}\right)\right]-4Y$
SS/I or SS/AD	$u_G > C\left[\frac{(\rho_L-\rho_G)g\cos\alpha}{\rho_G}\frac{A_G}{dA_L/dh_L}\right]^{1/2}$	$F^2\left[\frac{1}{C^2}\frac{\tilde{u}_G d\tilde{A}_L/d\tilde{h}_L}{\tilde{A}_G}\right]\geq 1$
I/AD[a]	$X=1.15$	[-]
SS/SW	$u_G \geq \left[\frac{4\nu_L(\rho_L-\rho_G)g\cos\alpha}{s\rho_G u_L}\right]^{1/2}$	$K\geq\frac{2}{\sqrt{\tilde{u}_L\tilde{u}_G\sqrt{s}}}$
I/DB	$u_L \geq \left[\frac{4A_G}{S_i}\frac{g\cos\alpha}{C_L\left(\frac{4A_L}{S_L}\frac{u_L}{\nu_L}\right)^{-n}}\left(1-\frac{\rho_G}{\rho_L}\right)\right]^{1/2}$	$T^2\geq\frac{8\tilde{A}_G}{\tilde{S}_i\tilde{u}_L^2(\tilde{u}_L\tilde{D}_L)^{-n}}$

[a] This transition takes place at a constant value

Source: Author

5 RESULTS AND DISCUSSION

5.1 MODEL VERIFICATION

To demonstrate the reliability of the present model, it was confronted against two inclination scenarios: horizontal and vertical.

For the horizontal scenario (Fig.16), the present model was compared with the experimental data from Gschnaidtner (2014) - Fig.16 (a) - for co-current gas-liquid flow through a horizontal concentric annulus of $D_o = 51.5mm$ and $D_i = 33.3mm$ and from Ekberg *et al.* (1999) - Fig.16 (b) - for co-current gas-liquid flow through a horizontal concentric annulus of $D_o = 35.2mm$ and $D_i = 33.2mm$. Both works were performed at atmospheric pressure and room temperature $(25°C)$.

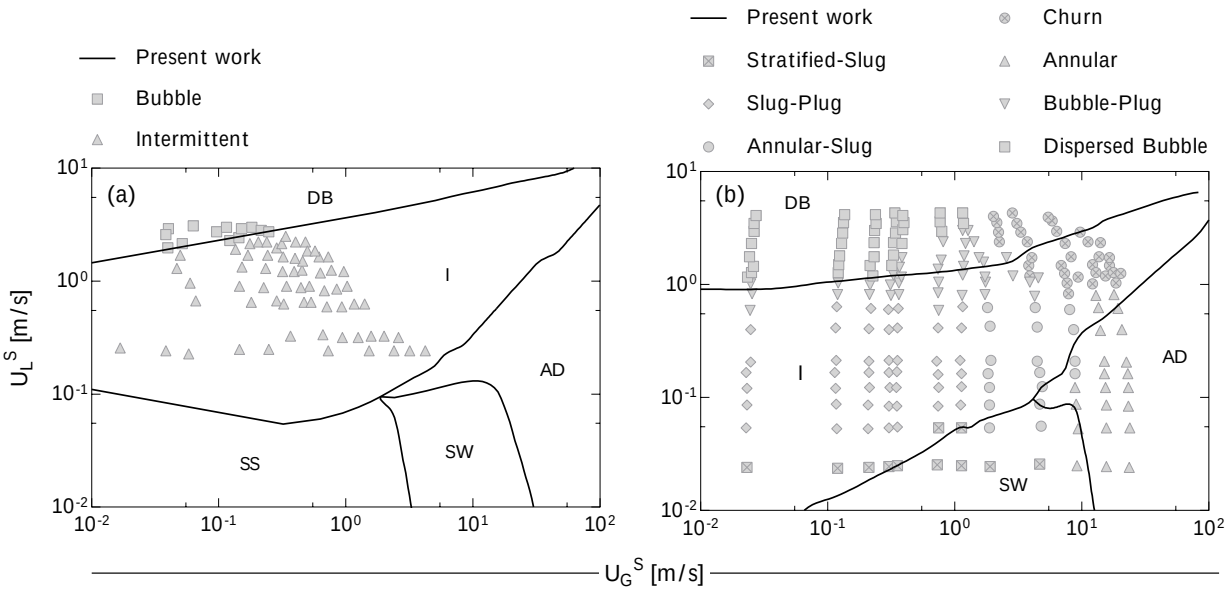

Figure 16 – Comparison between the present model with: (a) Gschnaidtner's work for co-current gas-liquid flow through a horizontal concentric annulus; (b) Ekberg et al. work for co-current gas-liquid flow through a horizontal concentric annulus. Both works were performed at atmospheric pressure and room temperature $(25°C)$.

Source: Author

When compared with the experimental data from Gschnaidtner (2014), the present model presents a very satisfactory performance since an excellent agreement exists between the experimental data and the theoretically predicted boundaries (solid lines), while, for the experimental data from Ekberg *et al.* (1999) the model also achieved a satisfactory performance, except for the churn flow pattern at high superficial liquid velocities. Yu *et al.* (2010) also

observed discrepancies in the churn flow pattern for high liquid velocities, when confronting their flow pattern prediction model for an upward vertical annulus with experimental data. They suggested that the transition to such a pattern appears to happen at a lower superficial gas velocity than the model predicts.

For the vertical scenario (Fig.17), the present work (solid line) was compared against two mechanistic models: the model from Kelessidis and Dukler (1989) (dashed line) and the model from Filho *et al.* (1992a) (dash-dotted line).

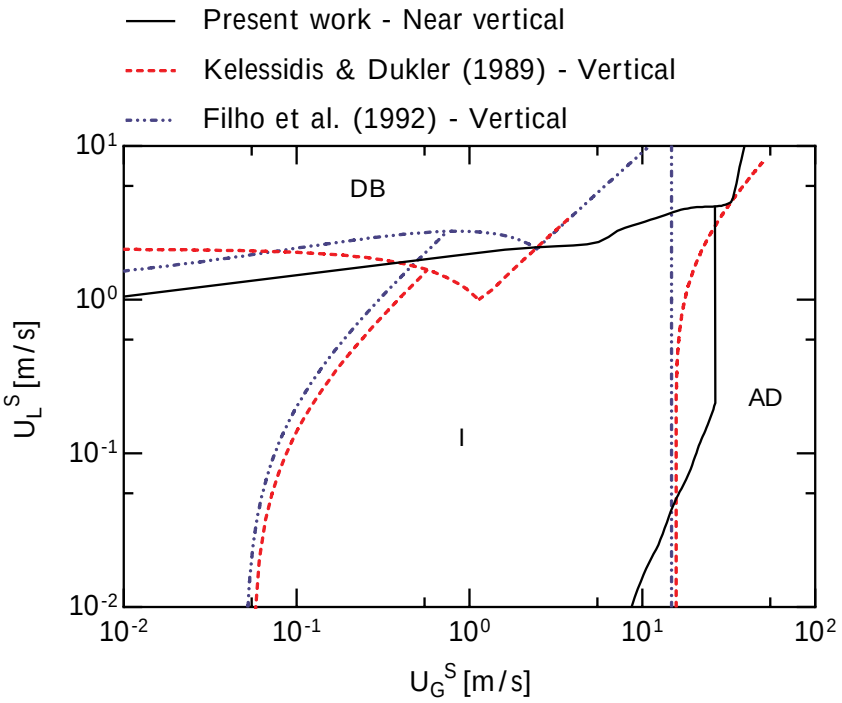

Figure 17 – Comparison between the present model (solid line) and the co-current gas-liquid flow through a vertical concentric annulus model from Kelessidis and Dukler (1989) (dashed line) and Filho *et al.* (1992a) (dash-dotted line). Note that the transition between the slug/churn flow patterns is predicted by the Kelessidis and Dukler (1989) and Filho *et al.* (1992a) models. However, these flow patterns are considered as a single pattern (intermittent pattern) in the present model.

Source: Author

All three models were evaluated under the same condition, i.e. an annulus of $D_o = 116.6mm$ and $D_i = 75mm$ and properties of the fluids at atmospheric pressure and temperature of $25°C$.

As one can see, there is good agreement between the three models; however, the transition to the annular flow pattern presents a more significant difference between the three models. The proposed model admits (for high liquid phase velocities) a higher gas-phase threshold velocity;

however, with a decrease in the liquid phase velocity, the threshold velocity decreases in a linear manner, which is to be expected since low velocities of liquid need low gas velocities to remain on the periphery of the tube.

When confronting the transition between the intermittent and dispersed bubble flow patterns, all three models present minor divergences from each other for low superficial gas velocities.

5.2 OVERALL RESULTS

The following results are presented according to the four sections shown in Fig.18.

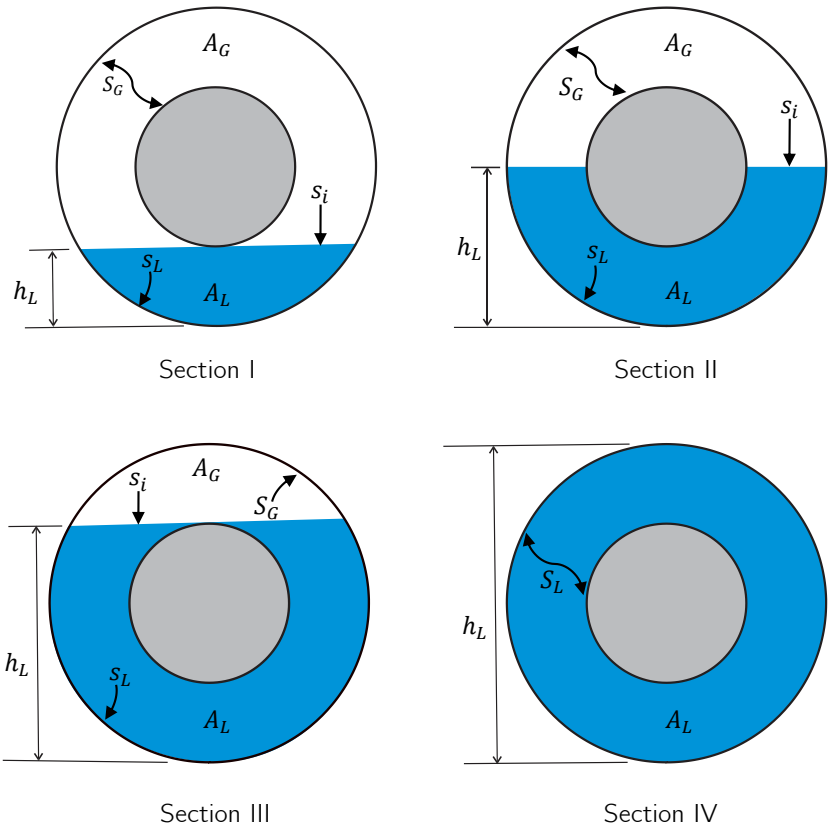

Figure 18 – Geometrical parameters and sections of an annulus dependent on the liquid height
Source: Author

Each section depends on the liquid height inside the tube. The section I is valid for $0 \leq h_L \leq r_o - r_i$; the section II is valid for $r_o - r_i \leq h_L \leq r_o$; the section III is valid for $r_o \leq h_L \leq r_o + r_i$; and the section IV is valid for $r_o + r_i \leq h_L \leq 2r_o$.

For all operational conditions (i.e. tube size, fluid properties, inclinations, and flow rates in which stratified flow patterns might exist), Eq.3.34 and Eq.3.35 assume a unique value of $\frac{h_L}{D_o}$. Therefore, Eq.3.33 can be plotted as a two-dimensional map for different values of Y. Figure

19 presents the solutions for turbulent flow of both phases (solid curves) and turbulent liquid with laminar gas flow (dotted curves[5]).

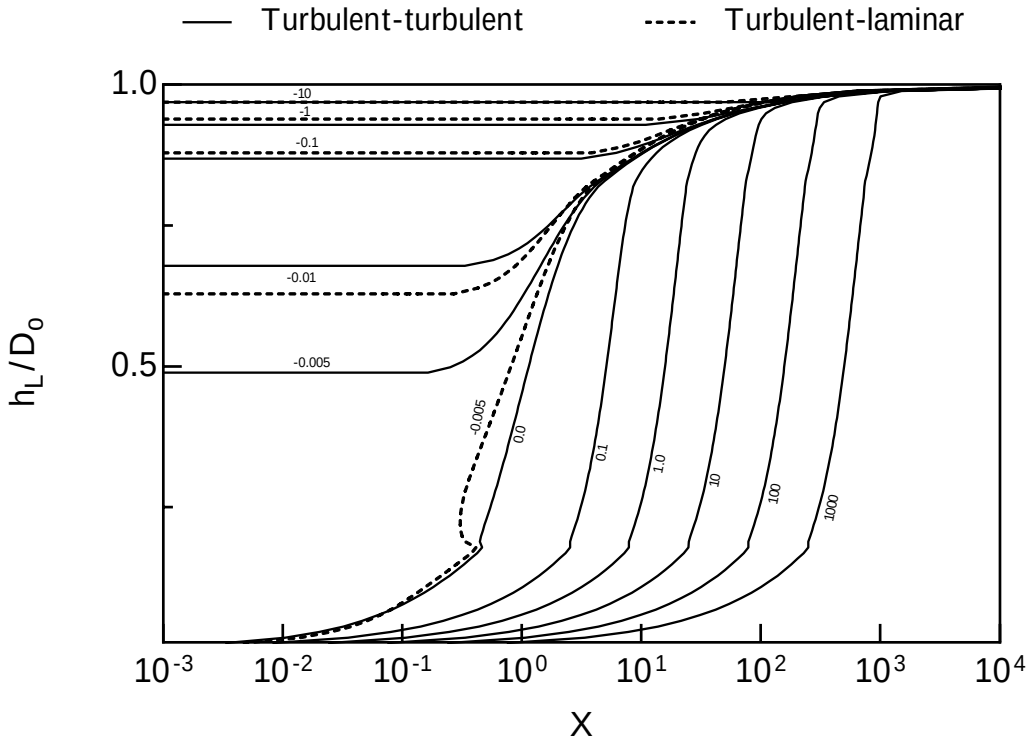

Figure 19 – Equilibrium liquid level for stratified flow with different dimensionless inclination parameter (Y). The solid curves are for the turbulent flow of both the liquid and gas phase, whereas the dotted curves are for turbulent flow in the liquid phase and laminar flow in the gas phase

Source: Author

The solution for the laminar-turbulent case is quite close to the turbulent-turbulent case curve for all scenarios except the dotted curve of $Y = 0.005$. Furthermore, in general, all curves for $Y \geq 0$ show a growth behavior marked by the four sections (see Fig.21).

For sections I and IV, in which the behavior resembles a pipe, the response is similar to the results obtained by Taitel and Dukler (1976), as expected. On the other hand, for sections II and III, which is the inner-tube region of influence, the curve presents an accentuated growth. For positive Y parameter curves, from section I to section II, there is an evident change in inclination, and a prominent corner - critical point (DEMIDOVICH, 1970). A critical point in the negative Y parameter curves is not observed in any section's transition, except for the $Y = -0.005$, which is close to zero; therefore, a behavior similar to the horizontal curve

[5] The turbulent-laminar case can occurs for transitions at low gas rate.

$(Y = 0)$ is expected.

Figure 20a and 20b show the equilibrium stratified flow surface for different combinations of gas and liquid superficial velocities in a pipe of $D_o = 116.6mm$ and an annulus of $D_o = 116.6mm$ and $D_i = 75mm$. Both surfaces are for $Y = 0$. The surface is obtained by iteratively solving Eq.3.32. Note that, as the superficial gas velocity increases, the dimensionless liquid height (h_L/D_o) required to maintain the stratified flow at equilibrium increases.

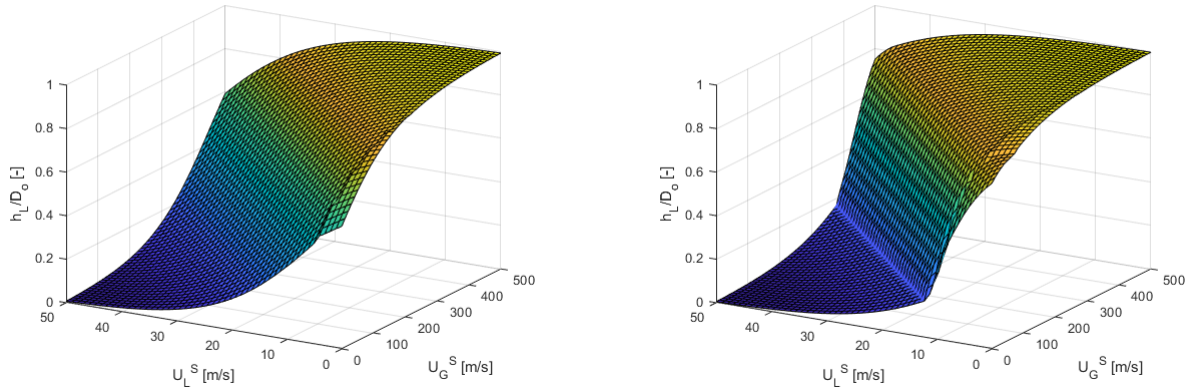

(a) Pipe (b) Annulus

Figure 20 – Surface of equilibrium stratified flow varying the superficial velocity of the gas and liquid for: a) pipe of $D_o = 116.6mm$ b) annulus of $D_o = 116.6mm$ and $D_i = 75mm$. Fluid properties at $25°C$ and 1 atm.

Source: Author

As expected, the growth behavior presented in Fig.19 is again observed in Fig.20, on the inner-tube region of influence. In addition, comparing both surfaces, one observes an evident change on the surface inclination of Fig.20b at ${U_L}^S \approx 20$ m/s and ${U_G}^S \approx 100$ m/s. This change takes place precisely in $\frac{h_L}{D_o} = 1 - \kappa$, which is the bottom of the inner tube. A less abrupt change takes place in $\frac{h_L}{D_o} = 1 + \kappa$ (top of inner tube). Hence, the inner-tube region of influence ranges from $1 - \kappa \leq \frac{h_L}{D_o} \leq 1 + \kappa$.

To expand the analysis, the derivative of the curve for $Y = 10$ was calculated and Fig.19 presents the corresponding curve. The other curves in Fig.7 present similar behavior.

The curve is divided into four sections (see Fig.18), corresponding to the liquid height in the annulus: the blue zone presents the results for $0 \leq h_L \leq r_o - r_i$; the red zone corresponds to the solution for $r_o - r_i \leq h_L \leq r_o$; the green zone shows the results for $r_o \leq h_L \leq r_o + r_i$; and the purple zone presents the solution for $r_o + r_i \leq h_L \leq 2r_o$.

From the bottom of the outer tube to the threshold height of $r_o - r_i$ (blue zone), the area

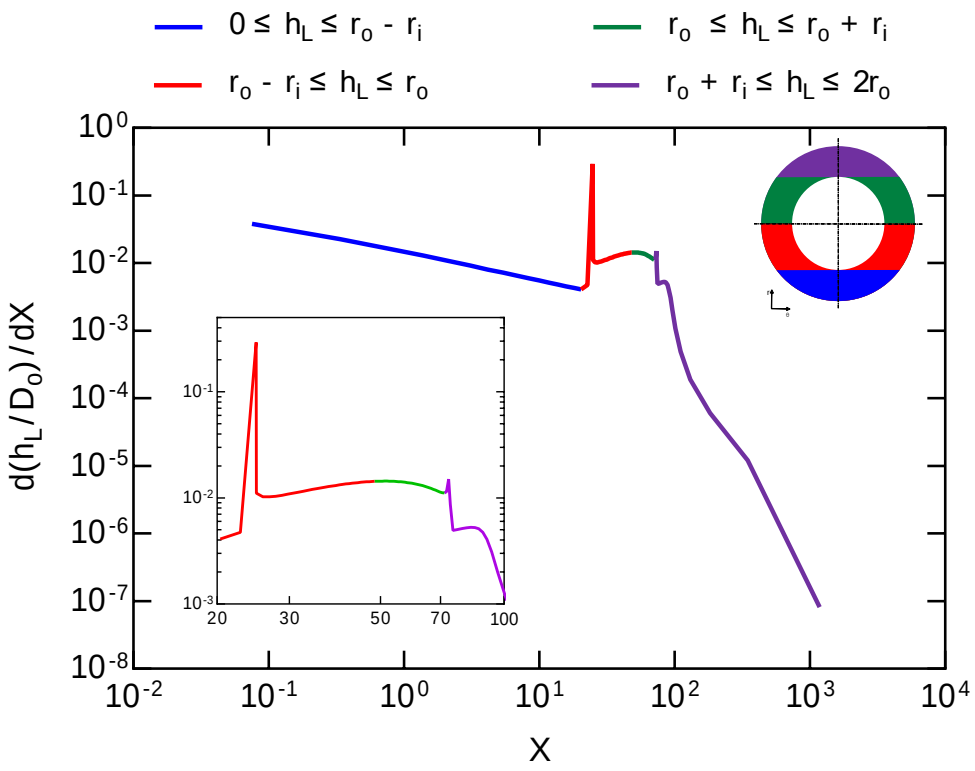

Figure 21 – Variation of dimensionless liquid level with the Lockhart-Martinelli (Eq. 3.34) parameter for the equilibrium's curve $Y = 10$. Each color represents a section into tube's height.

Source: Author

filled by the liquid shows a constant growth, so its derivative has an almost constant behavior, as shown by the blue section. From the bottom of the inner tube to the tube center (red zone), the liquid area's growth trend is influenced by the presence of the inner tube, resulting in the peak found at the beginning of the red curve ($\frac{h_L}{D_o} = 1 - \kappa$). As the liquid height increases, the influence of the inner tube and the consequent instability caused by it is attenuated. As a result, the curve recovers the asymptotic behavior.

There is no abrupt change from the center to the top of the inner tube (green zone) as in the previous transition, since the area filled by the liquid remains constant. Consequently, the presence/influence of the inner tube on the liquid height growth trend gradually decreases. Because of the lack of influence of the inner tube in the purple zone, the curve behaves as a pipe. However, there is a peak in the curve at ($\frac{h_L}{D_o} = 1 + \kappa$), with a smaller amplitude than at ($\frac{h_L}{D_o} = 1 - \kappa$) since it is more abrupt.

As seen in Fig.21, the change between the red-green sections is notoriously better-behaved

and defined, thus is is suggested that such zones can be observed as a single one. Therefore, rather than using four sets of equations (see Appendix A), one can use only three. Hence, the formulations proposed in Appendix A, which were developed as a function of h_L or h_G, were reworked and it is proposed to use two angles (that we called β and θ) to calculate all the necessary equations used in Section 4. Further details are given in Appendix C.

The generalized flow pattern map for horizontal tubes ($Y = 0$) is presented in Fig.22. The solid curves are the transition map for the annulus and the dotted curves are the transition map proposed by Taitel and Dukler (1976).

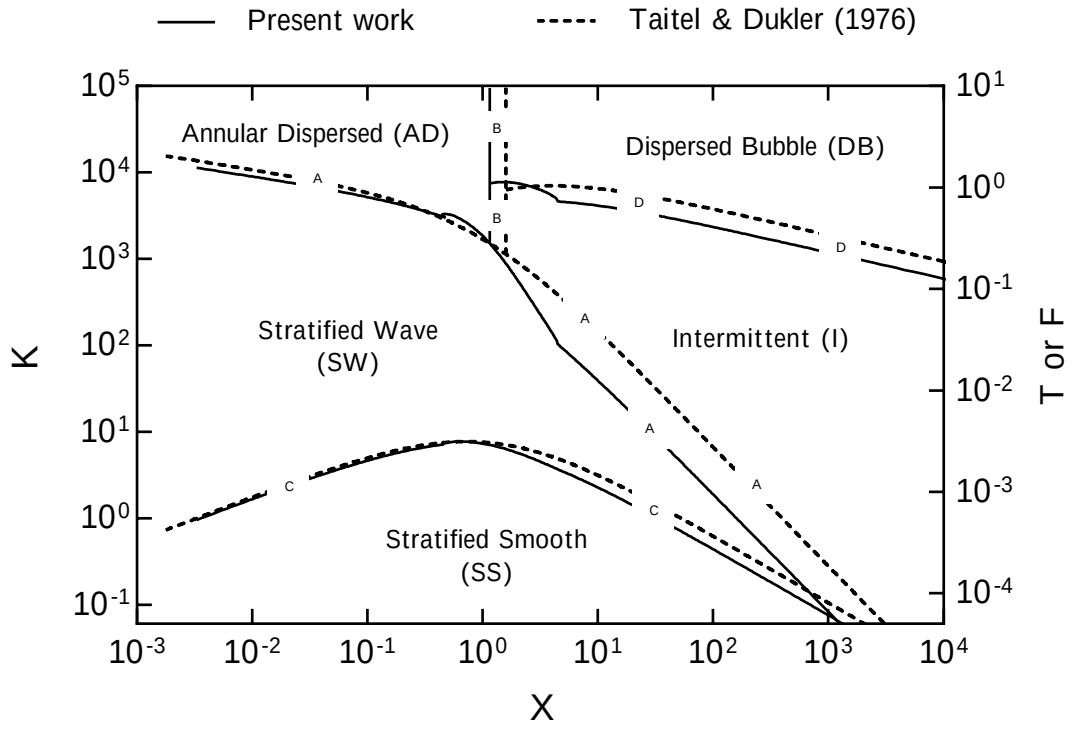

Figure 22 – Comparison between the present work and the Taitel and Dukler (1976) model for the generalized flow pattern map for horizontal gas-liquid flow. Each boundary between a two phase flow pattern to another is marked by a letter. The solid curves are for an annulus of 116.6 mm outer tube diameter and $75mm$ inner tube diameter. The dotted line is for a pipe of $116.6mm$. Fluid properties at $25°C$ and 1 atm

Source: Author

Curve A represents the transitions between stratified (S) and intermittent (I) or annular-dispersed liquid (AD) flow patterns; the curve is plotted in X vs. F coordinates. The $X - F$ ordered pairs are all the values that satisfy Eq.4.6, showing that finite-sized waves grow and tend to block or sweep around the tube as a result between the imbalance of the force generated

by the Bernoulli effect and the weight force acting on the wave. Therefore, every single value of X on the left-hand side of the curve represents conditions under which stratified flow patterns exist (TAITEL; DUKLER, 1976).

Curve B stipulates the transitions between annular dispersed liquid (AD) and intermittent (I) or a dispersed bubble (DB) flow pattern. The transition takes place at a constant value of X, which indicates that the growing waves need a minimum liquid supply in order to form a slug, which only occurs for $h_L/D_o \geq 0.5$.

Curve C delimits the transitions between stratified wavy (SW) and stratified smooth (SS) flow patterns; the curve is plotted in X vs. K coordinates. The $X - K$ ordered pairs are all the values that satisfy Eq.4.10, which is based on the assumption that the wave creation model made by Jeffreys (JEFFREYS; TAYLOR, 1925; JEFFREYS, 1926) is valid. Hence, values of K lower than curve C have a poor gas flow, even too low to form a wave.

Curve D specifies the transitions between dispersed bubble (DB) and intermittent (I) flow pattern, it lays in the $X - T$ plane and locates the $X - T$ ordered pair that satisfies Eq.4.16, which identifies the conditions where the buoyant force becomes equal to the turbulent fluctuations. Consequently, values of T below the curve D do not sustain the gas mixed into the liquid phase because of the little turbulence, and therefore the elongated gas bubbles flow pattern takes place (TAITEL; DUKLER, 1976).

Following the results presents in Fig.22, the difference in the behavior of the curves is noticeable between a scenario with a circular tube (dotted curve) to a scenario with an annulus (solid curve). For instance, for curve A, it is observed more predominantly the influence of the inner tube because of a change (critical point) in the inclination from around $X = 0.45$ to $X = 4.50$. For curve B, the transition changes from $X = 1.5$ for the circular scenario to $X = 1.15$ for the annulus one, i.e. the value of the Lockhart-Martinelli parameter for $\frac{h_L}{D_o} = 0.5$ and horizontal tube ($Y = 0$) decreases. For curve C, few differences are observed between both scenarios. For curve D, one observes a more direct influence of the inner tube as curve A. However, since curve D defines the transition to a pattern that is only observed for values of $\frac{h_L}{D_o} \geq 0.5$, the curve has only one critical point, at approximately $X = 4.5$.

During the development of these criteria, no tube wall's roughness was considered. The generalized flow map presented in Fig.22 was rebuilt with ${u_L}^S - {u_G}^S$ coordinates for an air-water system at $25°C$ and 1 atm pressure for a horizontal annulus of $116.6mm$ outer

diameter and $75mm$ inner diameter and a pipe of $116.6mm$. Once all dimensionless variables (F, X, K, and T) are fixed at the transitions boundaries, they are all expressed as a function of the superficial velocities of the liquid and gas. The result is presented in Fig.23, where the solid curves show the prediction for the theory developed herein, and the dotted curves represent the results for the theory developed by Taitel and Dukler (1976).

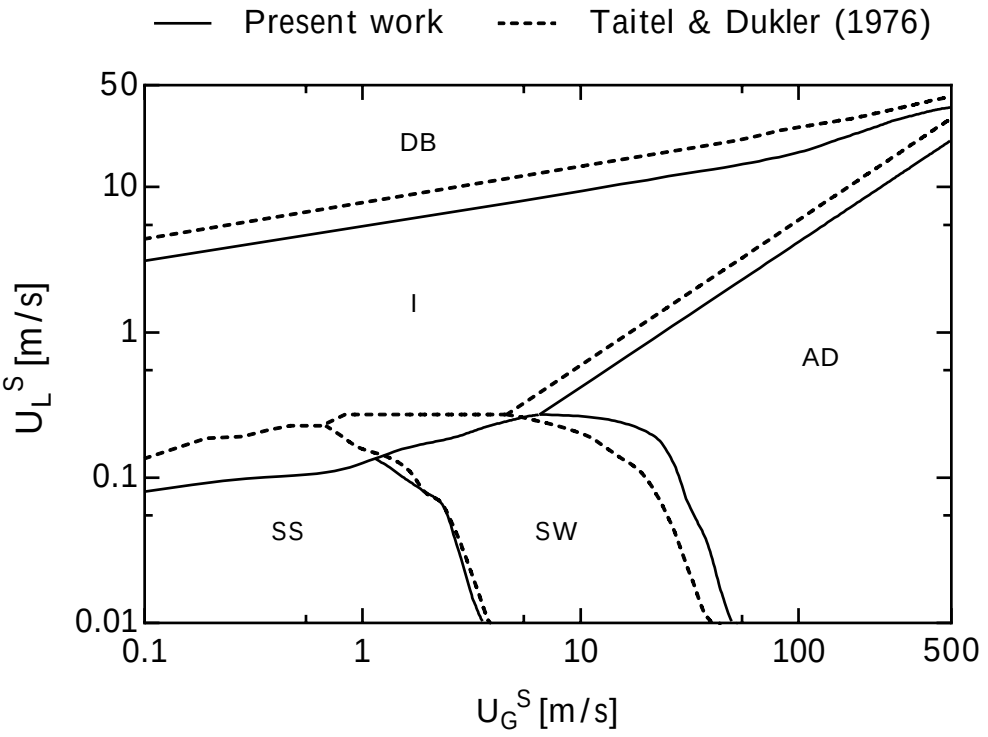

Figure 23 – Comparison between the present work and the Taitel and Dukler (1976) model for the superficial velocity map. Air-Water at $25°C$ and 1 atm for an annulus of $116.6mm$ outer diameter and $75mm$ inner diameter, and a pipe of $116.6mm$ diameter.

Source: Author

As expected, the curves changed as they derive from the results obtained in Fig.22. The threshold value of the superficial gas velocity in the transition between the intermittent flow pattern and the stratified smooth or wavy pattern had a slight drop. Minor differences were observed in the transition between stratified smooth and stratified wavy patterns. The transition curve between the stratified wavy and annular dispersed liquid flow pattern had a left shift, increasing the threshold value of the transitional superficial liquid velocity. The transition between annular dispersed liquid and intermittent flow patterns and the transition between intermittent and dispersed bubble flow patterns decreased, which in turn decreased the threshold value of the superficial gas velocity for both transitions.

The effect of the inclination on the boundaries is shown in Fig.24a to 24d for upward inclinations of $0°$, $30°$, $60°$, and $85°$, respectively. The scenario considers an air-water mixture at $25°C$ and $1atm$, in an annulus with $116.6mm$ outer diameter and $75mm$ inner diameter.

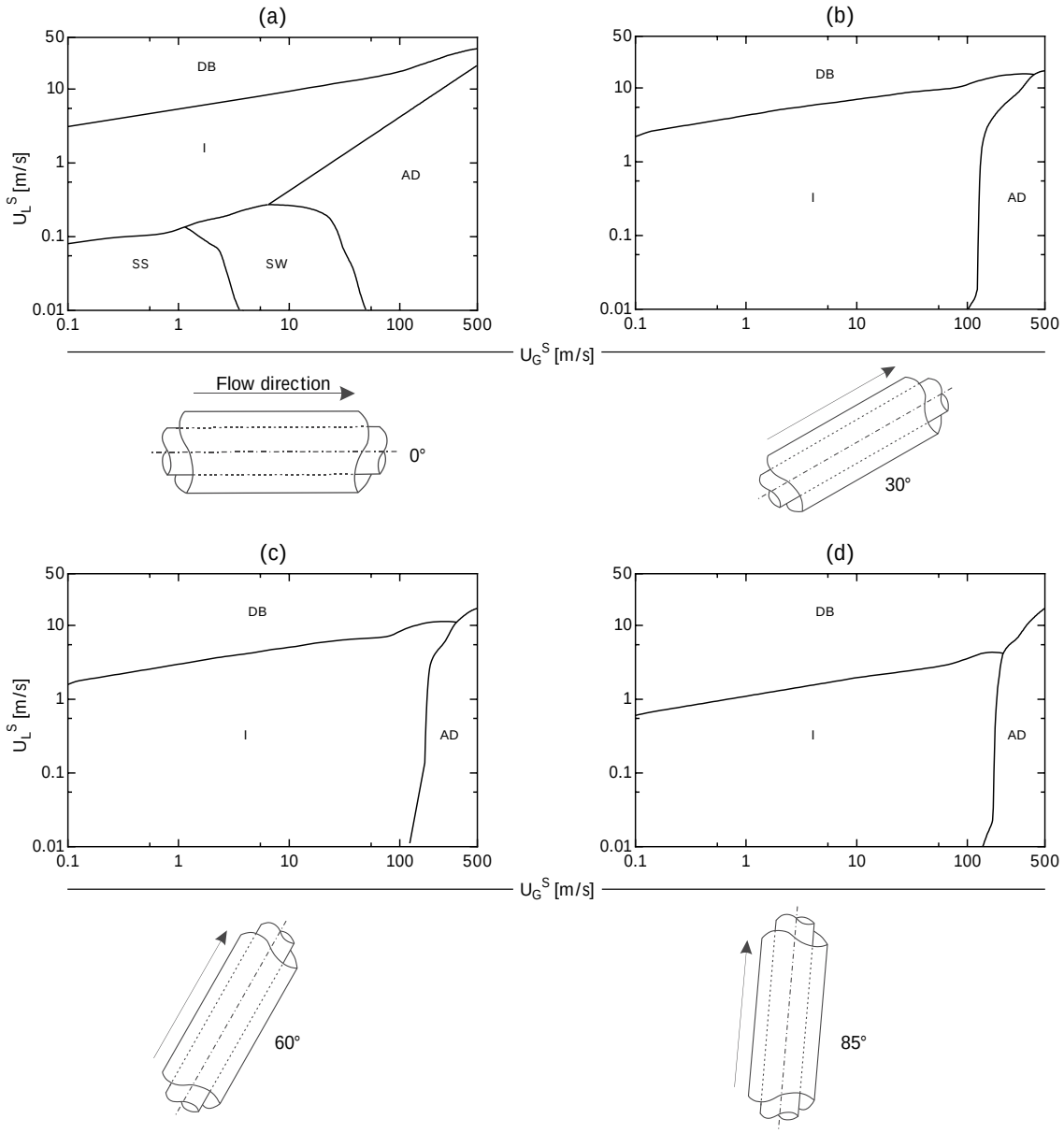

Figure 24 – Transition map boundaries for an annulus of $116.6mm$ outer diameter and $75mm$ inner diameter with upward inclination of: a) $0°$, b) $30°$, c) $60°$, and d) $85°$. Air-Water at $25°C$ and 1 atm.

Source: Author

It should be noted that the stratified flow pattern is the most affected since the tube inclination is upward; the acceleration of gravity acts in the direction opposite to the flow. Therefore, the liquid and gas flow rates are required to trigger the transition from stratified flow decrease, and the stratified flow area shrinks; besides, for large inclinations, such areas even vanish, resulting

in an increase in the intermittent flow pattern area.

The dispersed bubble flow pattern area has a modest increase as the inclination increases. It is assumed that such behavior is due to the acceleration of gravity against the direction of flow favoring the keeping of more air bubbles, even at lower liquid flow rates.

The effect of the inclination on the boundaries is shown in Fig. 13a to 13d for downward inclinations of $0°$, $30°$, $60°$, and $85°$, respectively. The scenario considers an air-water mixture at $25°C$ and $1atm$ in an annulus with $116.6mm$ outer diameter and $75mm$ inner diameter.

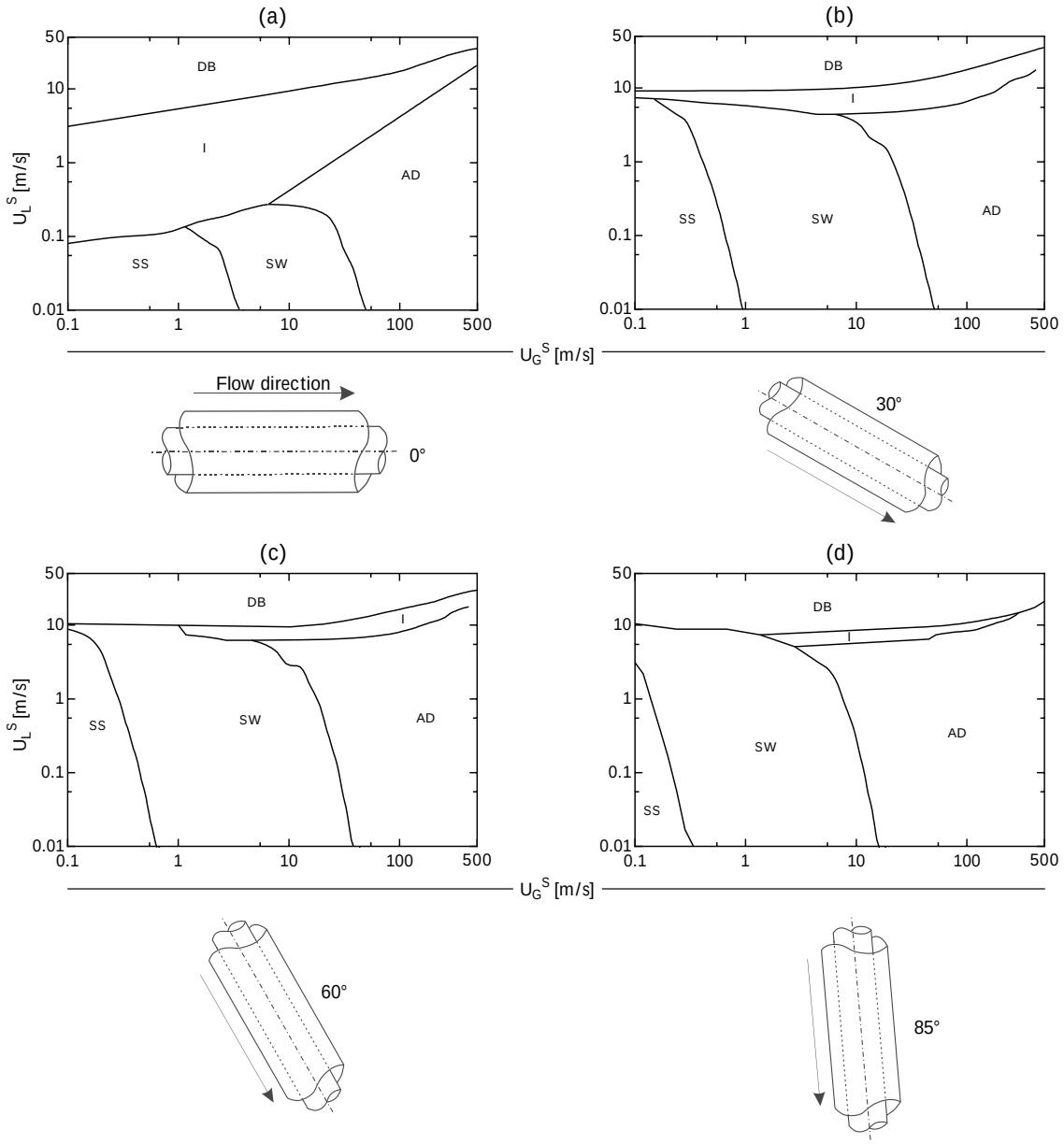

Figure 25 – Transition map boundaries for an annulus of $116.6mm$ outer diameter and $75mm$ inner diameter with downward inclination of: a) $0°$, b) $30°$, c) $60°$, and d) $85°$. Air-Water at $25°C$ and 1 atm.

Source: Author

A switch to a downward inclination also influences the stratified flow pattern because, contrary to upward flow, the gravity force favors the flow; hence, the liquid phase moves quicker. As a result, the liquid level within the tube is lower, resulting in higher gas and liquid flow rates required to cause the transition from the downward stratified flow. Consequently, the stratified flow area is expanded as the angle of inclination increases. Barnea *et al.* (1982) reported analog results for downward-inclined pipes.

The transition to dispersed bubble flow is relatively insensitive to the inclination since, at high liquid rates, the gas is dispersed into tiny bubbles because of the turbulent forces becoming almost unaffected by the acceleration due to gravity. On the other hand, the intermittent area decreases considerably as the inclination increases; hence, this flow pattern is only observed at very high liquid and gas flow rates. Similar behavior was predicted by Barnea *et al.* (1982).

To quantify the variation in the size of the area occupied by each flow pattern with the change in tube inclination, the area occupied by the respective flow patterns was calculated. Figure 26 shows the results considering two flow directions: upward and downward.

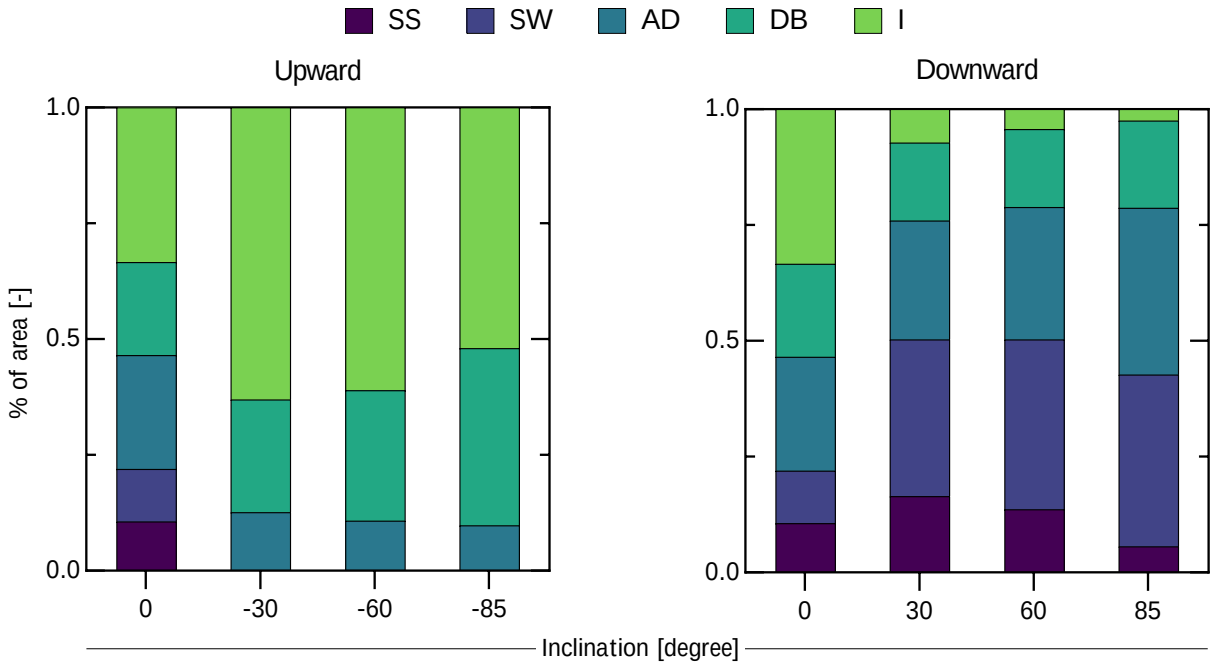

Figure 26 – Transition map boundaries for an annulus of $116.6mm$ outer diameter and $75mm$ inner diameter with downward inclination of: a) $0°$, b) $30°$, c) $60°$, and d) $85°$. Air-Water at $25°C$ and 1 atm.

Source: Author

Note that for the upward direction, the inclination is considered negative.

Table 3 presents the numerical values for the areas of each flow pattern shown in Fig.26.

Table 3 – Percentage area of each flow pattern

Angle	Upward					Downward				
	SS	SW	AD	DB	I	SS	SW	AD	DB	I
0	0.106	0.113	0.246	0.201	0.334	0.106	0.113	0.246	0.201	0.334
30	0.000	0.000	0.126	0.243	0.631	0.165	0.338	0.256	0.168	0.072
60	0.000	0.000	0.108	0.282	0.610	0.136	0.367	0.286	0.168	0.043
85	0.000	0.000	0.098	0.383	0.520	0.056	0.370	0.360	0.188	0.024

Source: Author

6 CONCLUSIONS

In the present work, the Taitel and Dukler (1976) model developed for pipes was generalized to take into account flow in annuli under inclinations from the horizontal to near-vertical. The two-phase flow pattern maps identified the transitions between stratified smooth/stratified wavy, stratified wavy/annular dispersed liquid, stratified/intermittent, annular dispersed liquid/intermittent, and intermittent/dispersed bubble. Since a mechanistic model was developed for flow in annuli, a new approach to obtain the shear stresses and the velocity profile had to be developed, emphasizing that this approach yields to the same results obtained for the classic situation of vertical pipes when the inner diameter tends to zero, thus the equation is still valid for pipes. The inclusion of the inner tube in the model - a concentric condition - could be evidenced through the model development (in the equilibrium liquid level for the stratified flow balance) and by plotting the so-called generalized flow pattern map, whit the dimensionless parameters (Lockhart-Martinelli and transition pattern parameters). Concerning the equilibrium liquid level for the stratified flow, the changes (inner tube inclusion) in the set of equations used to describe the variables of interest (such as the phases' occupied area and wetted perimeter) caused an evident change in the rate of liquid height rise/fall.

The present model was verified as two tube inclinations: horizontal (against experimental data) and vertical (against theoretical models). The model presented a satisfactory performance for both inclinations, except for the churn flow pattern that merits a deep investigation for validation at high superficial liquid velocities in horizontal annuli.

Once the model was tested at the inclination limits, the effect of four different inclinations ($0°$, $30°$, $60°$, and $85°$) was verified for two flow directions: downward and upward. Regardless of the direction, the stratified flow pattern was the most affected. In upward flows in annuli, the acceleration due to gravity acts in the opposite direction to the flow; the liquid and gas flow rate required to trigger the transition from stratified flow decreased, thus shrinking the stratified flow area in the map. The contrary effect was observed for downward flows, where the gravity favors the flow and, hence, the liquid phase moves quicker. As a result, the liquid height within the tube decreases, resulting in higher gas and liquid flow rates required to cause the transition from the downward stratified flow. Consequently, the stratified flow area was expanded as the angle of inclination increased.

Finally, authors should always provide the flow pattern map of dimensionless parameters, to

establish fair comparisons among the models and, consequently, to rebuild maps utilizing the typical ${u_L}^S - {u_G}^S$ coordinates, which should be utilized for engineering purposes only.

6.1 RECOMMENDATIONS FOR FUTURE RESEARCH

Literature review and results presented in this dissertation entice some proposals to further investigation.

- To evaluate the presence/influence of tube wall's roughness.
- To confront the present model against other works than those presented here.
- To investigate the source of the shift in the flow pattern prediction for the churn flow pattern for high superficial liquid velocity.
- To split the intermittent flow pattern into other flow patterns (slug, churn, elongated bubble) and formulate predictions for such models.

REFERENCES

AGRAWAL, S. S.; GREGORY, G. A.; GOVIER, G. W. An analysis of horizontal stratified two phase flow in pipes. **The Canadian Journal of Chemical Engineering**, v. 51, n. 3, p. 280–286, 1973. Available at: <https://onlinelibrary.wiley.com/doi/abs/10.1002/cjce.5450510303>.

AL-LABABIDI, S.; MBA, D.; ADDALI, A. Upstream multiphase flow assurance monitoring using acoustic emission. In: SIKORSKI, W. (Ed.). **Acoustic Emission**. Rijeka: IntechOpen, 2012. chap. 10. Available at: <https://doi.org/10.5772/31332>.

ANUMBE, N. C. **Experimental Investigation of Two-Phase (Gas/Liquid) Flow in Intermediate Sized, Horizontal and Inclined Pipes**. 231 p. PHD Thesis — University of South Carolina, 2018. Available at: <https://scholarcommons.sc.edu/etd/5052/?utm_source=scholarcommons.sc.edu%2Fetd%2F5052&utm_medium=PDF&utm_campaign=PDFCoverPages>.

BAKER, O. Design of pipelines for the simultaneous flow of oil and gas. In: . [s.n.], 1953. (SPE Annual Technical Conference and Exhibition, All Days). SPE-323-G. Available at: <https://doi.org/10.2118/323-G>.

BARCELLAR, F. R. R. **Proposta de Controle Automático e Monitoramento Operacional do Bombeio Centrifugo Submerso em Sistemas de Produção Offshore.** 2016. 92 p. Master's Thesis (Mestrado em Engenharia Elétrica) — Centro Tecnológico, Programa de Pós-Graduação em Engenharia Elétrica, Universidade Federal do Espírito Santo, Vitória, Brazil, 2016. Available at: <http://repositorio.ufes.br/handle/10/9676>.

BARNEA, D.; SHOHAM, O.; TAITEL, Y. Flow pattern characterization in two phase flow by electrical conductance probe. **International Journal of Multiphase Flow**, v. 6, n. 5, p. 387–397, 1980. ISSN 0301-9322. Available at: <https://www.sciencedirect.com/science/article/pii/0301932280900014>.

BARNEA, D.; SHOHAM, O.; TAITEL, Y. Flow pattern transition for downward inclined two phase flow; horizontal to vertical. **Chemical Engineering Science**, v. 37, p. 735–740, 1982.

BENJAMIN, T. B. Shearing flow over a wavy boundary. **Journal of Fluid Mechanics**, Cambridge University Press, v. 6, n. 2, p. 161–205, 1959.

BIRD, R. B.; STEWART, W. E.; LIGHTFOOT, E. N. **Transport phenomena**. 2nd, wiley international ed. ed. [S.l.]: J. Wiley, 2002. ISBN 9780471410775,0471410772.

BOLARINWA, O. D. **A study of two-phase gas-liquid flow with viscous oil in a vertical pipe and annuli channel.** 2016. 102 p. Master's Thesis (Master thesis) — Department of Energy and Process Engineering, Norwegian University of Science and Technology, Trondheim, Norway, 2016. Available at: <http://hdl.handle.net/11250/2410772>.

BP. Report, **Statistical Review of World Energy**. 2021. British Petroleum Statistical Review. Available at: <https://www.bp.com/content/dam/bp/business-sites/en/global/corporate/pdfs/energy-economics/statistical-review/bp-stats-review-2021-full-report.pdf>. Accessed on: octuber - 12 - 2021.

BRENNEN, C. E. Introduction to multiphase flow. In: _____. **Fundamentals of Multiphase Flow**. 1. ed. Cambridge: Cambridge University Press, 2005. chap. 1, p. 1–29.

BRILL, J.; ARIRACHAKARAN, S. State of the Art in Multiphase Flow. **Journal of Petroleum Technology**, v. 44, n. 05, p. 538–541, 05 1992. ISSN 0149-2136. Available at: <https://doi.org/10.2118/23835-PA>.

BRILL, J. P.; MUKHERJEE, H. **Multiphase flow in wells**. 1st. ed. [S.l.: s.n.], 1999. 149 p.

CHAN, A.; BANERJEE, S. Design aspects of gamma densitometers for void fraction measurements in small scale two-phase flows. **Nuclear Instruments and Methods in Physics Research**, v. 190, n. 1, p. 135–148, 1981. ISSN 0167-5087. Available at: <https://www.sciencedirect.com/science/article/pii/0029554X81902147>.

CHAN, A.; BZOVEY, D. Measurement of mass flux in high temperature high pressure steam–water two-phase flow using a combination of pitot tubes and a gamma densitometer. **Nuclear Engineering and Design**, v. 122, n. 1, p. 95–104, 1990. ISSN 0029-5493. Available at: <https://www.sciencedirect.com/science/article/pii/0029549390901998>.

CHEN, X.; CAI, X.; BRILL, J. A general model for transition to dispersed bubble flow. **Chemical Engineering Science**, v. 52, n. 23, p. 4373–4380, 1997. ISSN 0009-2509. Available at: <https://www.sciencedirect.com/science/article/pii/S0009250997808573>.

CHENG, L.; RIBATSKI, G.; THOME, J. R. Two-Phase Flow Patterns and Flow-Pattern Maps: Fundamentals and Applications. **Applied Mechanics Reviews**, v. 61, n. 5, 07 2008. ISSN 0003-6900. 050802. Available at: <https://doi.org/10.1115/1.2955990>.

The New Deepwater Oil and Gas Province in Brazil: Flow Assurance and Artificial Lift: Innovations for Jubarte Heavy Oil, All Days of **OTC Offshore Technology Conference**, (OTC Offshore Technology Conference, All Days). OTC-19083-MS. Available at: <https://doi.org/10.4043/19083-MS>.

COSTIGAN, G.; WHALLEY, P. Slug flow regime identification from dynamic void fraction measurements in vertical air-water flows. **International Journal of Multiphase Flow**, v. 23, n. 2, p. 263–282, 1997. ISSN 0301-9322. Available at: <https://www.sciencedirect.com/science/article/pii/S030193229600050X>.

DAS, G.; DAS, P.; PUROHIT, N.; MITRA, A. Phase distribution of gas–liquid mixtures in concentric annuli-inception and termination of asymmetry. **International Journal of Multiphase Flow**, v. 26, n. 5, p. 857–876, 2000. ISSN 0301-9322. Available at: <https://www.sciencedirect.com/science/article/pii/S0301932299000348>.

DAS, G.; DAS, P. K.; PUROHIT, N. K.; MITRA, A. K. Flow Pattern Transition During Gas Liquid Upflow Through Vertical Concentric Annuli—Part I: Experimental Investigations. **Journal of Fluids Engineering**, v. 121, n. 4, p. 895–901, 12 1999. ISSN 0098-2202. Available at: <https://doi.org/10.1115/1.2823552>.

DAS, G.; DAS, P. K.; PUROHIT, N. K.; MITRA, A. K. Flow Pattern Transition During Gas Liquid Upflow Through Vertical Concentric Annuli—Part II: Mechanistic Models. **Journal of Fluids Engineering**, v. 121, n. 4, p. 902–907, 12 1999. ISSN 0098-2202. Available at: <https://doi.org/10.1115/1.2823553>.

De Schepper, S. C.; HEYNDERICKX, G. J.; MARIN, G. B. Cfd modeling of all gas–liquid and vapor–liquid flow regimes predicted by the baker chart. **Chemical Engineering Journal**, v. 138, n. 1, p. 349–357, 2008. ISSN 1385-8947. Available at: <https://www.sciencedirect.com/science/article/pii/S1385894707004044>.

DEMIDOVICH, B. **Problems in mathematical analysis**. [S.l.]: Mir, 1970.

EKBERG, N.; GHIAASIAAN, S.; ABDEL-KHALIK, S.; YODA, M.; JETER, S. Gas–liquid two-phase flow in narrow horizontal annuli. **Nuclear Engineering and Design**, v. 192, n. 1, p. 59–80, 1999. ISSN 0029-5493. Available at: <https://www.sciencedirect.com/science/article/pii/S0029549399000783>.

EYO, E. N.; LAO, L. Gas-liquid flow regimes in horizontal annulus. **Journal of Petroleum Science and Engineering**, v. 175, p. 573–586, 2019. ISSN 0920-4105. Available at: <https://www.sciencedirect.com/science/article/pii/S0920410518311616>.

FILHO, C. E.; SHOHAM, O.; BRILL, J. Upward vertical t wo-phase flow through an annulus—part i: Single-phase friction factor, taylor bubble rise velocity, and flow pattern prediction. **Journal of Energy Resources Technology-transactions of The Asme - J ENERG RESOUR TECHNOL**, v. 114, p. 13, 03 1992.

FILHO, C. E.; SHOHAM, O.; BRILL, J. Upward vertical two-phase flow through an annulus—part ii: Modeling bubble, slug, and annular flow. **Journal of Energy Resources Technology; (United States)**, v. 114:1, p. 17, 03 1992.

FIROUZI, M.; TOWLER, B. F.; RUFFORD, T. E. Mechanistic modelling of counter-current slug flows in vertical annuli. In: . [s.n.], 2015. (SPE Asia Pacific Unconventional Resources Conference and Exhibition, All Days). SPE-176885-MS. Available at: <https://doi.org/10.2118/176885-MS>.

FRANCO, L.; RAMOS, R. **Introducing NEMOG lab - The Research Group for Oil & Gas Flow and Measurement**. 2021. 6 p. Available at: <https://www.researchgate.net/publication/351094220_Introducing_NEMOG_lab_-_The_Research_Group_for_Oil_Gas_Flow_and_Measurement>.

FRANCO, L. G. **Methodologies to mitigate attenuating effects in flare gas flow measurement by ultrasonic technology at low pressure and high carbon dioxide concentration.** 2020. 135 p. Master's Thesis (Mestrado em Engenharia Mecânica) — Centro Tecnológico, Programa de Pós-Graduação em Engenharia Mecânica, Universidade Federal do Espírito Santo, Vitória, 2020. Available at: <https://engenhariamecanica.ufes.br/en/pos-graduacao/PPGEM/thesis-details?id=14415>.

FURUKAWA, T.; SEKOGUCHI, K. Phase distribution for air-water two-phase flow in annuli. **Bulletin of JSME**, v. 29, n. 255, p. 3007–3014, 1986.

GAZLEY, C. J. **Interfacial Shear Stress and Stability in two-phase flow**. PHD Thesis — University of Delaware, 1948.

GSCHNAIDTNER, T. **Two Phase Flow (Air-Water) Characteristics in Annulus.** 2014. 121 p. Master's Thesis (Master Degree in Science) — School of Engineering, Energy Systems and Thermal Processes, Cranfield University, Cranfield, England, 2014.

HAND, N.; SPEDDING, P. Horizontal gas liquid flow at close to atmospheric conditions. **Chemical Engineering Science**, v. 48, n. 12, p. 2283–2305, 1993. ISSN 0009-2509. Available at: <https://www.sciencedirect.com/science/article/pii/000925099380244K>.

HARVEL, G.; HORI, K.; KAWANISHI, K.; CHANG, J. Real-time cross-sectional averaged void fraction measurements in vertical annulus gas-liquid two-phase flow by neutron radiography and x-ray tomography techniques. **Nuclear Instruments and Methods in Physics Research Section A: Accelerators, Spectrometers, Detectors and Associated Equipment**, v. 371, n. 3, p. 544–552, 1996. ISSN 0168-9002. Available at: <https://www.sciencedirect.com/science/article/pii/0168900295008071>.

HASAN, A.; KABIR, C. Two-phase flow in vertical and inclined annuli. **International Journal of Multiphase Flow**, v. 18, n. 2, p. 279–293, 1992. ISSN 0301-9322. Available at: <https://www.sciencedirect.com/science/article/pii/030193229290089Y>.

HEWITT, G.; HALL-TAYLOR, N. Chapter 2 - regimes of flow. In: HEWITT, G.; HALL-TAYLOR, N. (Ed.). **Annular Two-phase Flow**. Amsterdam: Pergamon, 1970. p. 4–20. ISBN 978-0-08-015797-9. Available at: <https://www.sciencedirect.com/science/article/pii/B9780080157979500054>.

HEWITT, G. F.; ROBERTS, D. N. Studies of two-phase flow patterns by simultaneous x-ray and flast photography. 2 1969. Available at: <https://www.osti.gov/biblio/4798091>.

HIBIKI, T.; SITU, R.; MI, Y.; ISHII, M. Local flow measurements of vertical upward bubbly flow in an annulus. **International Journal of Heat and Mass Transfer**, v. 46, n. 8, p. 1479–1496, 2003. ISSN 0017-9310. Available at: <https://www.sciencedirect.com/science/article/pii/S0017931002004210>.

IBARRA, R.; NOSSEN, J.; TUTKUN, M. Two-phase gas-liquid flow in concentric and fully eccentric annuli. part ii: Model development, flow regime transition algorithm and pressure gradient. **Chemical Engineering Science**, v. 203, p. 501–510, 2019. ISSN 0009-2509. Available at: <https://www.sciencedirect.com/science/article/pii/S0009250919301836>.

INCROPERA, F. P.; DEWITT, D. P. **Fundamentos de Transferência de Calor e de Massa**. 6. ed. Rio de Janeiro: LTC, 2006. ISBN 0470055545,9780470055540.

JEFFREYS, H. Formation of water waves by wind. **Proceedings of the Royal Society of London. Series A, Containing Papers of a Mathematical and Physical Character**, v. 110, n. 754, p. 241–247, 1926. Available at: <https://royalsocietypublishing.org/doi/abs/10.1098/rspa.1926.0014>.

JEFFREYS, H.; TAYLOR, G. I. On the formation of water waves by wind. **Proceedings of the Royal Society of London. Series A, Containing Papers of a Mathematical and Physical Character**, v. 107, n. 742, p. 189–206, 1925. Available at: <https://royalsocietypublishing.org/doi/abs/10.1098/rspa.1925.0015>.

JONES, O. C.; ZUBER, N. The interrelation between void fraction fluctuations and flow patterns in two-phase flow. **International Journal of Multiphase Flow**, v. 2, n. 3, p. 273–306, 1975. ISSN 0301-9322. Available at: <https://www.sciencedirect.com/science/article/pii/0301932275900154>.

JULIA, J. E.; OZAR, B.; DIXIT, A.; JEONG, J.-J.; HIBIKI, T.; ISHII, M. Axial Development of Flow Regime in Adiabatic Upward Two-Phase Flow in a Vertical Annulus. **Journal of Fluids Engineering**, v. 131, n. 2, 01 2009. ISSN 0098-2202. 021302. Available at: <https://doi.org/10.1115/1.3059701>.

JULIA, J. E.; OZAR, B.; JEONG, J.-J.; HIBIKI, T.; ISHII, M. Flow regime development analysis in adiabatic upward two-phase flow in a vertical annulus. **International Journal of Heat and Fluid Flow**, v. 32, n. 1, p. 164–175, 2011. ISSN 0142-727X. Available at: <https://www.sciencedirect.com/science/article/pii/S0142727X10001591>.

KELESSIDIS, V.; DUKLER, A. Modeling flow pattern transitions for upward gas-liquid flow in vertical concentric and eccentric annuli. **International Journal of Multiphase Flow**, v. 15, n. 2, p. 173–191, 1989. ISSN 0301-9322. Available at: <https://www.sciencedirect.com/science/article/pii/0301932289900694>.

LAGE, A. C.; TIME, R. W. Mechanistic Model for Upward Two-Phase Flow in Annuli. All Days, 10 2000. SPE-63127-MS. Available at: <https://doi.org/10.2118/63127-MS>.

LEVIC, B.; LEVIČ, V.; TECHNICA, I. S.; HALL, P.; LTD, S. T. **Physicochemical Hydrodynamics**. Prentice-Hall, 1962. (Prentice-Hall international series in the physical and chemical engineering sciences). Available at: <https://books.google.com.br/books?id=EtoIAQAAIAAJ>.

LIMA, M. P. **Afericao do Modelo VOF na Caracterizacao de Padroes de Escoamento Multifasico em Tubulacao Horizontal e Inclinada.** 2016. 117 p. Master's Thesis (Mestrado em Engenharia Mecânica) — Centro Tecnológico, Programa de Pós-Graduação em Engenharia Mecânica, Universidade Federal do Espírito Santo, Vitória, Brazil, 2016. Available at: <http://repositorio.ufes.br/handle/10/9809>.

LOCKHART, R. W.; MARTINELLI, R. C. Proposed correlation of data for isothermal two-phase, two-component flow in pipes. **Chemical Engineering Progress**, v. 45, n. 1, p. 39–48, 1949.

MANDHANE, J.; GREGORY, G.; AZIZ, K. A flow pattern map for gas—liquid flow in horizontal pipes. **International Journal of Multiphase Flow**, v. 1, n. 4, p. 537–553, 1974. ISSN 0301-9322. Available at: <https://www.sciencedirect.com/science/article/pii/0301932274900068>.

MARTINS, R.; ANDRADE, J. R.; RAMOS, R. On the effect of the mounting angle on single-path transit-time ultrasonic flow measurement of flare gas: a numerical analysis. **Journal of the Brazilian Society of Mechanical Sciences and Engineering**, v. 42, n. 1, p. 13, Dec 2019. ISSN 1806-3691. Available at: <https://doi.org/10.1007/s40430-019-2097-9>.

MATSUI, G. Automatic identification of flow regimes in vertical two-phase flow using differential pressure fluctuations. **Nuclear Engineering and Design**, v. 95, p. 221–231, 1986. ISSN 0029-5493. Available at: <https://www.sciencedirect.com/science/article/pii/002954938690049X>.

MENDES, F. A. A.; RODRIGUEZ, O. M. H.; ESTEVAM, V.; LOPES, D. The influence of fluid properties and duct geometry on gas-liquid flow patterns. In: **International Congress of Mechanical Engineering - COBEM**. ABCM, 2013. Available at: <https://abcm.org.br/anais/cobem/2013/_web/>.

MILNE-THOMSON, L. **Theoretical Hydrodynamics**. 4th. ed. [S.l.]: The MacMillan Co, 1960.

NRSC. **Nuclear Reactor**. 201? Available at: <https://nrsc-am.com/blog/nuclear-reactors/>. Accessed on: 2021-09-02.

OLIVEIRA, M.; LIMA, M.; MARTINS, M.; MARTINS, R.; RAMOS, R. Experimental and numerical evaluation of churn and slug air-water flow in horizontal and inclined pipes. In: INTERNATIONAL CONGRESS OF MECHANICAL ENGINEERING - COBEM, 25th., 2019, Uberlândia, Brazil. **Anais...** Uberlândia, Brazil: ABCM, 2019. p. 10.

OSAMUSALI, S. I. **Study of gas-liquid two-phase flow pattern transitions in horizontal pipe, annulus and nuclear fuel type rod bundle flow systems**. Doctor of Philosophy — McMaster University, july 1988. Available at: <http://hdl.handle.net/11375/6680>.

OSGOUEI, R. E.; OZBAYOGLU, A. M.; OZBAYOGLU, E. M.; YUKSEL, E.; ERESEN, A. Pressure drop estimation in horizontal annuli for liquid–gas 2 phase flow: Comparison of mechanistic models and computational intelligence techniques. **Computers and Fluids**, v. 112, p. 108–115, 2015. ISSN 0045-7930. Available at: <https://www.sciencedirect.com/science/article/pii/S0045793014004253>.

OZAR, B.; JEONG, J.; DIXIT, A.; JULIá, J.; HIBIKI, T.; ISHII, M. Flow structure of gas–liquid two-phase flow in an annulus. **Chemical Engineering Science**, v. 63, n. 15, p. 3998–4011, 2008. ISSN 0009-2509. Available at: <https://www.sciencedirect.com/science/article/pii/S0009250908002418>.

OZBAYOGLU, M. E.; OMURLU, C. Modelling of two-phase flow through concentric annuli. **Petroleum Science and Technology**, Taylor and Francis, v. 25, n. 8, p. 1027–1040, 2007. Available at: <https://www.tandfonline.com/doi/abs/10.1080/10916460600695132>.

PALADINO, E. E. **Estudo do Escoamento Multifasico em Medidores de Vazao do tipo Pressao Differencial**. 263 p. PHD — Federal University of Santa Catarina, April 2005. Available at: <https://sinmec.ufsc.br/site/arquivos/x-xwrkamlvmz_2005_emilio_tese.pdf>.

PETALAS, N.; AZIZ, K. A Mechanistic Model for Multiphase Flow in Pipes. **Journal of Canadian Petroleum Technology**, v. 39, n. 06, 06 2000. ISSN 0021-9487. Available at: <https://doi.org/10.2118/00-06-04>.

RIBEIRO, M. P.; OLIVEIRA, P. da S.; MATOS, J. Siqueira de; SILVA, J. Mendonça da. Field Applications Of Subsea Electrical Submersible Pumps In Brazil. All Days, 05 2005. OTC-17415-MS. Available at: <https://doi.org/10.4043/17415-MS>.

RODRIGUES, R.; SOARES, R.; MATOS, J. de; PEREIRA, C.; RIBEIRO, G. A New Approach For Subsea Boosting - Pumping Module On The Seabed. All Days, 05 2005. OTC-17398-MS. Available at: <https://doi.org/10.4043/17398-MS>.

RODRIGUES, R.; SOARES, R.; MATOS, J. de; PEREIRA, C.; RIBEIRO, G. A new approach for subsea boosting-pumping module on the seabed. In: ONEPETRO. **Offshore Technology Conference**. [S.l.], 2005.

ROMERO, O. J.; HUPP, A. Subsea electrical submersible pump significance in petroleum offshore production. **Journal of Energy Resources Technology**, American Society of Mechanical Engineers Digital Collection, v. 136, n. 1, 2014.

ROUHANI, S.; SOHAL, M. Two-phase flow patterns: A review of research results. **Progress in Nuclear Energy**, v. 11, n. 3, p. 219–259, 1983. ISSN 0149-1970. Available at: <https://www.sciencedirect.com/science/article/pii/0149197083900124>.

SADATOMI, M.; SATO, Y.; SARUWATARI, S. Two-phase flow in vertical noncircular channels. **International Journal of Multiphase Flow**, v. 8, n. 6, p. 641–655, 1982. ISSN 0301-9322. Available at: <https://www.sciencedirect.com/science/article/pii/0301932282900684>.

SALCUDEAN, M.; CHUN, J.; GROENEVELD, D. C. Effect of flow obstruction on void distribution in horizontal air-water flow. **International Journal of Multiphase Flow**, v. 9, p. 91–96, 1983.

SALCUDEAN, M.; GROENEVELD, D. C.; LEUNG, L. Effect of flow-obstruction geometry on pressure drops in horizontal air-water flow. **International Journal of Multiphase Flow**, v. 9, n. 1, p. 73–85, 1983. ISSN 0301-9322. Available at: <https://www.sciencedirect.com/science/article/pii/0301932283900071>.

SCOTT, D. S. Properties of cocurrent gas-liquid flow. In: DREW, T. B.; HOOPES, J. W.; VERMEULEN, T. (Ed.). Academic Press, 1964, (Advances in Chemical Engineering, v. 4). p. 199–277. Available at: <https://www.sciencedirect.com/science/article/pii/S0065237708602410>.

SOO, S. L. **Multiphase fluid dynamics**. [S.l.]: Science Press, 1990.

SPEDDING, P.; NGUYEN, V. T. Regime maps for air water two phase flow. **Chemical Engineering Science**, v. 35, n. 4, p. 779–793, 1980. ISSN 0009-2509. Available at: <https://www.sciencedirect.com/science/article/pii/0009250980850627>.

SPEDDING, P.; SPENCE, D. Flow regimes in two-phase gas-liquid flow. **International Journal of Multiphase Flow**, v. 19, n. 2, p. 245–280, 1993. ISSN 0301-9322. Available at: <https://www.sciencedirect.com/science/article/pii/030193229390002C>.

SUN, X.; KURAN, S.; ISHII, M. Cap bubbly-to-slug flow regime transition in a vertical annulus. **Experiments in Fluids**, v. 37, n. 3, p. 458–464, Sep 2004. ISSN 1432-1114. Available at: <https://doi.org/10.1007/s00348-004-0809-z>.

TAITEL, Y. Flow pattern transition in two phase flow. In: . [s.n.], 1990. (9th International Heat Transfer Conference, v. 1), p. 237–253. Available at: <https://ihtcdigitallibrary.com/conferences/6ec9fdc764f29109,058deef014a8f7e6,0843c2c70d7127cb.html>.

TAITEL, Y.; DUKLER, A. E. A model for predicting flow regime transitions in horizontal and near horizontal gas-liquid flow. **AIChE Journal**, v. 22, n. 1, p. 47–55, 1976. Available at: <https://aiche.onlinelibrary.wiley.com/doi/abs/10.1002/aic.690220105>.

TAITEL, Y.; LEE, N.; DUKLER, A. E. Transient gas-liquid flow in horizontal pipes: Modeling the flow pattern transitions. **AIChE Journal**, v. 24, n. 5, p. 920–934, 1978. Available at: <https://aiche.onlinelibrary.wiley.com/doi/abs/10.1002/aic.690240518>.

TSOUKALAS, L. H.; ISHII, M.; MI, Y. A neurofuzzy methodology for impedance-based multiphase flow identification. **Engineering Applications of Artificial Intelligence**, v. 10, n. 6, p. 545–555, 1997. ISSN 0952-1976. Available at: <https://www.sciencedirect.com/science/article/pii/S0952197697000377>.

TUTU, N. K. Pressure fluctuations and flow pattern recognition in vertical two phase gas-liquid flows. **International Journal of Multiphase Flow**, v. 8, n. 4, p. 443–447, 1982. ISSN 0301-9322. Available at: <https://www.sciencedirect.com/science/article/pii/0301932282900532>.

VINCE, M.; LAHEY, R. On the development of an objective flow regime indicator. **International Journal of Multiphase Flow**, v. 8, n. 2, p. 93–124, 1982. ISSN 0301-9322. Available at: <https://www.sciencedirect.com/science/article/pii/030193228290012X>.

WONGWISES, S.; PIPATHATTAKUL, M. Flow pattern, pressure drop and void fraction of two-phase gas–liquid flow in an inclined narrow annular channel. **Experimental Thermal and Fluid Science**, v. 30, n. 4, p. 345–354, 2006. ISSN 0894-1777. Available at: <https://www.sciencedirect.com/science/article/pii/S0894177705001019>.

WU, B.; FIROUZI, M.; MITCHELL, T.; RUFFORD, T. E.; LEONARDI, C.; TOWLER, B. A critical review of flow maps for gas-liquid flows in vertical pipes and annuli. **Chemical Engineering Journal**, v. 326, p. 350–377, 2017. ISSN 1385-8947. Available at: <https://www.sciencedirect.com/science/article/pii/S1385894717308938>.

WU, B.; FIROUZI, M.; RUFFORD, T. E.; TOWLER, B. Characteristics of counter-current gas-liquid two-phase flow and its limitations in vertical annuli. **Experimental Thermal and Fluid Science**, v. 109, p. 109899, 2019. ISSN 0894-1777. Available at: <https://www.sciencedirect.com/science/article/pii/S0894177719305199>.

WU, X.; SHEN, J.; LI, Y.; LEE, K. Y. Steam power plant configuration, design, and control. **WIREs Energy and Environment**, v. 4, n. 6, p. 537–563, 2015. Available at: <https://wires.onlinelibrary.wiley.com/doi/abs/10.1002/wene.161>.

YADIGAROGLU, G.; HETSRONI, G. Nature of multiphase flows and basic concepts. In: _____. **Introduction to Multiphase Flow: Basic Concepts, Applications and Modelling**. Cham: Springer International Publishing, 2018. p. 1–37. ISBN 978-3-319-58718-9. Available at: <https://doi.org/10.1007/978-3-319-58718-9_1>.

YU, T. T.; ZHANG, H.-Q. Q.; LI, M. X.; SARICA, C. A Mechanistic Model for Gas/Liquid Flow in Upward Vertical Annuli. **SPE Production & Operations**, v. 25, n. 03, p. 285–295, 07 2010. ISSN 1930-1855. Available at: <https://doi.org/10.2118/124181-PA>.

ZEROCO2. **Single cycle steam turbine power plant**. 2017? Available at: <http://www.zeroco2.no/capture/sources-of-co2/single-cycle-steam-turbine-power-plant>. Accessed on: 2021-09-02.

ZHAO, X. **Mechanistic-based models for slug flow in vertical pipes**. 144 p. PHD thesis — Texas Tech University, May 2005. Available at: <https://ttu-ir.tdl.org/handle/2346/1073>. Accessed on: 09-17-2021.

APPENDIX A – ADAPTATION OF EQUATIONS - GEOMETRIC APPROACH

Taitel and Dukler (1976) model is based on geometrical correlations for pipes; hence, such equations must be modified to take the annulus into account. Depending on either the liquid height (h_L) or gas height (h_G), the annulus area might be divided into four sections:

- Section I: $0 < h_L \leq r_o - r_i$
- Section II: $r_o - r_i < h_L \leq r_o$
- Section III: $r_o < h_L \leq r_o + r_i$
- Section IV: $r_o + r_i < h_L \leq 2r_o$

Figure 27 shows the perimeter over which each phase acts depending on the liquid height.

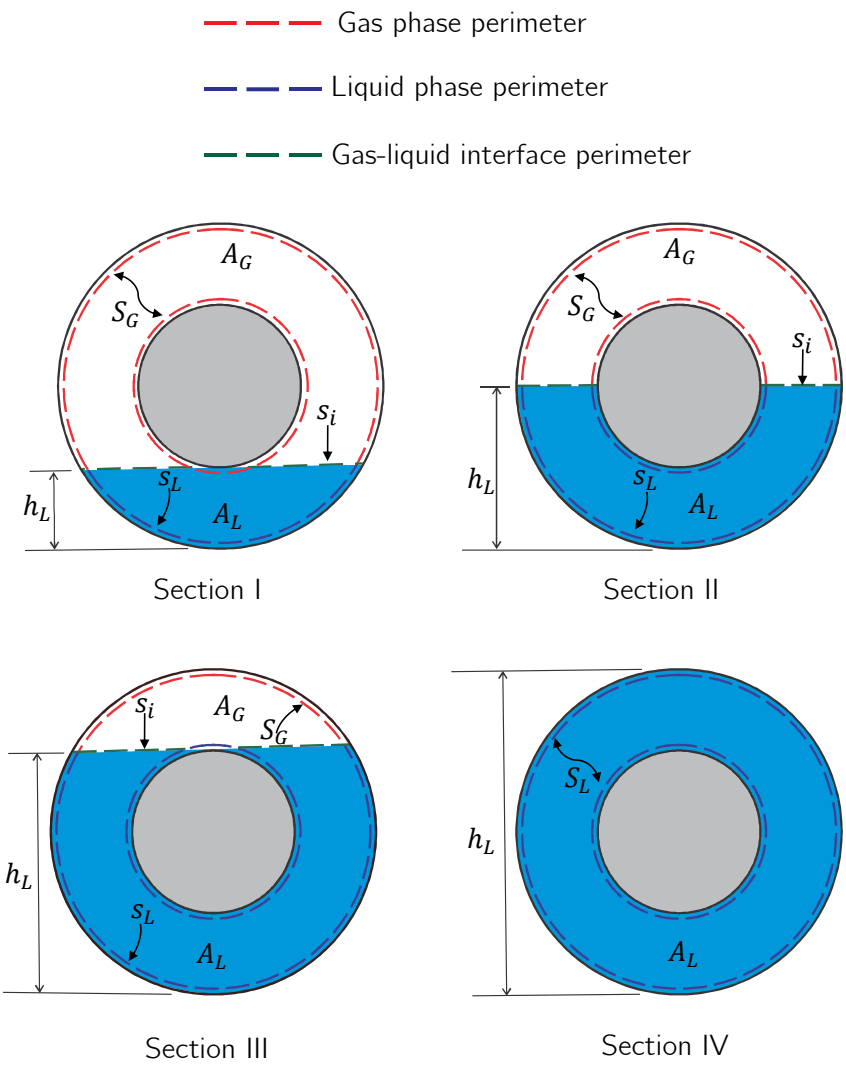

Figure 27 – Gas and liquid phases acting perimeter depending on the liquid height
Source: Author

For all sections, the equations were modified to describe the perimeter wetted by the liquid (S_L), by the gas (S_G) and, by the gas-liquid interface (S_i), the area occupied by the liquid (A_L), and by the gas (A_G), and $\frac{dA_L}{dh_L}$.

- **SECTION I**

Section I is valid for h_L from the bottom of the outer tube to the bottom of the inner tube. The $\triangle_{ABC}$ height, h, in Fig.28 is given by the Eq.A.1.

$$h = r_o - h_L \tag{Eq.A.1}$$

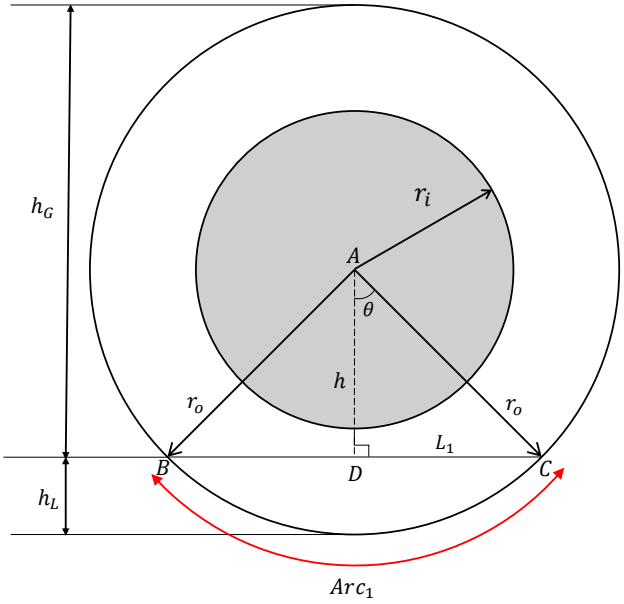

Figure 28 – Cross-section area for section I
Source: Author

The $\triangle_{ADC}$ base, L_1, is given by the Eq.A.2.

$$L_1 = \sqrt{r_o^2 - h^2} \rightarrow L_1 = \sqrt{h_L(2r_o - h_L)} \tag{Eq.A.2}$$

From the $\triangle_{ADC}$, the angle θ is given by Eq.A.3.

$$\cos\theta = \frac{h}{r_o} \rightarrow \cos\theta = \frac{r_o - h_L}{r_o} \rightarrow \theta = \arccos\left(1 - \frac{h_L}{r_o}\right) \tag{Eq.A.3}$$

The area filled by the liquid phase (A_L) is equivalent to the area of the circular segment whose height is h_L and radius is r_o. In other words, this area is equivalent to the area of the circular sector minus the area of the $\triangle_{ABC}$. Eq.A.4 describes this area.

$$A_L = \arccos\left(1 - \frac{h_L}{r_o}\right) r_o^2 - \sqrt{h_L(2r_o - h_L)}(r_o - h_L) \qquad \text{(Eq.A.4)}$$

The area filled by the gas phase (A_G) is given by Eq.A.5, which is equivalent to the annulus area minus the area filled by the liquid.

$$A_G = \pi(ro^2 - r_i^2) - A_L \qquad \text{(Eq.A.5)}$$

The perimeter wetted by the liquid phase (S_L) is equal to the length of the Arc_1; therefore, S_L is:

$$S_L = 2r_o\theta \rightarrow S_L = 2r_o \arccos\left(1 - \frac{h_L}{r_o}\right) \qquad \text{(Eq.A.6)}$$

By simple inspection, it is clear that the perimeter of the gas (S_G) is the remaining perimeter of the largest circumference (radius r_o) plus the perimeter of the smallest circumference (radius r_i), that is,

$$S_G = (2\pi r_o - S_L) + 2\pi r_i \rightarrow S_G = \pi(D_o + D_i) - D_o \arccos\left(1 - \frac{h_L}{r_o}\right) \qquad \text{(Eq.A.7)}$$

The air-water interface perimeter, Si, is given by Eq.A.8.

$$Si = 2L_1 \rightarrow Si = 2\sqrt{h_L(2r_o - h_L)} \qquad \text{(Eq.A.8)}$$

The variation of the area occupied by the liquid with regard to its height is given by Eq.A.9.

$$\frac{dA_L}{dh_L} = 2L_1 \rightarrow \frac{dA_L}{dh_L} = 2\sqrt{h_L(2r_o - h_L)} \qquad \text{(Eq.A.9)}$$

Eq.A.5 is also valid for the Section II, while Eq.A.9 for the Section IV.

- **SECTION II**

Section II is valid for h_L from the bottom of the inner tube to the center. In this case, the inner tube effect must be taken into account.

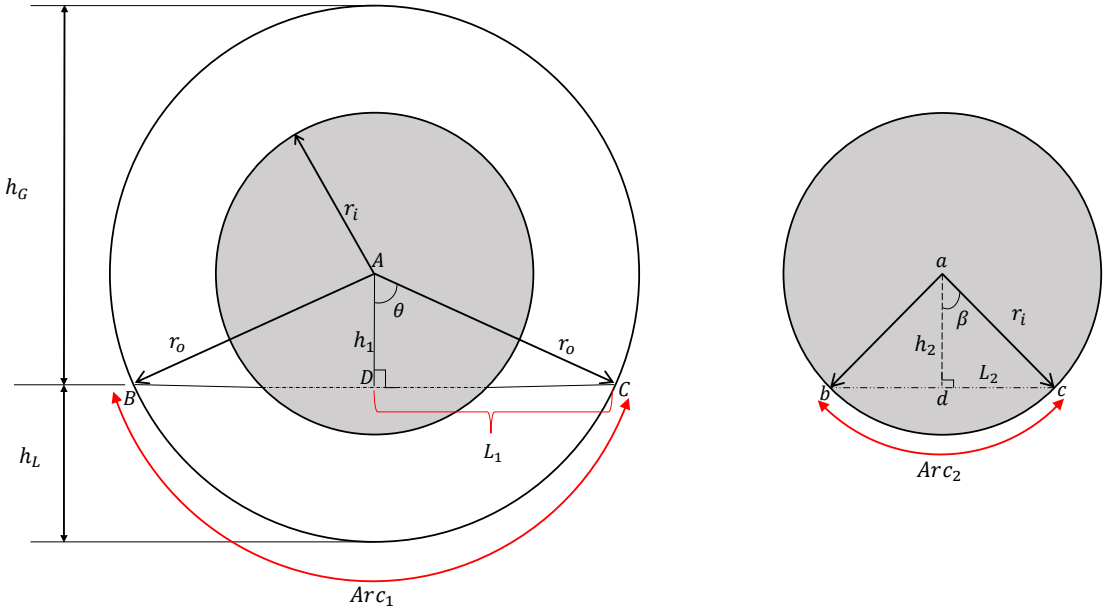

Figure 29 – Cross-section area for section II
Source: Author

The $\triangle_{ABC}$ height, h_1 in Fig.29 is described analogously as Fig.28 by the Eq.A.1, that is,

$$h_1 = r_o - h_L \tag{Eq.A.10}$$

The $\triangle_{ADC}$ base, L_1, is the same as Eq.A.2. The $\triangle_{adc}$ base, L_2, it is given by the Eq.A.11. The $\triangle_{abc}$ height is the same as $\triangle_{ABC}$ height, h_1.

$$L_2 = \sqrt{r_i^2 - h_2^2} \rightarrow L_2 = \sqrt{r_i^2 - (r_o - h_L)^2} \tag{Eq.A.11}$$

From the $\triangle_{ADC}$, the angle θ is given by Eq.A.12.

$$\cos\theta = \frac{h_1}{r_o} \rightarrow \cos\theta = \frac{r_o - h_L}{r_o} \rightarrow \theta = \arccos\left(1 - \frac{h_L}{r_o}\right) \tag{Eq.A.12}$$

Analogously, from the $\triangle_{adc}$, the angle β is given by Eq.A.13.

$$\cos\beta = \frac{h_2}{r_i} \rightarrow \cos\beta = \frac{r_o - h_L}{r_i} \rightarrow \beta = \arccos\left(\frac{r_o - h_L}{r_i}\right) \quad \text{(Eq.A.13)}$$

The area filled by the liquid phase (A_L) is equivalent to the area of the circular segment whose height is h_L, and radius is r_o minus the area of the circular segment whose height is $h_L - (r_o - r_i)$ and radius is r_i.

$$\begin{aligned} A_L = {} & \arccos\left(1 - \frac{h_L}{r_o}\right) r_o^2 - \sqrt{h_L(2r_o - h_L)}(r_o - h_L) \\ & - \left[\arccos\left(1 - \frac{h_L - (r_o - r_i)}{r_i}\right) {r_i}^2 - \sqrt{2h_L r_o + r_i^2 - r_o^2 - h_L^2}(r_o - h_L)\right] \end{aligned} \quad \text{(Eq.A.14)}$$

The perimeter wetted by the liquid phase (S_L) is equal to the length of the Arc_1 plus Arc_2 , hence, S_L is given by Eq.A.15:

$$S_L = 2r_o\theta + 2r_i\beta \rightarrow S_L = 2r_o \arccos\left(1 - \frac{h_L}{r_o}\right) + 2r_i \arccos\left(\frac{r_o - h_L}{r_i}\right) \quad \text{(Eq.A.15)}$$

Analogously to the previous section, S_G is given by Eq.A.16.

$$S_G = (2\pi r_o - Arc_1) + (2\pi r_i - Arc_2) \rightarrow S_G = \pi(D_o + D_i) - S_L \quad \text{(Eq.A.16)}$$

The air-water interface perimeter, Si, is given by Eq.A.17.

$$Si = 2L_1 - 2L_2 \rightarrow Si = 2\sqrt{h_L(2r_o - h_L)} - 2\sqrt{r_i^2 - (r_o - h_L)^2} \quad \text{(Eq.A.17)}$$

The variation of the area occupied by the liquid with regard its height is given by Eq.A.18.

$$\frac{dA_L}{dh_L} = 2L_1 - 2L_2 \rightarrow 2\frac{dA_L}{dh_L} = \sqrt{h_L(2r_o - h_L)} - 2\sqrt{r_i^2 - (r_o - h_L)^2} \quad \text{(Eq.A.18)}$$

Eq.A.18 is valid for Section III.

- **SECTION III**

Section III is valid for h_L from the center to the top of the inner tube. Similarly to Section II, the effect of the inner tube must be taken into account.

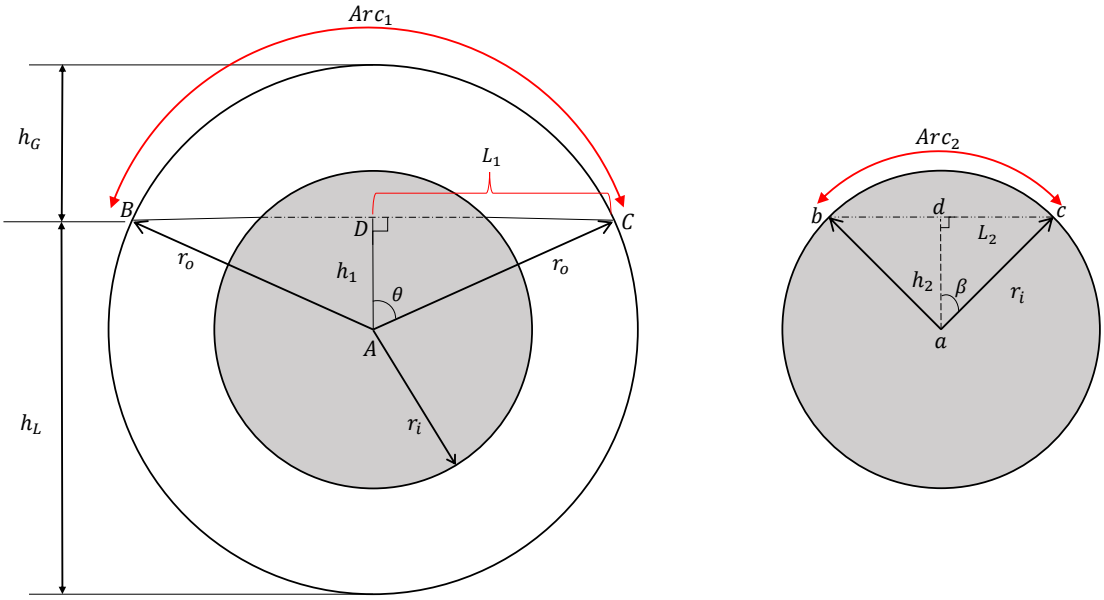

Figure 30 – Cross-section area for section III
Source: Author

The $\triangle_{ABC}$ height, h_1, in Fig.30 is given by the Eq.A.19.

$$h_1 = h_L - r_o \tag{Eq.A.19}$$

The $\triangle_{ADC}$ basis, L_1, is the same as Eq.A.2. The $\triangle_{adc}$ basis, L_2, is described by the Eq.A.20.

$$L_2 = \sqrt{r_i^2 - h_2^2} \rightarrow L_2 = \sqrt{r_i^2 - (h_L - r_o)^2} \tag{Eq.A.20}$$

From the $\triangle_{ADC}$, the angle θ is given by Eq.A.21.

$$\cos\theta = \frac{h_1}{r_o} \rightarrow \cos\theta = \frac{h_L - r_o}{r_o} \tag{Eq.A.21}$$

Similarly, from the $\triangle_{adc}$, the angle β is given by Eq.A.22.

$$\cos\beta = \frac{h_2}{r_i} \rightarrow \cos\beta = \frac{h_L - r_o}{r_i} \quad \text{(Eq.A.22)}$$

The area filled by the gas phase (A_G) is equivalent to the area of the circular segment whose height is h_G and radius is r_o, minus the area of the circular segment whose height is $(r_o+r_i)-h_L$ and radius is r_i.

$$A_G = \arccos\left(1 - \frac{h_G}{r_o}\right) r_o^2 - \sqrt{h_G(2r_o - h_G)}(r_o - h_G) - \left[\arccos\left(1 - \frac{r_o + r_i - h_L}{r_i}\right) {r_i}^2 - \sqrt{2h_L r_o + r_i^2 - r_o^2 - h_L^2}(h_L - r_o)\right] \quad \text{(Eq.A.23)}$$

The area filled by the liquid phase (A_L) is equivalent to the annulus area minus the area occupied by the gas phase (A_G).

$$A_L = \pi(r_o^2 - r_i^2) - A_G \quad \text{(Eq.A.24)}$$

The perimeter wetted by the gas phase (S_G) is equal to the length of the Arc_1 plus Arc_2; hence S_G is given by Eq.A.25:

$$S_G = 2r_o\theta + 2r_i\beta \rightarrow S_G = 2r_o \arccos\left(\frac{h_L}{r_o} - 1\right) + 2r_i \arccos\left(\frac{h_L - r_o}{r_i}\right) \quad \text{(Eq.A.25)}$$

Analogously to the previous section, S_L is given by Eq.A.26.

$$S_L = (2\pi r_o - Arc_1) + (2\pi r_i - Arc_2) \rightarrow S_L = \pi(D_o + D_i) - S_G \quad \text{(Eq.A.26)}$$

The air-water interface perimeter, Si, is given by Eq.A.27.

$$Si = 2L_1 - 2L_2 \rightarrow Si = 2\sqrt{h_L(2r_o - h_L)} - 2\sqrt{r_i^2 - (h_L - r_o)^2} \quad \text{(Eq.A.27)}$$

Eq.A.24 is valid for Section IV.

- **SECTION IV**

Section IV is valid for h_G from the top of the inner pipe to the top of the outer pipe.

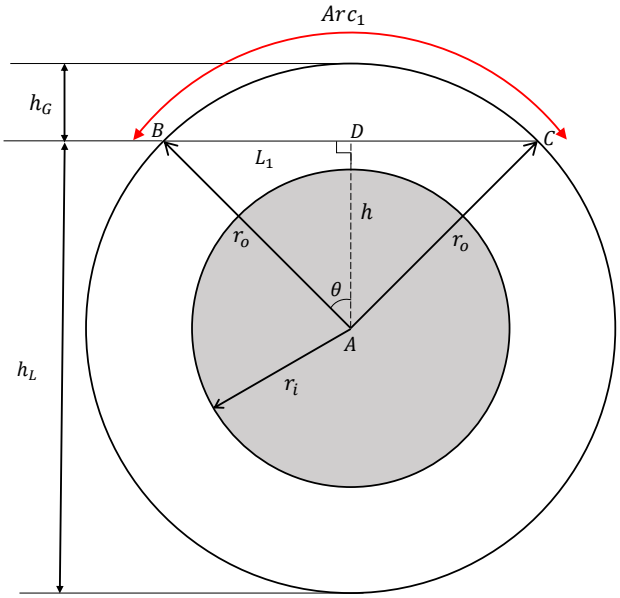

Figure 31 – Cross-section area for section IV
Source: Author

The $\triangle_{ABC}$ height, h, in Fig.31 is given by the Eq.A.28.

$$h = r_o - h_G \tag{Eq.A.28}$$

The $\triangle_{ADC}$ base, L_1, is given by the Eq.A.29.

$$L_1 = \sqrt{r_o^2 - h^2} \rightarrow L_1 = \sqrt{h_G(2r_o - h_G)} \tag{Eq.A.29}$$

From the $\triangle_{ADC}$, the angle θ is given by Eq.A.30.

$$\cos\theta = \frac{h}{r_o} \rightarrow \cos\theta = \frac{r_o - h_G}{r_o} \rightarrow \theta = \arccos\left(1 - \frac{h_G}{r_o}\right) \tag{Eq.A.30}$$

The area filled by the gas phase (A_G) is equivalent to the area of the circular segment whose height is h_G and radius is r_o, it is given by Eq.A.31.

$$A_G = \arccos\left(1 - \frac{h_G}{r_o}\right) r_o^2 - \sqrt{h_G(2r_o - h_G)}(r_o - h_G) \qquad \text{(Eq.A.31)}$$

The perimeter wetted by the gas phase (S_G) is equivalent to the length of the Arc_1.

$$S_G = 2r_o\theta \rightarrow S_G = 2r_o \arccos\left(1 - \frac{h_G}{r_o}\right) \qquad \text{(Eq.A.32)}$$

Analogously to Section I, it is clear that the perimeter of the liquid (S_L) is the remaining perimeter of the largest circumference (radius r_o) plus the perimeter of the smallest circumference (radius r_i), that is,

$$S_L = (2\pi r_o - S_G) + 2\pi r_i \rightarrow S_L = \pi(D_o + D_i) - D_o \arccos\left(1 - \frac{h_G}{r_o}\right) \qquad \text{(Eq.A.33)}$$

The air-water interface perimeter, Si, is given by Eq.A.34.

$$Si = 2L_1 \rightarrow Si = 2\sqrt{h_G(2r_o - h_G)} \qquad \text{(Eq.A.34)}$$

APPENDIX B – DIMENSIONLESS EQUATIONS

This section presents the development of all equations developed in Appendix A in a dimensionless form. The reference variables are D_o for length; ${D_o}^2$ for area; ${u_L}^S$ for the liquid velocity; and ${u_G}^S$ for the gas velocity.

▪ SECTION I

From Eq.A.4,

$$A_L = \arccos\left(1 - \frac{h_L}{r_o}\right) r_o^2 - \sqrt{h_L(2r_o - h_L)}(r_o - h_L)$$

The above equation can be rewritten by substituting r_o by $D_o/2$ as,

$$\begin{aligned}
A_L &= \arccos\left(1 - \frac{2h_L}{D_o}\right)\left(\frac{{D_o}^2}{4}\right) - \left(\frac{D_o}{2} - h_L\right)\sqrt{h_L(D_o - h_L)} \\
&= \arccos\left(1 - \frac{2h_L}{D_o}\right)\left(\frac{{D_o}^2}{4}\right) - \left(1 - \frac{2h_L}{D_o}\right)\sqrt{h_L D_o - {h_L}^2}\left(\frac{D_o}{2}\right) \\
&= \arccos\left(1 - \frac{2h_L}{D_o}\right)\left(\frac{{D_o}^2}{4}\right) - \left(1 - \frac{2h_L}{D_o}\right)\sqrt{h_L D_o\left(\frac{2}{D_o}\frac{D_o}{2}\right)^2 - {h_L}^2\left(\frac{2}{D_o}\frac{D_o}{2}\right)^2}\left(\frac{D_o}{2}\right) \\
&= \arccos\left(1 - \frac{2h_L}{D_o}\right)\left(\frac{{D_o}^2}{4}\right) - \left(1 - \frac{2h_L}{D_o}\right)\sqrt{\frac{4h_L}{D_o} - \frac{4{h_L}^2}{D_o}}\left(\frac{{D_o}^2}{4}\right) \quad \text{(By using } \tilde{h}_L = h_L/D_o\text{)} \\
&= \arccos(1 - 2\tilde{h}_L)\left(\frac{{D_o}^2}{4}\right) - (1 - 2\tilde{h}_L)\sqrt{4\tilde{h}_L - 4\tilde{h}_L^2}\left(\frac{{D_o}^2}{4}\right)
\end{aligned}$$

So, the dimensionless form for the area occupied by the liquid phase at section I is given by Eq.B.1.

$$\tilde{A}_L = \frac{A_L}{{D_o}^2} = \frac{1}{4}\left[\arccos(1 - 2\tilde{h}_L) - (1 - 2\tilde{h}_L)\sqrt{1 - (1 - 2\tilde{h}_L)^2}\right] \qquad \text{(Eq.B.1)}$$

From Eq.A.5

$$A_G = \pi(ro^2 - r_i^2) - A_L$$

By substituting r_o and r_i by $D_o/2$ and $D_i/2$ respectively, the above equation can be rewritten as,

$$\begin{aligned} A_G &= \pi\left(\frac{{D_o}^2}{4} - \frac{{D_i}^2}{4}\right) - A_L \quad \text{(By using the relationship given in Eq.3.1)} \\ &= \pi\left(\frac{{D_o}^2}{4} - \kappa^2\frac{{D_o}^2}{4}\right) - A_L \\ &= \pi\left(\frac{{D_o}^2}{4}\right)(1-\kappa^2) - A_L \end{aligned}$$

So, the dimensionless form for the area occupied by the gas phase at section I is given by Eq.B.2.

$$\tilde{A}_G = \frac{A_G}{{D_o}^2} = \frac{1}{4}\pi(1-\kappa^2) - \tilde{A}_L \qquad \text{(Eq.B.2)}$$

From Eq.A.6,

$$S_L = 2r_o \arccos\left(1 - \frac{h_L}{r_o}\right)$$

By substituting $2r_o$ as D_o in above equation,

$$\begin{aligned} S_L &= D_o \arccos\left(1 - \frac{2h_L}{D_o}\right) \\ &= D_o \arccos(1 - 2\tilde{h}_L) \end{aligned}$$

Thus, the dimensionless form for the perimeter wetted by the liquid phase is presented by Eq.B.3.

$$\tilde{S}_L = \frac{S_L}{D_o} = \arccos(1 - 2\tilde{h}_L) \qquad \text{(Eq.B.3)}$$

From Eq.A.7,

$$S_G = \pi(D_o + D_i) - D_o \arccos\left(1 - \frac{h_L}{r_o}\right)$$

By changing r_o to $D_o/2$,

$$\begin{aligned} S_G &= \pi(D_o + D_i) - D_o \arccos\left(1 - \frac{2h_L}{D_o}\right) \quad \text{(By using the relationship given in Eq.3.1)} \\ &= \pi(D_o + \kappa D_o) - D_o \arccos\left(1 - \frac{2h_L}{D_o}\right) \\ &= \pi D_o(1+\kappa) - D_o \arccos(1 - 2\tilde{h}_L) \end{aligned}$$

Hence, the dimensionless form for the perimeter wetted by the gas phase is presented by Eq.B.4.

$$\tilde{S}_G = \frac{S_G}{D_o} = \pi(1+\kappa) - \arccos(1 - 2\tilde{h}_L) \qquad \text{(Eq.B.4)}$$

From Eq.A.8

$$Si = 2\sqrt{h_L(2r_o - h_L)}$$

By changing r_o to $D_o/2$,

$$\begin{aligned} Si &= 2\sqrt{h_L D_o - {h_L}^2} \\ &= 2\sqrt{h_L D_o \left(\frac{2}{D_o}\frac{D_o}{2}\right)^2 - {h_L}^2 \left(\frac{2}{D_o}\frac{D_o}{2}\right)^2} \\ &= D_o\sqrt{4\tilde{h}_L - 4\tilde{h_L}^2} \end{aligned}$$

Therefore, the dimensionless form for the perimeter at the gas-liquid interface is given by Eq.B.5.

$$\tilde{S}_i = \frac{S_i}{D_o} = \sqrt{1 - (1 - 2\tilde{h}_L)^2} \qquad \text{(Eq.B.5)}$$

From, Eq.A.9

$$\frac{dA_L}{dh_L} = 2\sqrt{h_L(2r_o - h_L)}$$

The above equation has the same development as Eq.B.5, consequently, the dimensionless form are equal, Eq.B.6 presents the result.

$$\frac{d\tilde{A}_L}{d\tilde{h}_L} = \frac{dA_L/{D_o}^2}{dh_L/D_o} = \sqrt{1-(1-2\tilde{h}_L)^2} \qquad \text{(Eq.B.6)}$$

Eq.B.6 is also valid for section IV.

- **SECTION II**

From Eq.A.14,

$$A_L = \arccos\left(1-\frac{h_L}{r_o}\right){r_o}^2 - \sqrt{h_L(2r_o-h_L)}(r_o-h_L) - \left[\arccos\left(1-\frac{h_L-(r_o-r_i)}{r_i}\right){r_i}^2 - \sqrt{2h_Lr_o+r_i^2-r_o^2-h_L^2}(r_o-h_L)\right]$$

The above equation can be rewritten switching r_o to $D_o/2$ as,

$$\begin{aligned}
A_L &= \Gamma - \left[\arccos\left(\frac{2D_o}{2D_i}-\frac{2h_L}{D_i}\right)\frac{{D_i}^2}{4} - \left(\frac{D_o}{2}-h_L\right)\sqrt{h_LD_o+\frac{{D_i}^2}{4}-\frac{{D_o}^2}{4}-h_L^2}\right] \\
&= \Gamma - \left[\arccos\left(\frac{D_o}{\kappa D_o}-\frac{2h_L}{\kappa D_o}\right)\kappa^2\frac{{D_o}^2}{4} - \left(\frac{D_o}{2}-h_L\right)\sqrt{h_LD_o+\kappa^2\frac{{D_o}^2}{4}-\frac{{D_o}^2}{4}-h_L^2}\right] \\
&= \Gamma - \left[\arccos\left(\frac{1-2h_L}{\kappa D_o}\right)\kappa^2\frac{{D_o}^2}{4} - \left(\frac{D_o}{2}\right)\left(1-\frac{2h_L}{D_o}\right)\sqrt{\left(\frac{{D_o}^2}{4}\right)\left(\frac{4h_L}{D_o}+\kappa^2-1-\frac{4{h_L}^2}{{D_o}^2}\right)}\right] \\
&= \Gamma - \left[\arccos\left(\frac{1-2h_L}{\kappa D_o}\right)\kappa^2\frac{{D_o}^2}{4} - \left(\frac{D_o}{2}\right)\left(1-\frac{2h_L}{D_o}\right)\sqrt{\left(\frac{{D_o}^2}{4}\right)\left(\frac{4h_L}{D_o}+\kappa^2-1-\frac{4{h_L}^2}{{D_o}^2}\right)}\right] \\
&= \Gamma - \left[\kappa^2\arccos\left(\frac{1-2\tilde{h}_L}{\kappa}\right)\frac{{D_o}^2}{4} - \left(\frac{{D_o}^2}{4}\right)(1-2\tilde{h}_L)\sqrt{4\tilde{h}_L-4\tilde{h}_L^2+\kappa^2-1}\right]
\end{aligned}$$

Where $\Gamma = \arccos\left(1-\frac{2h_L}{D_o}\right)\left(\frac{{D_o}^2}{4}\right) - \left(\frac{D_o}{2}-h_L\right)\sqrt{h_L(D_o-h_L)}$ which is the same as seen in the development of Eq.B.1. Hence, the area occupied by the liquid phase at section II in dimensionless form is given by Eq.B.7.

$$\tilde{A}_L = \frac{A_L}{{D_o}^2} = \frac{1}{4}\Big[\arccos(1-2\tilde{h}_L) - (1-2\tilde{h}_L)\sqrt{1-(1-2\tilde{h}_L)^2} - \kappa^2 \arccos\left(\frac{1-2\tilde{h}_L}{\kappa}\right) + (1-2\tilde{h}_L)\sqrt{\kappa^2-(1-2\tilde{h}_L)^2}\Big] \quad \text{(Eq.B.7)}$$

The expression for the area occupied by the gas phase in dimensionless form follows the same development as the previous section; equation below presents the result - Eq.B.2.

$$\tilde{A}_G = \frac{A_G}{{D_o}^2} = \frac{1}{4}\left[\pi(1-\kappa^2) - \tilde{A}_L\right]$$

From Eq.A.15,

$$S_L = 2r_o \arccos\left(1-\frac{h_L}{r_o}\right) + 2r_i \arccos\left(\frac{r_o - h_L}{r_i}\right)$$

The above equation is rewritten by substituting $2r_o$ and $2r_i$ by D_o and D_i respectively.

$$\begin{aligned} S_L &= D_o \arccos\left(1-\frac{2h_L}{D_o}\right) + D_i \arccos\left(\frac{2D_o}{2D_i} - \frac{2h_L}{D_i}\right) \\ &= D_o \arccos\left(1-\frac{2h_L}{D_o}\right) + \kappa D_o \arccos\left(\frac{2D_o}{2\kappa D_o} - \frac{2h_L}{\kappa D_o}\right) \\ &= D_o \arccos(1-2\tilde{h}_L) + \kappa D_o \arccos\left(\frac{1-2\tilde{h}_L}{\kappa}\right) \end{aligned}$$

Hence, the dimensionless liquid perimeter is expressed by Eq.B.8.

$$\tilde{S}_L = \frac{S_L}{D_o} = \arccos(1-2\tilde{h}_L) + \kappa \arccos\left(\frac{1-2\tilde{h}_L}{\kappa}\right) \quad \text{(Eq.B.8)}$$

From Eq.A.15,

$$S_G = \pi(D_o + D_i) - S_L$$

Rewriting the above equation,

$$S_G = \pi(D_o + \kappa D_i) - S_L$$
$$= \pi D_o(1+\kappa) - S_L$$

Therefore, the dimensionless gas perimeter is given by Eq.B.9.

$$\tilde{S}_G = \frac{S_G}{D_o} = \pi(1+\kappa) - \left[\arccos(1-2\tilde{h}_L) + \kappa \arccos\left(\frac{1-2\tilde{h}_L}{\kappa}\right)\right] \quad \text{(Eq.B.9)}$$

From Eq.A.17,

$$Si = 2\sqrt{h_L(2r_o - h_L)} - 2\sqrt{r_i^2 - (r_o - h_L)^2}$$

Rewriting the above equation,

$$\begin{aligned} Si &= 2\sqrt{D_o h_L - {h_L}^2} - 2\sqrt{h_L D_o + \frac{{D_i}^2}{4} - \frac{{D_o}^2}{4} - {h_L}^2} \\ &= 2\sqrt{D_o h_L - {h_L}^2} - 2\sqrt{h_L D_o + \kappa^2\frac{{D_o}^2}{4} - \frac{{D_o}^2}{4} - {h_L}^2} \\ &= 2\sqrt{\left(\frac{{D_o}^2}{4}\right)\left(\frac{4h_L}{D_o} - \frac{4{h_L}^2}{D_o}\right)} - 2\sqrt{\left(\frac{{D_o}^2}{4}\right)\left(\frac{4h_L}{D_o} + \kappa^2 - 1 - \frac{4{h_L}^2}{{D_o}^2}\right)} \\ &= D_o\sqrt{1-(1-2\tilde{h}_L)^2} - D_o\sqrt{4\tilde{h}_L - 4\tilde{h}_L^2 + \kappa^2 - 1} \end{aligned}$$

Consequently, the perimeter at the gas-liquid interface is given byEq.B.10.

$$\tilde{S}_i = \frac{S_i}{D_o} = \sqrt{1-(1-2\tilde{h}_L)^2} - \sqrt{\kappa^2 - (1-2\tilde{h}_L)^2} \quad \text{(Eq.B.10)}$$

From Eq.A.18,

$$\frac{dA_L}{dh_L} = 2\sqrt{h_L(2r_o - h_L)} - 2\sqrt{r_i^2 - (r_o - h_L)^2}$$

The above equation can be rewritten as,

$$\begin{aligned}\frac{dA_L}{dh_L} &= 2\sqrt{D_o h_L - {h_L}^2} - 2\sqrt{h_L D_o + \frac{{D_i}^2}{4} - \frac{{D_o}^2}{4} - {h_L}^2} \\ &= D_o\sqrt{1-(1-2\tilde{h}_L)^2} - D_o\sqrt{4\tilde{h}_L - 4\tilde{h}_L^2 + \kappa^2 - 1}\end{aligned}$$

The expression is equal to the development of Eq.B.10, so the result is the same, and it is given by Eq.B.11

$$\frac{d\tilde{A}_L}{d\tilde{h}_L} = \frac{dA_L/{D_o}^2}{dh_L/D_o} = \sqrt{1-(1-2\tilde{h}_L)^2} - \sqrt{\kappa^2-(1-2\tilde{h}_L)^2} \qquad \text{(Eq.B.11)}$$

Eq.B.11 is also valid for section III.

- **SECTION III**

From Eq.A.23,

$$\begin{aligned}A_G = \arccos\left(1-\frac{h_G}{r_o}\right) r_o^2 - \sqrt{h_G(2r_o-h_G)}(r_o-h_G) \\ - \left[\arccos\left(1-\frac{r_o+r_i-h_L}{r_i}\right) {r_i}^2 - \sqrt{2h_L r_o + r_i^2 - r_o^2 - h_L^2}(h_L-r_o)\right]\end{aligned}$$

$$\begin{aligned}A_G &= \Omega - \left[\arccos\left(\frac{2h_L}{D_i} - \frac{2D_o}{2D_i}\right)\frac{{D_i}^2}{4} - \left(h_L - \frac{D_o}{2}\right)\sqrt{h_L D_o + \frac{{D_i}^2}{4} - \frac{{D_o}^2}{4} - h_L^2}\right] \\ &= \Omega - \left[\arccos\left(\frac{2h_L}{\kappa D_o} - \frac{D_o}{\kappa D_o}\right)\kappa^2\frac{{D_o}^2}{4} - \left(h_L - \frac{D_o}{2}\right)\sqrt{h_L D_o + \kappa^2\frac{{D_o}^2}{4} - \frac{{D_o}^2}{4} - h_L^2}\right] \\ &= \Omega - \left[\arccos\left(\frac{2h_L-1}{\kappa D_o}\right)\kappa^2\frac{{D_o}^2}{4} - \left(\frac{D_o}{2}\right)\left(\frac{2h_L}{D_o}-1\right)\sqrt{\left(\frac{{D_o}^2}{4}\right)\left(\frac{4h_L}{D_o} + \kappa^2 - 1 - \frac{4{h_L}^2}{{D_o}^2}\right)}\right] \\ &= \Omega - \left[\arccos\left(\frac{2h_L-1}{\kappa D_o}\right)\kappa^2\frac{{D_o}^2}{4} - \left(\frac{D_o}{2}\right)\left(\frac{2h_L}{D_o}-1\right)\sqrt{\left(\frac{{D_o}^2}{4}\right)\left(\frac{4h_L}{D_o} + \kappa^2 - 1 - \frac{4{h_L}^2}{{D_o}^2}\right)}\right] \\ &= \Omega - \left[\kappa^2\arccos\left(\frac{2\tilde{h}_L-1}{\kappa}\right)\frac{{D_o}^2}{4} - \left(\frac{{D_o}^2}{4}\right)(2\tilde{h}_L-1)\sqrt{4\tilde{h}_L - 4\tilde{h}_L^2 + \kappa^2 - 1}\right]\end{aligned}$$

Where $\Omega = \arccos\left(1 - \frac{h_G}{r_o}\right) r_o^2 - \sqrt{h_G(2r_o - h_G)}(r_o - h_G)$ which is the same as seen in the development of Eq.B.18. Hence, the area occupied by the gas phase at section III in dimensionless form is given by Eq.B.12.

$$\tilde{A}_G = \frac{A_G}{{D_o}^2} = \frac{1}{4}\Big[\arccos(2\tilde{h}_L - 1) - (2\tilde{h}_L - 1)\sqrt{1 - (2\tilde{h}_L - 1)^2} - \kappa^2 \arccos\left(\frac{2\tilde{h}_L - 1}{\kappa}\right) + (2\tilde{h}_L - 1)\sqrt{\kappa^2 - (1 - 2\tilde{h}_L)^2}\Big] \quad \text{(Eq.B.12)}$$

From Eq.A.24,

$$A_L = \pi(r_o^2 - r_i^2) - A_G$$

Now rewriting the above equation,

$$\begin{aligned} A_L &= \pi\left(\frac{{D_o}^2}{4} - \frac{{D_i}^2}{4}\right) - A_G \\ &= \pi\left(\frac{{D_o}^2}{4} - \kappa^2\frac{{D_o}^2}{4}\right) - A_G \\ &= \pi\left(\frac{{D_o}^2}{4}\right)(1 - \kappa^2) - A_G \end{aligned}$$

Hence, the dimensionless form for the area occupied by the liquid phase at section III is given by Eq.B.13.

$$\tilde{A}_L = \frac{A_L}{{D_o}^2} = \frac{1}{4}[\pi(1 - \kappa^2) - \tilde{A}_G] \quad \text{(Eq.B.13)}$$

From Eq.A.25,

$$S_G = 2r_o \arccos\left(\frac{h_L}{r_o} - 1\right) + 2r_i \arccos\left(\frac{h_L - r_o}{r_i}\right)$$

The above equation can be rewritten as,

$$
\begin{aligned}
S_G &= D_o \arccos\left(\frac{2h_L}{D_o} - 1\right) + D_i \arccos\left(\frac{2h_L}{D_i} - \frac{2D_o}{2D_i}\right) \\
&= D_o \arccos\left(\frac{2h_L}{D_o} - 1\right) + \kappa D_o \arccos\left(\frac{2h_L}{\kappa D_o} - \frac{D_o}{D_i}\right) \\
&= D_o \arccos(2\tilde{h}_L - 1) + \kappa D_o \arccos\left(\frac{2\tilde{h}_L - 1}{\kappa}\right)
\end{aligned}
$$

Therefore, the dimensionless gas perimeter is given by Eq.B.14.

$$
\tilde{S}_G = \frac{S_G}{D_o} = \arccos(2\tilde{h}_L - 1) + \kappa \arccos\left(\frac{2\tilde{h}_L - 1}{\kappa}\right) \tag{Eq.B.14}
$$

From Eq.A.26,

$$
S_L = 2\pi(r_o + r_i) - S_G \tag{Eq.B.15}
$$

The above equation can be rewritten as,

$$
\begin{aligned}
S_L &= \pi(D_o + D_i) - S_G \\
&= \pi(D_o + \kappa D_o) - S_G \\
&= \pi D_o(1 + \kappa) - S_G
\end{aligned}
$$

Thus, the dimensionless liquid perimeter is given by Eq.B.16.

$$
\tilde{S}_L = \frac{S_L}{D_o} = \pi(1 + \kappa) - \left[\arccos(2\tilde{h}_L - 1) + \kappa \arccos\left(\frac{2\tilde{h}_L - 1}{\kappa}\right)\right] \tag{Eq.B.16}
$$

From Eq.A.27,

$$
Si = 2\sqrt{h_L(2r_o - h_L)} - 2\sqrt{r_i^2 - (h_L - r_o)^2}
$$

The above equation can be rewritten as,

$$
\begin{aligned}
Si &= 2\sqrt{D_o h_L - {h_L}^2} - 2\sqrt{h_L D_o + \frac{{D_i}^2}{4} - \frac{{D_o}^2}{4} - {h_L}^2} \\
&= 2\sqrt{D_o h_L - {h_L}^2} - 2\sqrt{h_L D_o + \kappa^2 \frac{{D_o}^2}{4} - \frac{{D_o}^2}{4} - {h_L}^2} \\
&= 2\sqrt{\left(\frac{{D_o}^2}{4}\right)\left(\frac{4h_L}{D_o} - \frac{4{h_L}^2}{D_o}\right)} - 2\sqrt{\left(\frac{{D_o}^2}{4}\right)\left(\frac{4h_L}{D_o} + \kappa^2 - 1 - \frac{4{h_L}^2}{{D_o}^2}\right)} \\
&= D_o\sqrt{1-(1-2\tilde{h}_L)^2} - D_o\sqrt{4\tilde{h}_L - 4\tilde{h}_L^2 + \kappa^2 - 1}
\end{aligned}
$$

Consequently, the perimeter at the gas-liquid interface is presented in Eq.B.17.

$$
\tilde{S}_i = \frac{S_i}{D_o} = \sqrt{1-(1-2\tilde{h}_L)^2} - \sqrt{\kappa^2 - (1-2\tilde{h}_L)^2} \qquad \text{(Eq.B.17)}
$$

- **SECTION IV**

From Eq.A.31

$$
A_G = \arccos\left(1 - \frac{h_G}{r_o}\right) r_o^2 - \sqrt{h_G(2r_o - h_G)}(r_o - h_G)
$$

The above equation can be rewritten as,

$$
\begin{aligned}
A_G &= \arccos\left(1 - \frac{2h_G}{D_o}\right)\left(\frac{{D_o}^2}{4}\right) - \left(\frac{D_o}{2} - h_G\right)\sqrt{h_G(D_o - h_G)} \\
&= \arccos\left(1 - \frac{2h_G}{D_o}\right)\left(\frac{{D_o}^2}{4}\right) - \left(1 - \frac{2h_G}{D_o}\right)\sqrt{h_G D_o - {h_G}^2}\left(\frac{D_o}{2}\right) \\
&= \arccos\left(1 - \frac{2h_G}{D_o}\right)\left(\frac{{D_o}^2}{4}\right) - \left(1 - \frac{2h_G}{D_o}\right)\sqrt{h_G D_o\left(\frac{2}{D_o}\frac{D_o}{2}\right)^2 - {h_G}^2\left(\frac{2}{D_o}\frac{D_o}{2}\right)^2}\left(\frac{D_o}{2}\right) \\
&= \arccos\left(1 - \frac{2h_G}{D_o}\right)\left(\frac{{D_o}^2}{4}\right) - \left(1 - \frac{2h_G}{D_o}\right)\sqrt{\frac{4h_G}{D_o} - \frac{4{h_G}^2}{D_o}}\left(\frac{{D_o}^2}{4}\right) \quad \text{(By using } \tilde{h}_G = h_G/D_o\text{)} \\
&= \arccos(1-2\tilde{h}_G)\left(\frac{{D_o}^2}{4}\right) - (1-2\tilde{h}_G)\sqrt{4\tilde{h}_G - 4\tilde{h}_G^2}\left(\frac{{D_o}^2}{4}\right)
\end{aligned}
$$

So, the dimensionless form for the area occupied by the liquid phase at section IV is given by Eq.B.18.

$$\tilde{A}_G = \frac{A_G}{{D_o}^2} = \frac{1}{4}\left[\arccos(1-2\tilde{h}_G) - (1-2\tilde{h}_G)\sqrt{1-(1-2\tilde{h}_G)^2}\right] \quad \text{(Eq.B.18)}$$

The solution for the area occupied by the liquid phase in the section IV follows the same development as section III; therefore, it is given by Eq.B.13.

$$\tilde{A}_L = \frac{A_L}{{D_o}^2} = \frac{1}{4}[\pi(1-\kappa^2) - \tilde{A}_G]$$

With $\tilde{A}_G$ given by Eq.B.18.

From Eq.A.32,

$$S_G = 2r_o \arccos\left(1 - \frac{h_G}{r_o}\right)$$

Which can be rewritten by substituting r_o with $D_o/2$ as,

$$S_G = D_o \arccos\left(1 - \frac{2h_G}{D_o}\right)$$

Hence, the gas perimeter at section IV in dimensionless form is given by Eq.B.19.

$$\tilde{S}_G = \frac{S_G}{D_o} = \arccos(1-2\tilde{h}_G) \quad \text{(Eq.B.19)}$$

From Eq.A.33,

$$S_L = 2\pi(r_o + r_i) - 2r_o \arccos\left(1 - \frac{h_G}{r_o}\right)$$

Which can be rewritten as,

$$
\begin{aligned}
S_L &= \pi(D_o + D_i) - D_o \arccos\left(1 - \frac{2h_G}{D_o}\right) \\
&= \pi(D_o + \kappa D_o) - D_o \arccos\left(1 - \frac{2h_G}{D_o}\right) \\
&= \pi D_o(1+\kappa) - D_o \arccos(1 - 2\tilde{h}_G)
\end{aligned}
$$

Therefore, the liquid perimeter at section IV in dimensionless form is given by Eq.B.20.

$$
\tilde{S}_L = \frac{S_L}{D_o} = \pi(1+\kappa) - \arccos(1 - 2\tilde{h}_G) \qquad \text{(Eq.B.20)}
$$

From Eq.A.34,

$$
Si = 2\sqrt{h_G(2r_o - h_G)}
$$

Which can be rewritten as following,

$$
\begin{aligned}
Si &= 2\sqrt{h_G D_o - {h_G}^2} \\
&= 2\sqrt{\left(\frac{{D_o}^2}{4}\right)\left(\frac{4h_G}{D_o} - \frac{4{h_G}^2}{{D_o}^2}\right)} \\
&= D_o\sqrt{1 - (1 - 2\tilde{h}_G)^2}
\end{aligned}
$$

Hence, the perimeter at the gas-liquid interface at section IV in dimensionless form is given by Eq.B.21.

$$
\tilde{S}_i = \frac{S_i}{D_o} = \sqrt{1 - (1 - 2\tilde{h}_G)^2} \qquad \text{(Eq.B.21)}
$$

APPENDIX C – EVALUATION OF TRANSVERSAL AREAS OCCUPIED BY LIQUID AND GAS

This section details how to calculate the cross sections filled by liquid and gas. The cross-section of the cylinder is a circumference with radius r_o (as shown in Fig.32). Taking the Cartesian axes xyz, the circumference is placed onto the yz plane, and the traditional θ angle with the z axis as a reference. The first step is the calculation of the hatched area in Fig.32.

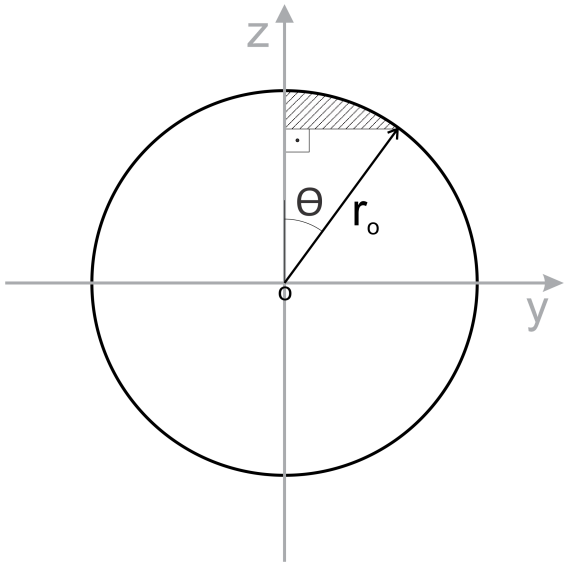

Figure 32 – Initial cross-section area
Source: Author

By evaluating the circle area that is covered by the angle θ. Its value is:

$$A_\theta = \frac{(r_o)^2\theta}{2}. \qquad \text{(Eq.C.1)}$$

Then it is also evaluated the area of the triangle that is formed having the projection of r_o on the z axis as the height,

$$A_T = \frac{1}{2} \times r_o \sin\theta \times \ r_o \cos\theta = \frac{(r_o)^2}{2} \sin\theta \cos\theta \qquad \text{(Eq.C.2)}$$

.

To reach the value of the area of interest (A_{int}), an intermediate step is required: the difference between circular area and discount the area of the triangle is calculated.

$$A_{int} = A_\theta - A_T = \frac{(r_o)^2}{2}(\theta - \sin\theta\cos\theta). \quad \text{(Eq.C.3)}$$

thus doubling the area above, the value of the final area is given by Eq.C.4.

$$A_f = 2A_{int} = (r_0)^2(\theta - \sin\theta\cos\theta) \quad \text{(Eq.C.4)}$$

Now, it is placed a cylinder of radius r_i inside the current cylinder ($r_i < r_o$), as shown in Fig.33. In this context, the area filled by the gas is related to the proposed model. Note that the angle β that appears in Fig.33 is smaller than the angle θ and will have an area analogous to the calculated above the shape,

$$A_{int} = (r_i)^2(\beta - \sin\beta\cos\beta). \quad \text{(Eq.C.5)}$$

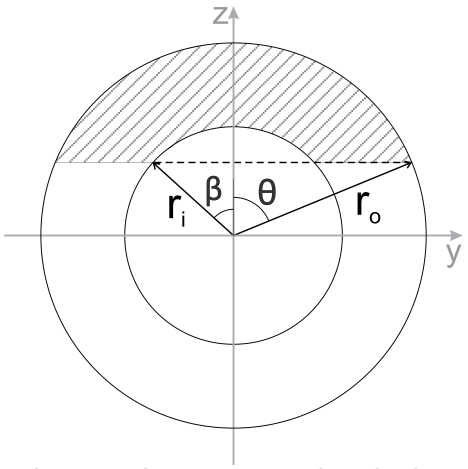

Figure 33 – Area occupied by the gas phase in cross hatched pattern
Source: Author

The area filled by the gas A_G (as shown in crosshatched Fig.33) is the difference between the calculated areas in the cylinder with radius r_o and r_i,

$$A_G = (r_o)^2(\theta - \sin\theta\cos\theta) - (r_i)^2(\beta - \sin\beta\cos\beta). \quad \text{(Eq.C.6)}$$

APPENDIX D – CODES IN MATLAB

Code 1 – Main code for solving equation 3.33 iterations

```
clc();
clear
close all

%Comparacao
D_o = (125-2*4.2)/1000;
D_i =  75/1000;
nu_L = 8.931E-7;%/1000;
nu_G = 1.579E-5;%*1000;
rho_L = 997.1; %kg/m3
rho_G = 1.169; %kg/m3
sigma = 71.97E-3; %N/m

angulo = 0;
gamma = (angulo)*pi/180; %radianos
g = 9.81; %m/s2
A = 0.25*pi*(D_o^2-D_i^2); %m2
s = 0.01;
kappa = D_i/D_o;
R = 0.5*D_o;
r = 0.5*D_o;
psi = (r/R)-((1-kappa^2)/(2*log(1/kappa)))*(R/r);
discretizacao = 50;
tol = 0.01;

[save_hl,U_GS_vector,U_LS_vector] = ...
    find_zero_4_equacoes(discretizacao,tol,A,D_o,D_i,r,R,
```

```
27 gamma,nu_L, nu_G,rho_L,rho_G );
28
29 matrix_SS = zeros(discretizacao,discretizacao);
30 matrix_AD = zeros(discretizacao,discretizacao);
31 matrix_I = zeros(discretizacao,discretizacao);
32 matrix_DB = zeros(discretizacao,discretizacao);
33 matrix_SW = zeros(discretizacao,discretizacao);
34 matrix_SS_SW = zeros(discretizacao,discretizacao);
35
36 SS_X = zeros(discretizacao,discretizacao);
37 SS_Y = zeros(discretizacao,discretizacao);
38
39 SW_X = zeros(discretizacao,discretizacao);
40 SW_Y = zeros(discretizacao,discretizacao);
41
42 AD_X = zeros(discretizacao,discretizacao);
43 AD_Y = zeros(discretizacao,discretizacao);
44
45 I_X = zeros(discretizacao,discretizacao);
46 I_Y = zeros(discretizacao,discretizacao);
47
48 DB_X = zeros(discretizacao,discretizacao);
49 DB_Y = zeros(discretizacao,discretizacao);
50
51 SS_SW_X = zeros(discretizacao,discretizacao);
52 SS_SW_Y = zeros(discretizacao,discretizacao);
53
54 for i = 1:discretizacao
55 for j = 1:discretizacao
56
57 U_GS = U_GS_vector(1,i);
58 U_LS = U_LS_vector(1,j);
```

```
hl = save_hl(i,j);

tilde_hl = hl/D_o;

%section I
if tilde_hl ≤ (1-kappa)/2

tilde_hl = hl/D_o;
beta = acos(1-2*tilde_hl);

alpha_L = (2*beta-sin(2*beta))/(2*pi*(1-kappa^2));
alpha_G = 1 - alpha_L;

S_L = D_o*acos(1-2*tilde_hl);
S_G = D_o*(pi*(1+kappa)- acos(1-2*tilde_hl));
Si = D_o*sqrt(1-(1-2*tilde_hl)^2);

tilde_dAL_dhl = sqrt(tilde_hl*(1-tilde_hl));
tilde_AL = 0.25*(acos(1-2*tilde_hl)-(1-2*tilde_hl)
*sqrt(1-(1-2*tilde_hl)^2));
tilde_AG = 0.25*(pi*(1-kappa^2))-tilde_AL;
tilde_Si = sqrt(1-(1-2*tilde_hl)^2);
end

%Section II
if tilde_hl > (1-kappa)/2 && tilde_hl ≤ 0.5
tilde_hl = hl/D_o;
beta = acos(1-2*tilde_hl);
alpha = acos((1-2*tilde_hl)/kappa);

alpha_L = ...
    (2*beta-sin(2*beta)-kappa^2*(2*alpha-sin(2*alpha))) / ...
```

```
    (2*pi*(1-kappa^2));
alpha_G = 1 - alpha_L;

S_L = D_o*(acos(1-2*tilde_hl)+kappa*acos((1-2*tilde_hl) ...
    / kappa));
S_G = D_o*pi*(1+kappa)-S_L;
Si = D_o*(sqrt(1-(1-2*tilde_hl)^2) - ...
    sqrt(kappa^2-(1-2*tilde_hl)^2));

tilde_dAL_dhl = sqrt(1-(1-2*tilde_hl)^2) - ...
    sqrt(kappa^2-(1-2*tilde_hl)^2);
tilde_AL = 0.25*(acos(1-2*tilde_hl) - ...
    (1-2*tilde_hl)*sqrt(1-(1-2*tilde_hl)^2) - ...
    kappa^2*acos((1-2*tilde_hl) / kappa) + ...
    (1-2*tilde_hl)*sqrt(kappa^2 - (1-2*tilde_hl)^2));
tilde_AG = 0.25*(pi*(1-kappa^2))-tilde_AL;
tilde_Si = ...
    sqrt(1-(1-2*tilde_hl)^2)-sqrt(kappa^2-(1-2*tilde_hl)^2);
end

%Section III
if tilde_hl > 0.5 && tilde_hl ≤ (1+kappa)/2
tilde_hl = hl/D_o;
hg = 1-tilde_hl;
beta = acos(1-2*hg);
alpha = acos((1-2*hg)/kappa);

alpha_G = (2*beta-sin(2*beta) - ...
    kappa^2*(2*alpha-sin(2*alpha))) / (2*pi*(1-kappa^2));
alpha_L = 1- alpha_G;

```

```
112 S_G = D_o*(acos(2*tilde_hl-1) + ...
      kappa*acos((2*tilde_hl-1) / kappa));
113 S_L = D_o*pi*(1+kappa)-S_G;
114 Si = D_o*(sqrt(1-(1-2*tilde_hl)^2) - ...
      sqrt(kappa^2-(1-2*tilde_hl)^2));
115
116 tilde_dAL_dhl = sqrt(1-(1-2*tilde_hl)^2) - ...
      sqrt(kappa^2-(1-2*tilde_hl)^2);
117 tilde_AG = ...
      0.25*(acos(1-2*hg)-(1-2*hg)*sqrt(1-(1-2*hg)^2) - ...
      kappa^2*acos((2*tilde_hl-1)/kappa) + ...
      (2*tilde_hl-1)*sqrt(kappa^2-(1-2*tilde_hl)^2));
118 tilde_AL = 0.25*(pi*(1-kappa^2))-tilde_AG;
119 tilde_Si = sqrt(1-(1-2*tilde_hl)^2) - ...
      sqrt(kappa^2-(1-2*tilde_hl)^2);
120 end
121
122 %Section IV
123 if tilde_hl > (1+kappa)/2 && tilde_hl ≤ 1
124 tilde_hl = hl/D_o;
125 hg = 1-tilde_hl;
126 beta = acos(1-2*hg);
127
128 alpha_G = (2*beta-sin(2*beta))/(2*pi*(1-kappa^2));
129 alpha_L = 1- alpha_G;
130
131 S_G = D_o*acos(2*tilde_hl-1);
132 S_L = D_o*pi*(1+kappa)-S_G;
133 Si = D_o*sqrt(1-(1-2*tilde_hl)^2);
134
135 tilde_dAL_dhl = sqrt(tilde_hl*(1-tilde_hl));
136 tilde_AG = 0.25*(acos(1-2*hg)-(1-2*hg)*sqrt(1-(1-2*hg)^2));
```

```
137 tilde_AL = 0.25*(pi*(1-kappa^2))-tilde_AG;
138 tilde_Si = sqrt(1-(1-2*tilde_hl)^2);
139
140 end
141
142 U_G = U_GS/alpha_G;
143 U_L = U_LS/alpha_L;
144
145 A_G = A*alpha_G;
146 A_L = A*alpha_L;
147
148 D_L = 4*A_L/S_L;
149 D_G = 4*A_G/(S_G+Si);
150
151 Re_G = (U_G*D_G)/nu_G;
152 Re_L = (U_L*D_L)/nu_L;
153
154 if Re_G ≥ 2000
155 C_G = 0.046;
156 m = 0.2;
157 else
158 C_G = 16;
159 m = 1;
160 end
161
162 if Re_L ≥ 2000
163 C_L = 0.046;
164 n = 0.2;
165
166 else
167 C_L = 16;
168 n = 1;
```

```
169 end
170
171 f_L = C_L*((D_L*U_L)/nu_L)^(-n);
172 f_G = C_G*((D_G*U_G)/nu_G)^(-m);
173
174 tau_wg = 0.5*f_G*rho_G*U_G^2*psi;
175 tau_wl = 0.5*f_L*rho_L*U_L^2*psi;
176 tau_i = 0.5*f_G*rho_G*U_G^2*psi;
177
178 tilde_UL = (A/D_o^2)/tilde_AL; %VERIFICAR
179 tilde_UG = (A/D_o^2)/tilde_AG; %VERIFICAR
180 tilde_DL = D_L/D_o;
181 C2 = 1-tilde_hl;
182
183 %ADIMENSIONAIS
184 square_x = ((4*C_L/D_o)*(((U_LS*D_o)/nu_L)^(-n)) * ...
       (0.5*rho_L*U_LS^2)) / ((4*C_G/D_o) * ...
       (((U_GS*D_o)/nu_G)^(-m)) * (0.5*rho_G*U_GS^2));
185 X = sqrt(square_x);
186 T = sqrt(((4*C_L/D_o) * (((U_LS*D_o)/nu_L)^(-n)) * ...
       (0.5*rho_L*U_LS^2)) / ((rho_L-rho_G)*g*cos(gamma)));
187 F = sqrt(rho_G/(rho_L-rho_G)) * ...
       (U_GS/sqrt(D_o*g*cos(gamma)));
188 K = F*sqrt(D_o*U_LS/nu_L);
189
190 %TRANSICAO REGIMES
191 S_to_NS_eq_25 = ...
       F^2*((tilde_UG*tilde_dAL_dhl)/(tilde_AG*C2^2));
192 S_to_NS_eq_23 = ...
       C2*sqrt(((rho_L-rho_G)*g*cos(gamma)*A_G) / ...
       (rho_G*D_o*tilde_dAL_dhl));
193 I_to_AD = tilde_hl;
```

```
194 I_to_DB = (8*tilde_AG) / ...
      (tilde_Si*tilde_UL^2*((tilde_UL*tilde_DL)^(-n)));
195 SS_to_SW = ...
      sqrt((4*nu_L*(rho_L-rho_G)*g*cos(gamma))/(s*rho_G*U_L));
196
197 if U_G ≤ S_to_NS_eq_23 && U_G < SS_to_SW
198 matrix_SS(i,j) = 1;
199 matrix_SS_SW(i,j) = 6;
200 SS_X(i,j) = U_GS;
201 SS_Y(i,j) = U_LS;
202
203 SS_SW_X(i,j) = U_GS;
204 SS_SW_Y(i,j) = U_LS;
205 end
206
207 if U_G ≤ S_to_NS_eq_23 && U_G ≥ SS_to_SW
208 matrix_SW(i,j) = 2;
209 matrix_SS_SW(i,j) = 6;
210
211 SW_X(i,j) = U_GS;
212 SW_Y(i,j) = U_LS;
213
214 SS_SW_X(i,j) = U_GS;
215 SS_SW_Y(i,j) = U_LS;
216 end
217
218 if U_G > S_to_NS_eq_23 && I_to_AD < 0.5
219 matrix_AD(i,j) = 3;
220 AD_X(i,j) = U_GS;
221 AD_Y(i,j) = U_LS;
222 end
223
```

```
224 if U_G > S_to_NS_eq_23 && I_to_AD ≥ 0.5 && T^2 ≥ I_to_DB
225 matrix_DB(i,j) = 4;
226 DB_X(i,j) = U_GS;
227 DB_Y(i,j) = U_LS;
228 end
229
230 if U_G > S_to_NS_eq_23 && I_to_AD ≥ 0.5 && T^2 < I_to_DB
231 matrix_I(i,j) = 5;
232 I_X(i,j) = U_GS;
233 I_Y(i,j) = U_LS;
234 end
235 end
236 end
237
238 %TRANSFORMANDO AS MATRIZES EM VECTOR E REMOVENDO ZEROS
239
240 vector_SS_X = SS_X';
241 vector_SS_X = vector_SS_X(:);
242 vector_SS_Y = SS_Y';
243 vector_SS_Y = vector_SS_Y(:);
244
245 vector_SW_X = SW_X';
246 vector_SW_X = vector_SW_X(:);
247 vector_SW_Y = SW_Y';
248 vector_SW_Y = vector_SW_Y(:);
249
250 vector_AD_X = AD_X';
251 vector_AD_X = vector_AD_X(:);
252 vector_AD_Y = AD_Y';
253 vector_AD_Y = vector_AD_Y(:);
254
255 vector_DB_X = DB_X';
```

```
256 vector_DB_X = vector_DB_X(:);
257 vector_DB_Y = DB_Y';
258 vector_DB_Y = vector_DB_Y(:);
259
260 vector_I_X = I_X';
261 vector_I_X = vector_I_X(:);
262 vector_I_Y = I_Y';
263 vector_I_Y = vector_I_Y(:);
264 %%
265 figure(1)
266 plot(vector_SS_X,vector_SS_Y,'oc')
267 hold on
268 plot(vector_SW_X,vector_SW_Y,'ok')
269 plot(vector_AD_X,vector_AD_Y,'og')
270 plot(vector_DB_X,vector_DB_Y,'ob')
271 plot(vector_I_X,vector_I_Y,'or')
272 set(gca,'xscale','log')
273 set(gca,'yscale','log')
274
275 xlim([0.01 100])
276 ylim([0.01 10])
277 % xticks([0.1 1 10 100 500])
278 % yticks([0.01 0.1 1 10 50 100])
279 xlabel('U_{GS} [m/s]')
280 ylabel('U_{LS} [m/s]')
281 legend('SS','SW','AD','DB','I','Location','eastoutside')
282
283 %% CONTORNOS DO MAPA
284 matrix_save_I = matrix_I;
285 for i = 2:discretizacao-1
286 for j = 2:discretizacao-1
```

```
287 if matrix_I(i,j+1) == 5 && matrix_I(i,j-1) == 5 && ...
      matrix_I(i+1,j) == 5 && matrix_I(i-1,j-1) == 5
288 matrix_save_I(i,j) = 0;
289 end
290 end
291 end
292
293 for i = 1:discretizacao
294 for j = 1:discretizacao
295 if i == 1 || i == discretizacao || j == 1 || j == ...
      discretizacao
296 matrix_save_I(i,j) = 0;
297
298 end
299 end
300 end
301
302 figure(3)
303 surf(matrix_save_I)
304
305 save_index = zeros(1,discretizacao);
306 transicao_x_to_SW_1 = zeros(1,discretizacao); %primeiro
307 transicao_y_to_SW_1 = zeros(1,discretizacao); %primeiro
308 transicao_x_to_SW_2 = zeros(1,discretizacao); %primeiro
309 transicao_y_to_SW_2 = zeros(1,discretizacao); %primeiro
310 %
311 transicao_x_to_SS_SW_1 = zeros(1,discretizacao); %segundo
312 transicao_y_to_SS_SW_1 = zeros(1,discretizacao); %segundo
313 transicao_x_to_SS_SW_2 = zeros(1,discretizacao); %segundo
314 transicao_y_to_SS_SW_2 = zeros(1,discretizacao); %segundo
315
316 transicao_x_SS_to_SW_left = zeros(1,discretizacao);
```

```
317 transicao_y_SS_to_SW_left = zeros(1,discretizacao);
318
319 transicao_x_to_AD = zeros(1,discretizacao);
320 transicao_y_to_AD = zeros(1,discretizacao);
321
322 transicao_x_to_DB = zeros(1,discretizacao);
323 transicao_y_to_DB = zeros(1,discretizacao);
324
325 transicao_x_to_SS = zeros(1,discretizacao);
326 transicao_y_to_SS = zeros(1,discretizacao);
327
328 transicao_x_to_I = zeros(1,discretizacao);
329 transicao_y_to_I = zeros(1,discretizacao);
330
331 %SS-SW - Variando em X - PRIMEIRO
332 for i = 1:discretizacao
333 changedIndexes = diff(matrix_SW(i,:))≠0;
334 change = find(changedIndexes == 1);
335
336 if change ≠ 1
337 U_LS = U_LS_vector(1,i);
338 U_GS = U_GS_vector(1,change(1,1));
339 transicao_x_to_SW_1(1,i) = U_GS;
340 transicao_y_to_SW_1(1,i) = U_LS;
341 end
342 end
343 %SS-SW - Variando em Y - PRIMEIRO
344 for j = 1:discretizacao
345 changedIndexes = diff(matrix_SW(:,j))≠0;
346 change = find(changedIndexes == 1);
347
348 if change ≠ 1
```

```
U_LS = U_LS_vector(1,change(1,1));
U_GS = U_GS_vector(1,j);
transicao_x_to_SW_2(1,j) = U_GS;
transicao_y_to_SW_2(1,j) = U_LS;
end
end
%-----------------------------------------
%SW-I - Variando em X - SEGUNDO
for i = 1:discretizacao
changedIndexes = diff(matrix_SS_SW(i,:))≠0;
change = find(changedIndexes == 1);

if change ≠ 1
U_LS = U_LS_vector(1,i);
U_GS = U_GS_vector(1,(change(1,end)));
transicao_x_to_SS_SW_1(1,i) = U_GS;
transicao_y_to_SS_SW_1(1,i) = U_LS;
end
end
%SW-I - Variando em Y - SEGUNDO
for j = 1:discretizacao
changedIndexes = diff(matrix_SS_SW(:,j))≠0;
change = find(changedIndexes == 1);

if change ≠ 1
U_LS = U_LS_vector(1,(change));
U_GS = U_GS_vector(1,j);
transicao_x_to_SS_SW_2(1,j) = U_GS;
transicao_y_to_SS_SW_2(1,j) = U_LS;
end
end
%-----------------------------------------------
```

```
381 for i = 1:discretizacao
382
383 changedIndexes = diff(matrix_SS(i,:))≠0;
384 change = find(changedIndexes == 1);
385
386 if change ≠ 1
387 U_LS = U_LS_vector(1,i);
388 U_GS = U_GS_vector(1,change(1,length(change)));
389 transicao_x_SS_to_SW_left(1,i) = U_GS;
390 transicao_y_SS_to_SW_left(1,i) = U_LS;
391 end
392 end
393
394 for i = 1:discretizacao
395
396 changedIndexes = diff(matrix_AD(i,:))≠0;
397 change = find(changedIndexes == 1);
398
399 if change ≠ 1
400 U_LS = U_LS_vector(1,i);
401 U_GS = U_GS_vector(1,change(1,end));
402 transicao_x_to_AD(1,i) = U_GS;
403 transicao_y_to_AD(1,i) = U_LS;
404 end
405 end
406
407 for j = 1:discretizacao
408
409 changedIndexes = diff(matrix_DB(:,j))≠0;
410 change = find(changedIndexes == 1);
411
412 if change ≠ 1
```

```
413 U_LS = U_LS_vector(1,change);
414 U_GS = U_GS_vector(1,j);
415 transicao_x_to_DB(1,j) = U_GS;
416 transicao_y_to_DB(1,j) = U_LS;
417 end
418 end
419
420 for j = 1:discretizacao
421 changedIndexes = diff(matrix_SS(:,j))≠0;
422 change = find(changedIndexes == 1);
423
424 if change ≠ 1
425 U_LS = U_LS_vector(1,change);
426 U_GS = U_GS_vector(1,j);
427 transicao_x_to_SS(1,j) = U_GS;
428 transicao_y_to_SS(1,j) = U_LS;
429 end
430
431 end
432
433 for j = 1:discretizacao
434 changedIndexes = diff(matrix_I(:,j))≠0;
435 change = find(changedIndexes == 1);
436
437 if change ≠ 1
438 U_LS = U_LS_vector(1,(change(1,1)));
439 U_GS = U_GS_vector(1,j);
440 transicao_x_to_I(1,j) = U_GS;
441 transicao_y_to_I(1,j) = U_LS;
442 end
443 end
444
```

```
445 %%
446 % EXCLUINDO ITENS REPETIDOS
447
448 valor_y = find(transicao_y_to_SW_2 == ...
      transicao_y_to_SS_SW_2);
449
450 transicao_x_to_SW_2(valor_y) = [];
451 transicao_y_to_SW_2(valor_y) = [];
452
453 transicao_x_to_SW = [transicao_x_to_SW_1 ...
      transicao_x_to_SW_2]; %Combina os dois vetores em ...
      somente um
454 transicao_y_to_SW = [transicao_y_to_SW_1 ...
      transicao_y_to_SW_2]; %Combina os dois vetores em ...
      somente um
455 transicao_x_to_SW(transicao_x_to_SW == 0) = []; % ...
      Remove os zeros
456 transicao_y_to_SW(transicao_y_to_SW == 0) = []; % ...
      Remove os zeros
457
458 [¬, uniqueIdx] = unique(transicao_x_to_SW,'first'); ...
      %Verifica onde ha repeticao de x's
459 excluir = setdiff(1:numel(transicao_x_to_SW), uniqueIdx);
460
461 transicao_x_to_SW(excluir) = []; %Exclui as repeticoes
462 transicao_y_to_SW(excluir) = []; %Exclui as repeticoes
463
464 [¬, uniqueIdx] = unique(transicao_y_to_SW,'first'); ...
      %Verifica onde ha repeticao de x's
465 excluir = setdiff(1:numel(transicao_y_to_SW), uniqueIdx);
466
467 transicao_x_to_SW(excluir) = []; %Exclui as repeticoes
```

```
468 transicao_y_to_SW(excluir) = []; %Exclui as repeticoes
469
470 %-----SEGUNDO-INICIO------
471 [transicao_x_to_SS_SW,transicao_y_to_SS_SW] = ...
      second_vector(transicao_x_to_SS_SW_1,
472 transicao_y_to_SS_SW_1,
473 transicao_x_to_SS_SW_2,transicao_y_to_SS_SW_2);
474
475 %-----TERCEIRO-INICIO-----
476 transicao_x_to_AD(transicao_x_to_AD == 0) = []; % ...
      Remove os zeros
477 transicao_y_to_AD(transicao_y_to_AD == 0) = []; % ...
      Remove os zeros
478
479 [Lia,Locb] = ...
      ismember(transicao_x_to_SS_SW,transicao_x_to_AD);
480 [Lia2,Locb2] = ...
      ismember(transicao_y_to_SS_SW,transicao_y_to_AD);
481 [Lia3,Lo2cb3] = ismember(Locb,Locb2);
482 Lo2cb3(Lo2cb3 == 0) = [];
483 posicao = Locb(min(Lo2cb3),1);
484 valor_y = transicao_y_to_AD(1,posicao);
485 valor_x = transicao_x_to_AD(1,posicao);
486
487 excluir = find(transicao_y_to_AD < valor_y);
488 transicao_x_to_AD(excluir) = []; %Exclui as repeticoes
489 transicao_y_to_AD(excluir) = []; %Exclui as repeticoes
490
491 matrix = [transicao_x_to_AD' transicao_y_to_AD'];
492 matrix_out = sortrows(matrix,2);
493
494 transicao_x_to_AD = matrix_out(:,1);
```

```
495 transicao_y_to_AD = matrix_out(:,2);
496
497 [¬, uniqueIdx] = unique(transicao_x_to_AD,'last'); ...
      %Verifica onde ha repeticao de x's
498 excluir = setdiff(1:numel(transicao_x_to_AD), uniqueIdx);
499 transicao_x_to_AD(excluir) = []; %Exclui as repeticoes
500 transicao_y_to_AD(excluir) = []; %Exclui as repeticoes
501 %---------------------------------------
502 excluir = find(transicao_y_to_SS_SW > valor_y);
503 transicao_x_to_SS_SW(excluir) = []; %Exclui as repeticoes
504 transicao_y_to_SS_SW(excluir) = []; %Exclui as repeticoes
505
506 %---------------------------------------
507 excluir = find(transicao_x_to_I > valor_x);
508 transicao_x_to_I(excluir) = []; %Exclui as repeticoes
509 transicao_y_to_I(excluir) = []; %Exclui as repeticoes
510
511 [¬, uniqueIdx] = unique(transicao_y_to_I,'first'); ...
      %Verifica onde ha repeticao de x's
512 excluir = setdiff(1:numel(transicao_y_to_I), uniqueIdx);
513 transicao_x_to_I(excluir) = []; %Exclui as repeticoes
514 transicao_y_to_I(excluir) = []; %Exclui as repeticoes
515
516 transicao_x_to_I(transicao_x_to_I == 0) = [];
517 transicao_y_to_I(transicao_y_to_I == 0) = [];
518
519 %-----------------------------------------------
520 [¬, uniqueIdx] = unique(transicao_y_to_DB,'first'); ...
      %Verifica onde ha repeticao de x's
521 excluir = setdiff(1:numel(transicao_y_to_DB), uniqueIdx);
522
523 transicao_x_to_DB(excluir) = []; %Exclui as repeticoes
```

```
524 transicao_y_to_DB(excluir) = []; %Exclui as repeticoes
525
526 % INTERPOLACAO
527
528 x_inter_to_SW = linspace(min(transicao_x_to_SW), ...
      max(transicao_x_to_SW), 50);
529 y_inter_to_SW = ...
      interp1(transicao_x_to_SW,transicao_y_to_SW,
530 x_inter_to_SW,'makima');
531
532 x_inter_to_SS_SW = linspace(min(transicao_x_to_SS_SW), ...
      max(transicao_x_to_SS_SW), 50);
533 y_inter_to_SS_SW = ...
      interp1(transicao_x_to_SS_SW,transicao_y_to_SS_SW,
534 x_inter_to_SS_SW,'makima');
535
536 x_inter_to_AD = linspace(min(transicao_x_to_AD), ...
      max(transicao_x_to_AD), 50);
537 y_inter_to_AD = ...
      interp1(transicao_x_to_AD,transicao_y_to_AD,
538 x_inter_to_AD,'makima');
539
540 %%Save files
541 data_1 = [x_inter_to_SS_SW'  y_inter_to_SS_SW'];
542 data_2 = [x_inter_to_SW' y_inter_to_SW'];
543 data_3 = [x_inter_to_AD' y_inter_to_AD'];
544 data_4 = [x_inter_DB' y_inter_DB'];
545 data_5 = [x_inter_to_I' y_inter_to_I'];
546
547 writematrix(data_1,filename,'Sheet',1,'Range','A1:B100')
548 writematrix(data_2,filename,'Sheet',1,'Range','D1:E100')
549 writematrix(data_3,filename,'Sheet',1,'Range','G1:H100')
```

```
writematrix(data_4,filename,'Sheet',1,'Range','J1:K100')
writematrix(data_5,filename,'Sheet',1,'Range','M1:N100')
```

Code 2 – Function "find-zero.m" used in the main algorithm

```
function [save_hl,U_GS_vector,U_LS_vector] = ...
    find_zero_4_equacoes(discretizacao, tol, A, D_o, ...
    D_i, r, R, gamma, nu_L, nu_G, rho_L, rho_G)

kappa = D_i/D_o;
psi = (r/R)-((1-kappa^2)/(2*log(1/kappa)))*(R/r);
g = 9.81; %m/s2

U_GS_vector = ...
    logspace(-2,log(100)/log(10),discretizacao);
U_LS_vector = logspace(-2,log(10)/log(10),discretizacao);
save_hl = ...
    zeros(length(discretizacao),length(discretizacao));
save_maximo= ...
    zeros(length(discretizacao),length(discretizacao));

for i = 1:length(U_GS_vector)
for j = 1:length(U_LS_vector)

U_GS = U_GS_vector(1,i);
U_LS = U_LS_vector(1,j);

comprimento = 10^3;

equilibrio = zeros(1, comprimento);

```

```
22  valor_antes = 0;
23  valor_depois = D_o;
24  iter = 0;
25  itermax = 50;
26  valor = 2*tol;
27
28  while abs(valor) ≥ tol && iter ≤itermax
29
30  hl_vector = linspace(valor_antes,valor_depois, ...
        comprimento);
31
32  for k = 1:comprimento
33  %section I
34  if hl_vector(1,k) ≤ D_o/2-D_i/2
35  tilde_hl = hl_vector(1,k)/D_o;
36  beta = acos(1-2*tilde_hl);
37
38  alpha_L = (2*beta-sin(2*beta))/(2*pi*(1-kappa^2));
39  alpha_G = 1 - alpha_L;
40
41  S_L = D_o*acos(1-2*tilde_hl);
42  S_G = D_o*(pi*(1+kappa)- acos(1-2*tilde_hl));
43  Si = D_o*sqrt(1-(1-2*tilde_hl)^2);
44  end
45
46  %Section II
47  if hl_vector(1,k) > D_o/2-D_i/2 && hl_vector(1,k) ≤ D_o/2
48  tilde_hl = hl_vector(1,k)/D_o;
49  beta = acos(1-2*tilde_hl);
50  alpha = acos((1-2*tilde_hl)/kappa);
51
52  alpha_L = (2*beta-sin(2*beta) - kappa^2 * ...
```

```
      (2*alpha-sin(2*alpha))) / (2*pi*(1-kappa^2));
53    alpha_G = 1 - alpha_L;
54
55    S_L = D_o*(acos(1-2*tilde_hl) + ...
      kappa*acos((1-2*tilde_hl)/kappa));
56    S_G = D_o*pi*(1+kappa)-S_L;
57    Si = D_o*(sqrt(1-(1-2*tilde_hl)^2) - ...
      sqrt(kappa^2-(1-2*tilde_hl)^2));
58    end
59
60    %Section III
61    if hl_vector(1,k) > D_o/2 && hl_vector(1,k) ≤ D_o/2+D_i/2
62    tilde_hl = hl_vector(1,k)/D_o;
63    h_G = 1-tilde_hl;
64    beta = acos(1-2*h_G);
65    alpha = acos((1-2*h_G)/kappa);
66
67    alpha_G = (2*beta-sin(2*beta) - ...
      kappa^2*(2*alpha-sin(2*alpha))) / (2*pi*(1-kappa^2));
68    alpha_L = 1- alpha_G;
69
70    S_G = D_o*(acos(2*tilde_hl-1) + ...
      kappa*acos((2*tilde_hl-1)/kappa));
71    S_L = D_o*pi*(1+kappa)-S_G;
72    Si = D_o*(sqrt(1-(1-2*tilde_hl)^2) - ...
      sqrt(kappa^2-(1-2*tilde_hl)^2));
73    end
74
75    %Section IV
76    if hl_vector(1,k) > D_o/2+D_i/2 && hl_vector(1,k) ≤ D_o
77    tilde_hl = hl_vector(1,k)/D_o;
78    h_G = 1-tilde_hl;
```

```
beta = acos(1-2*h_G);

alpha_G = (2*beta-sin(2*beta))/(2*pi*(1-kappa^2));
alpha_L = 1- alpha_G;

S_G = D_o*acos(2*tilde_hl-1);
S_L = D_o*pi*(1+kappa)-S_G;
Si = D_o*sqrt(1-(1-2*tilde_hl)^2);
end

U_G = U_GS/alpha_G;
U_L = U_LS/alpha_L;

A_G = A*alpha_G;
A_L = A*alpha_L;

D_L = 4*A_L/S_L;
D_G = 4*A_G/(S_G+Si);

Re_G = (U_G*D_G)/nu_G;
Re_L = (U_L*D_L)/nu_L;

if Re_G ≥ 2000
C_G = 0.046;
m = 0.2;
else
C_G = 16;
m = 1;
end

if Re_L ≥ 2000
C_L = 0.046;
```

```
111    n = 0.2;
112    else
113    C_L = 16;
114    n = 1;
115    end
116
117    f_L = C_L*((D_L*U_L)/nu_L)^(-n);
118    f_G = C_G*((D_G*U_G)/nu_G)^(-m);
119
120    tau_wg = 0.5*f_G*rho_G*U_G^2*psi;
121    tau_wl = 0.5*f_L*rho_L*U_L^2*psi;
122    tau_i = 0.5*f_G*rho_G*U_G^2*psi;
123
124    equilibrio(1,k) = tau_wg*S_G/A_G - tau_wl*S_L/A_L + ...
          tau_i*Si*(1/A_L + 1/A_G)+(rho_L-rho_G)*g*sin(gamma);
125    end
126
127    vector = find(equilibrio > 0);
128    vector_2 = find(equilibrio ≤ 0);
129
130    if isempty(vector_2) == 1
131    depois = vector(1,1);
132    valor_antes = 0;
133    valor_depois = hl_vector(1,depois);
134    valor = 2*tol;
135    elseif isempty(vector) == 1
136    antes = vector_2(1,end);
137    valor_antes = hl_vector(1,antes);
138    valor_depois = D_o;
139    valor = 2*tol;
140    else
141    antes = vector_2(1,end);
```

```
142   depois = vector(1,1);
143   eq_antes = equilibrio(1,antes);
144   eq_depois = equilibrio(1,depois);
145   valor_antes = hl_vector(1,antes);
146   valor_depois = hl_vector(1,depois);
147   valor = eq_antes-eq_depois;
148   end
149
150   iter = iter+1;
151   %               fprintf('%d \t %d \t %d \t ...
        %.5f\n',i,j,iter, abs(valor))
152   end
153   save_hl(i,j) = hl_vector(1,antes);
154   save_maximo(i,j) = max(abs(valor));
155   end
156   end
157
158   eixo_x = linspace(0.1,500,discretizacao);
159   eixo_y = linspace(0.01,50,discretizacao);
160   %%
161   close all
162   figure(1)
163   surf(U_GS_vector,U_LS_vector,save_hl)
164   plano_1 = zeros(discretizacao,discretizacao);
165   plano_2 = zeros(discretizacao,discretizacao);
166
167   plano_1(:,:) = 0.5*(D_o-D_i)/D_o;
168   plano_2(:,:) = 0.5*(D_o+D_i)/D_o;
169
170   figure(2)
171   surf(eixo_x,eixo_y,save_hl/D_o);
172   h = rotate3d;
```

```
173    h.RotateStyle = 'box';
174    h.Enable = 'on';
175    shading interp
176
177    hold on
178    surf(eixo_x,eixo_y,plano_1)
179    surf(eixo_x,eixo_y,plano_2)
180    xlim([0 500])
181    xticks([0 100 200 300 400 500])
182    ylim([0 50])
183    view(-60,23)
184    xlabel('{U_G}^S [m/s]')
185    ylabel('{U_L}^S [m/s]')
186    zlabel('h_L/D_o [-]')
187    figure(3)
188    contourf(eixo_x,eixo_y,save_hl/D_o)
189    colorbar
190    figure(4)
191    surf(save_maximo)
192    zlim([0 2*tol])
193    figure(5)
194    surf(save_maximo)
195    zlim([0 2*tol])
196      end
```